Bibliography Report
June 2013

Irradiated Assisted Corrosion of Stainless Steel in Light Water Reactors – Focus on Radiolysis and Corrosion Damage

Mi WANG [1, 2]

[1] Laboratoire des Solides Irradiés – Ecole Polytechnique, CNRS, CEA, Palaiseau, France
[2] Laboratoire d'Etude de la Corrosion Aqueuse – CEA/DEN/DPC/SCCME, Centre de Saclay, Gif-sur-Yvette, France

Contents

Chapter 1

Light Water Reactors

Nuclear power is one of the major sources of energy and electricity production. Nuclear power plants provide about 6% of the world's energy and 13 - 15% of the world's electricty [1, 2]. Nuclear power plants are conventional thermal power stations in which the heat sources are nuclear reactors. They are devices to initiate and control sustained nuclear chain reactions and the heat from nuclear fission is passed to a thermal fluid (water or gas), which runs through turbines to generate power. Most of the nuclear reactors use energy form the the fission of the nucleus of the Uranium 235 isotope, ^{235}U. In France, the nuclear fuel is used in the form of uranium dioxide enriched to 3.5 - 4% in $^{235}UO_2$ [3].

The most common types of nuclear reactors are thermal reactors, among which the most popular are Light Water Reactors (LWRs). Because the LWRs are simple and less expressive to build compared to other nuclear reactors, they make up the vast majority of civil nuclear reactors and naval propulsion reactors in service. The LWRs can be subdivided into three categories: Boiling Water Reactors (BWRs), Pressurised Water Reactors (PWRs) and Supercritical Water Reactors (SWRs). SWRs, now named as KERENA, are based on the successful tradition of BWR technology and is currently still at the design stage [4]. PWRs are the most common civil nuclear reactors in the world. In France, they are the only ones in operation today.

1.1 General Introduction

1.1.A Main Components

The Reactor Pressure Vessel (RPV) is the highest priority key component in a nuclear power plant because it houses the nuclear reactor core and all associated support and alignment devices. It is the major part of the Reactor Coolant System (RCS). The major components of RPV are the reactor vessel, the core barrel, the reactor core and the upper internals package. Nuclear fuel is housed in the core barrel slides down inside of the reactor vessel [5, 6]. They are the places that nuclear reactions take place.

Most **nuclear fuels** used inside nuclear reactor core contain heavy fissile elements that are capable of nuclear fission, and the most common fissile nuclear fuels are Uranium 235. When a fissile atomic nuclei ^{235}U, absorbs a neutron, it splits into two or more fast-moving lighter nuclei (the fission products), releasing kinetic energy, γ radiation and free neutrons. A portion of these neutrons may later be absorbed by other fissile atoms and trigger further fission events, which release more neutrons. This is called a **nuclear chain reaction**.

The reactor core generates heat in several ways:

- The kinetic energy of fission products is converted to thermal energy when these nuclei collide with nearby atoms.
- Some of the γ rays produced during fission are absorbed by the reactor, their energy being converted to heat.
- Heat is produced by the radioactive decay of fission products and materials that have been activated by neutron absorption.

As a matter of fact, not all these neutrons can initiate further fission reactions due to their low cross section of capturing ^{235}U, so for most nuclear reactors, a **neutron moderator** is necessary. It is

a medium that reduces the speed of fast neutrons, thereby turning them into thermal neutrons which are capable of sustaining a nuclear chain reaction involving Uranium 235. Since energy is conserved, the reduction of the neutron kinetic energy takes place by transferring energy to a moderator. This process of the reduction of the initial high kinetic energy of free neutrons, *neutron slowing down*, is called **moderation**, or **thermalisation**.

For the safety of nuclear reactors, reactivity control of nuclear chain reaction is necessary to sustain the core at a low level of power efficiency. The continuous chain reactions of a nuclear fission reactor depends upon at least one neutron from each fission being absorbed by another fissionable nucleus, thus the reaction can be controlled by using materials which absorb neutrons. Therefore, despite the fact that absorbing neutrons is normally an undesirable effect, **control rods** made of **neutron poisons** are intentionally inserted into some types of reactors in order to lower high reactivity of their initial fresh fuel load. They are the substances with a large neutron absorption cross section. There are many types of poisons used in different aims, some of these poisons deplete as they absorb neutrons during reactor operation, while others remain relatively constant. For example, the positive reactivity due to the excess fuel must be balanced with negative reactivity from neutron-absorbing material. Soluble poisons, also known as chemical shim, produce a spatially uniform neutron absorption when dissolved in the water coolant. One of the most soluble poison used in control rods is boron, which is often referred to as soluble boric acid. Movable control rods containing neutron-absorbing material is one method, but burnable poisons are also loaded into the core which can control large amounts of excess fuel reactivity without control rods. They are materials that have a high neutron absorption cross section that are converted into materials of relatively low absorption cross section as the result of neutron absorption.

Apart form the RPV, the nuclear power plants may also contain the **pressuriser**, the **reactor coolant pump**, the **steam generator** and the **connecting pipes**, depending on the different types of reactors. Last but not least, lead blocks and concrete enclosures of several meters thickness are used as **shielding** which prevents radiations reaching outside of the reactors.

In those reactors which uses enriched uranium, light water is the choice for both coolant and neutron moderator, which gives the definition and description of the Light Water Reactors (LWRs) [7]. The main reasons for choosing light water are: low cost, lack of toxicity, high coefficient of heat transport and its qualities as a moderator. On the contrary, using water can also cause some inconveniences: water become corrosive at high temperature and its decomposition under irradiation. This decomposition is so called *water radiolysis*, which produce oxygen, O_2, and hydrogen peroxide, H_2O_2, as soluble species. Both O_2 and H_2O_2 are oxidative and will accelerate the corrosion of metal parts in the nuclear reactors. As mentioned, the two operational types of light water reactors (LWRs) are boiling water reactors (BWRs) and pressurized water reactors (PWRs). The main difference between the BWRs and the PWRs is that the PWRs employ a cooling system that is physically separated from the water which will be boiled to produce pressurised steam for the turbines. For BWRs, the water for the steam turbines is boiled directly by the reactor core. It will be more detailed in the following sections.

1.2 Classification of Nuclear Reactors

Research on commercial nuclear reactors started around the mid-1950s. By the end of 1990$'s$, a large amount of nuclear power plants were in commercial operation or under construction [8]. Nowadays, the most widely used commercial reactors are the Light Water Reactors (LWRs), including Boiling Water Reactors (BWRs) and Pressurised Water Reactors (PWRs). They both use enriched uranium dioxide as nuclear fuel and light water as both moderator and coolant. Furthermore, in the very earliest design, Basic Gas-Cooled Reactors, called MAGNOX reactors in UK and UNGG in France, used graphite as moderator and gas as coolant. As the result of improving the cost effectiveness of this type of reactor, there evolved the Advanced Gas-Cooled Reactors (AGRs). The only design of heavy water moderated and cooled reactor in commercial use is the CANada Deuterium Uranium reactors (CANDUs), designed in Canadian. They use unenriched uranium dioxide as nuclear fuel and heavy water as moderator [9]. In addition, there are also Reaktor Bolshoy Moshchnosti Kanalniy (RBMKs) and Vodo-Vodyanoi Energetichesky Reactors (VVERs) designed in Russia. The RBMKs are water cooled and graphite moderated reactors and the VVERs are a series of PWRs. In order to classify different types of nuclear reactors, there exists several methods: nuclear reaction, coolant and moderator, generation and etc.

1.2.A Classified via Nuclear reaction

The principal of all commercial nuclear reactors are based on their nuclear fission. Fission reactors can be divided roughly into two classes depending on the energy of neutrons that sustain the fission chain reactions. They are thermal reactors and fast neutron reactors. Almost all current reactors are thermal reactors which use slowed or thermal neutrons [10]. The thermal reactors contain neutron moderators that slow neutrons down until their kinetic energy approaches the average kinetic energy of the surrounding particles. The other type is fast neutron reactors use fast neutrons to cause fission in their fuel. They do not have a neutron moderator and use less moderating coolant. However, the fast neutron reactors must use highly rich fissile materials as the fuel in order to maintain the nuclear chain reactions without neutron moderator.

1.2.B Classified by Coolant and Moderator

Nuclear reactors can be distinguished by their own coolants and moderators. For coolants, there are water cooled, liquid metal cooled, gas cooled and molten salt cooled nuclear reactors. On the other hand, there exists different types of moderators such as graphite, heavy or light water, light element like lithium or beryllium and organic products.

1.2.C Classified via Generation

In general, all the nuclear power plants can be classified by **generation**: Generation I, II, III, III+, and IV. Nuclear reactors of Generation I refers to the earliest prototype reactors build form the 1950s to the 1960s. All of them have been retired except for the Wylfa Nuclear Power Station in north Wales which will be retired in 2014 [12]. Most current nuclear reactors are classified in Generation II, the commercial reactors built up from the 1970s to the 1990s, including LWRs which means PWRs

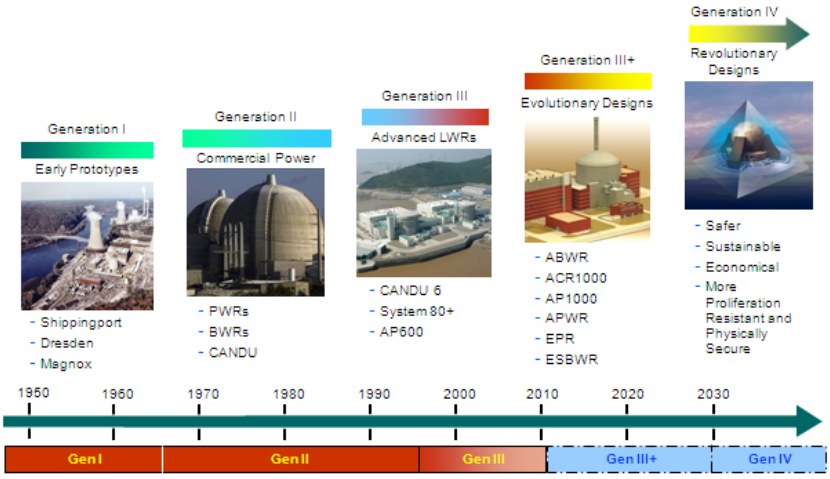

Figure 1.1: Road map of Generations of Nuclear Reactors. [11]

and BWRs, CANDUs, AGRs, and VVERs. Normally Generation II reactor designs had an original design life of 30 or 40 years. However, in order to give these reactors a longer operational life, there comes Generation III and Generation III+ nuclear reactors. Generation III reactors are essentially Generation II reactors with an evolutionary improvements: improved fuel technology, superior thermal efficiency, passive safety systems and standardized design for reduced maintenance and capital costs. Generation III+ nuclear reactors are based on the Generation III reactors' designs and have an enormous improvements of passive safety features which avoid active controls or operator intervention. As a result, reactors of Generation III and III+ can have 60 years operational life, and potentially can greatly exceed 60 years [11]. Reactors of Generation IV still remain at the theoretical and research stage, they are generally not expected to be available for commercial construction before 2030 [13–15]. A road map of Generations of nuclear reactors is presented by Fig.1.1.

Among these different classifications, the most popular one is still the generation method. The evolution and development of nuclear reactor generations depend on many factors: cost-effectiveness, safety, security and nonproliferation features, grid appropriateness, commercialisation road map including constructibility and licensability, management of the fuel cycle, etc. These are also the main factors to appraise the nuclear reactors. However each country has its own preferences for certain types of nuclear reactors. For example, the BWRs and the ABWRs are the most widely built in Japan, the CANDUs are mostly used in Canada and the VVERs for the Russian. In France, all the operating plants today are pressurised water reactors (PWRs). Actually, nuclear power is the primary source in France, nearly 80% of electric power which is the highest percentage in the world [3].

1.3 Boiling Water Reactors (BWRs)

1.3.A Introduction

Boiling Water Reactors (BWRs) are a set of Light Water Reactors (LWRs), they are also the second common type of commercial electricity-generating nuclear reactors. The BWRs were first designed

and developed in USA in the mid-1950s, and now is mainly manufactured by GE Hitachi Nuclear Energy [16]. In the late 1980s and 1990s, an improved version of BWRs was designed and has been further ameliorated until the present day, the so-called Advanced Boiling Water Reactors (ABWRs). They have used advanced technologies to reform the basic BWRs in many domains. In addition, they have a completely standardised design which is more convenient for construction. Other than BWRs and ABWRs, there are also Simplified BWRs (SBWRs) and Economic Simplified BWRs (ESBWRs).

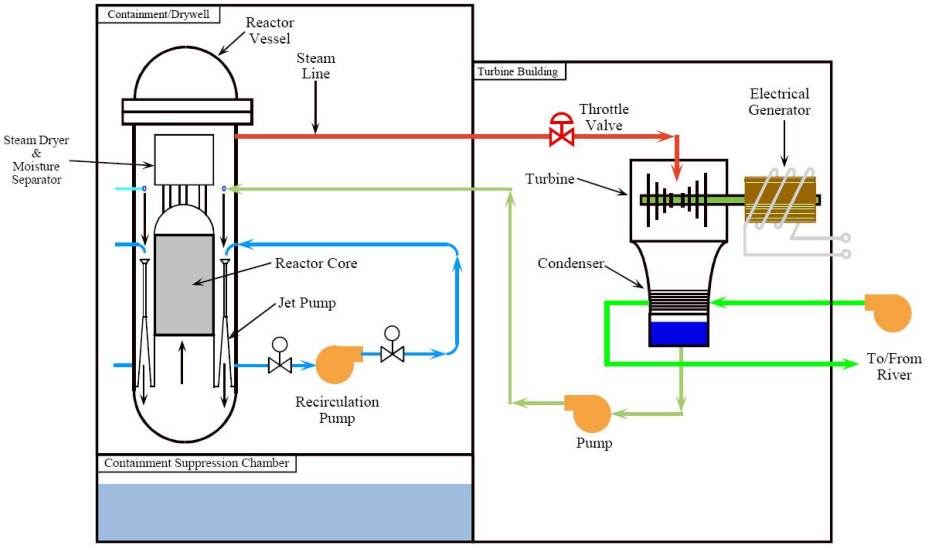

Figure 1.2: Scheme of Boiling Water Reactors (BWRs). [17]

BWRs use enriched uranium dioxide of ^{235}U as nuclear fuels, demineralised water as coolant and neutron moderator. The fuel is assembled into control rods that are submerged in demineralised water and housed in a steel reactor vessel. The nuclear fissions produce heat and causes the coolant water to boil, converting into water-steam mixtures in the upper part of the reactor vessel. This is the biggest different of BWRs compares to the other nuclear systems, the void formation in the reactor core. The droplets of the water-steam mixtures are removed by moisture separator and the steam flows directly through pipes into turbines to generate electricity. Afterwards, the steam is condensed into water and sent back to the reactor vessel. In addition, the recirculation pumps and jet pumps enable varying the coolant flow through the core which is a convenient method for controlling reactor power in BWRs [17]. A simplified scheme of BWRs has been presented in Fig.1.2. One thing should be clearly pointed out there is no steam generator and pressuriser in the system which is often regarded as the basic characteristic of BWRs.

1.3.B Water Chemistry Control in BWRs

Water chemistry control in BWRs is essentially important not only because it is the key factor of material degradation but also links to the fact that it can strongly impact Intergranular Stress Corrosion Cracking (IGSCC) in BWRs. Either material degradation or IGSCC can easily influence the life extension of BWRs, thus a complete and optimised process of water chemistry control is very necessary and has been advanced in recent years. For different types of BWRs and different countries, the guidelines may have some differences, but still the main interactions are more or less the same,

shown in Fig.1.3. It indicates that eliminating impurities, minimising material degradation, controlling radiation fields, avoiding fuel performance issues are the main factors need to be optimised for BWRs water chemistry control.

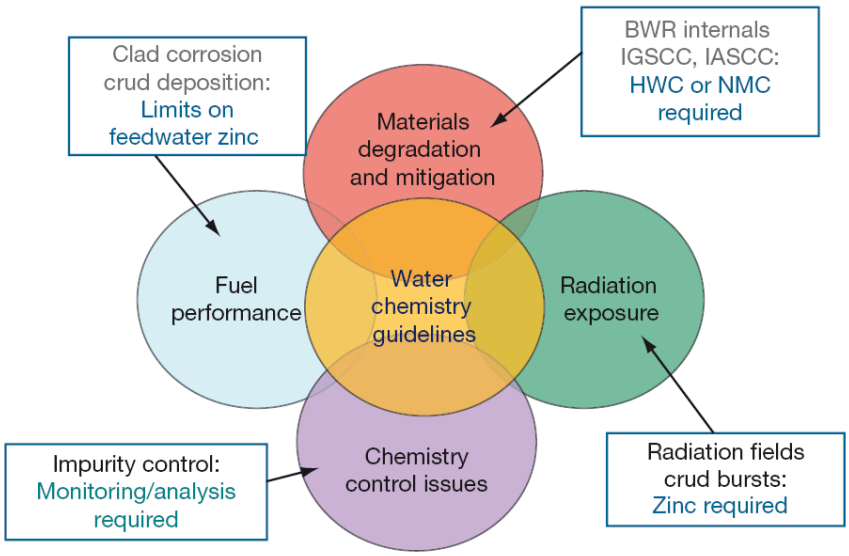

Figure 1.3: Boiling water reactors (BWRs) chemistry interactions. [18]

1.3.B.1 Impurities

Impurities in the coolant water, like chloride and sulfate, can cause a major corrosion problems, thus they need to be removed as much as possible. By using purification systems, the concentration of impurities can be reduced significantly and the water remain pure in all coolant systems.

1.3.B.2 Mitigating Effects on Materials Degradation

Intergranular stress corrosion cracking (IGSCC) is responsible for internal cracking in the reactor internal components which may lead to core failure. However, water chemistry control in BWRs plays an important role in IGSCC process. Electrochemical corrosion potential (ECP) is the key parameter affecting IGSCC: cracking growth reduces with a lower oxygen concentration in the water. Thus, Hydrogen Water Chemistry (HWC), injecting hydrogen continuously into the BWRs water which reduces ECP, has a mitigating effect on IGSCC. Normally, ECP is recommended under $-230mV$(SHE) in order to control IGSCC initiation and propagation [19]. Water decomposition happens in the radiation fields of BWRs, called *Water Radiolysis*. Water radiolysis will produce oxygen and hydrogen peroxide, stable oxidative species in the water. They will react with hydrogen in the water and reduce ECP. In the out-of-core region, a relatively low hydrogen concentration is preferred to reduce ECP. This low hydrogen injection is named HWC-L, indicates the hydrogen injection rate of 0.2-0.5 ppm. On the other hand, water radiolysis occurs in the core, the ECP reduced by the out-of-core region is normally not enough to protect the reactor core. As a result, HWC-M is nowadays used, it increases hydrogen concentration to 1.6-2.0 ppm. However, the rise of hydrogen concentration brings another problem: a carry-over, nitrogen-16 is left under reducing chemistry and hence the radiation field is enlarged in

the steam side. Therefore, Noble Metal Chemical Addition (NMCA) is added to the water in order to increase the efficiency of hydrogen in BWRs cores and to avoid high N-16 field at the same time. It has been demonstrated that with the help of NMCA, ECP can be kept below the -230 mV(SHE) threshold with a relatively low hydrogen injection rate, thus IGSCC can be prevented. Meanwhile, NMCA has also been proved that it has a slight improvement on out-of core region protection [20]. Nevertheless, replacing the original core material, 304 stainless steel, with a less susceptible to IGSCC material is also other way to prevent material degradation in BWRs cores. For instance, 347 stainless steel is used in German BWR reactors, 316 stainless steel (NG) in Sweden and Japan. In this case, oxygenated Normal Water Chemistry (NWC) is still used in these BWRs .

1.3.B.3 Chemistry Control Effects on Radiation Fields

^{60}Co, coming from the activation of soluble Ni in the core, is the primary source of radiation field easily deposited on the out-of-core surface in BWRs. ^{60}Co has a long half-life, accounts for 90% of the total dose, and it is also highly solube in the reactor coolant. Both soluble and insoluble forms of ^{60}Co can increase shutdown dose rates sharply, that is why zinc injection is quite necessary in BWRs water chemistry control. Zinc injection is normally regarded as a solution of reducing radiation field bulid-up. Comparer to ^{60}Co, Zn is much more preferred by oxide film formed on the out-of-core surface. It can be considered that Zn is added to decrease the presence of Ni, and its activated form ^{60}Co in the oxide film. For this reason, while there are Zn ions in the water, less ^{60}Co will be used to form the oxide film. Therefore, the longer and more ^{60}Co that stays in the water, the bigger the chance they have to be removed by the cleanup system. It is also worth mentioning that soluble iron in the feedwater needs to be eliminated in order to avoid and limit the deposits of iron oxide on the surface of fuel elements.

1.3.B.4 Fuels Performance Issues

Corrosion products deposits, so-called *CRUD*, are accumulated on the fuel oxide surface. It causes reduced heat transfer and leads an increase in fuel pin temperature, corrosion of fuel cladding and the risk of fuel failure eventually. Furthermore, Zn and noble metals from the NMAC in the water accelerates the CRUD deposits on the fuel. Therefore, an additional treatment is needed in BWRs water chemistry control in order to take care of the fuel performance issues. Actually, zinc concentration is limited to $0.4ppb$ for non-NMCA and $0.6ppb$ for NMCA reactors [21]. As mentioned before, feedwater iron may also reduce Zn in the water and hence reduce the amount of CRUD on the fuel [18].

1.3.B.5 Other factors

Other than these main factors for BWRs water chemistry control, Online Addition of Noble Metal (OLNM) and Flow-Assisted Corrosion (FAC) also have some influences. Nonetheless, it appears that OLNM has no adverse effects so far. And for FAC, the main factor is dissolved oxygen which needs to be maintained above $30ppb$ to minimise FAC of carbon and low-alloy steels in BWRs [18, 21]. Last but not least, there are always evaluation and diagnosis systems monitoring the water chemistry of BWRs [22].

BWRs have relatively simple and similar designs: fewer components, operate at lower temperature and lower pressure, less irradiation and less coolant loss comparer to PWRs. Therefore, it brings a greater thermal efficiency may lead to an economic advantage for BWRs. However, BWRs need a relatively large pressure vessel and it always exists contamination of activation products in steam turbines due to the fact that the steam produced in the core can enter directly into the turbine. Therefore, an extra cost is needed for the maintenance and operation of BWRs. Overall, BWRs are well developed and widely used nuclear power plant in the world currently, and they will be researched and ameliorated continuously in the future.

1.4 Pressurized Water Reactors (PWRs)

1.4.A The Primary and the Secondary Circuits of PWRs

Pressurised Water Reactors (PWRs) are the other type of Light Water Reactors (LWRs).[1] PWRs are actually the most common type of commercial nuclear power plants which are widely used allover the world. Like BWRs, the first commercial PWR was designed and constructed in the USA during the late 1950*s*. Gradually, big companys like Areva, EDF, Toshiba and Mitsubishi have joined in the development of PWRs. Nowadays, most PWRs under construction are the Generation III and III+ type. For instance, the European Pressurised Reactors (EPRs) designed by Areva, EDF and Siemens AG, the AP600 and AP1000 of Westinghouse Electric Company and the Mitsubishi Advanced Pressurised Water Reactor (Mitsubishi APWR) developed by Mitsubishi Heavy Industries.

PWRs have two major systems which are normally called the primary and the secondary circuits. The primary (or primary coolant) circuit is responsible for transferring the heat produced from the nuclear fuels to the steam generator. The steam formed in the steam generator is transferred to the main turbine generator in the secondary circuit where steam is converted into electricity. In a PWR, the pressuriser provides a way of controlling the system pressure. The nuclear reactor coolant, usually water, is circulated by the coolant pump in order to transfer the heat form the reactor core to the steam generator at a constant flow rate. The heat being generated by the fission process inside the reactor core is then used to generate steam in the steam generator which contains many tubes inside. The reactor coolant fluid comes in the bottom of the steam generator and flows through the inside of the tubes. The secondary feedwater which is used to pick up the heat flows around the outside of the tubes. After absorbing sufficient heat, the secondary feedwater starts to boil and generate steam. Afterwards, the condensate/feedwater system takes over the steam and sends to the main turbine for generating electricity. As the fact that the primary and the secondary circuits are physically separated, all the fission products stay inside of the primary circuit. A schema of a Pressurised Water Reactor (PWR) has shown in Fig.1.4.

The pressure in the primary coolant circuit is around 155 bars, which is the highest among all types of nuclear reactors. Thanks to this high pressure, the primary circuit coolant enters the bottom of the reactor core at about 275°C and is heated as it flows upwards through the reactor core to a temperature of about 320 $\sim$ 325°C [23]. The high temperature and high pressure in the primary coolant circuit are always regarded as a specific characteristic of PWRs.

[1] In theory, SWRs (KERENA) are the third type of LWRs which are still at the design stage in practice.

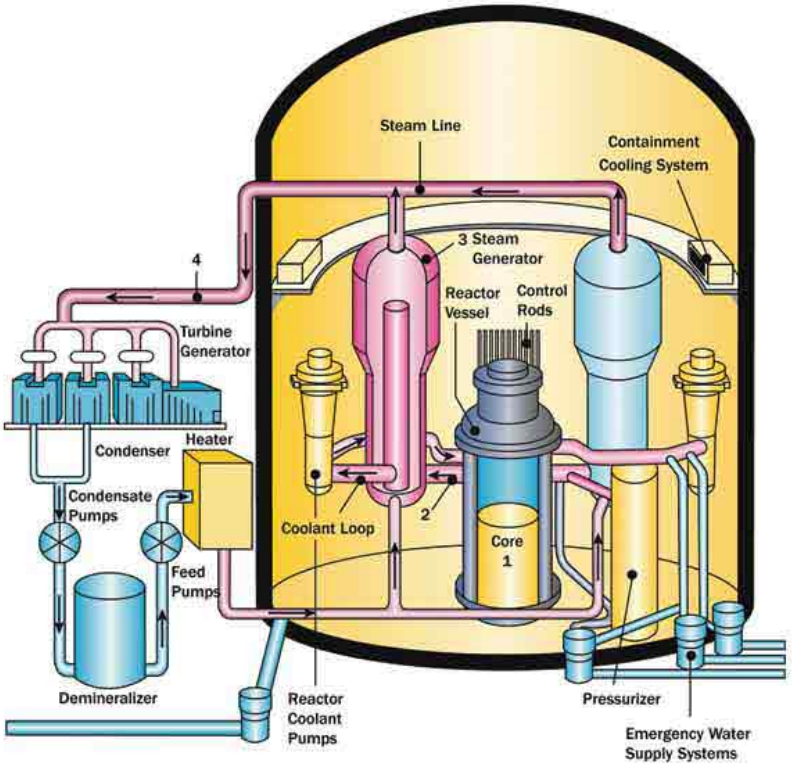

Figure 1.4: Schema of Pressurised Water Reactor.

PWRs normally use enriched uranium dioxide of ^{235}U, clad in a corrosion-resistant zirconium metal alloy Zircaloy, as the nuclear fuel. Light water is used as neutron moderator and coolant in PWRs. However, unlike BWRs, the coolant of PWRs is the demineralised water which contains Boron (B) and Lithium (Li). Boron, introduced in the form of boric acid (H_3BO_3 or $B(OH)_3$), a strong neutron absorber, is used as a neutron poison to slow down the fission reaction rate in PWRs. It can help to maintain the temperature of the primary coolant circuit at the desired point. A typical neutron absorption reaction in boron is written below Eq.1.1. This nuclear reaction leads to an increase of temperature. The energy is taken over by the primary circuit and transferred to the secondary circuit, reducing the power efficiency as the result.

$$^{10}_{5}B +^{1}_{0} n \rightarrow^{7}_{3} Li +^{4}_{2} He + 2.35MeV \tag{1.1}$$

The ^{10}B has a high cross section for absorption of thermal neutrons. For PWRs, boric acid used contains 19.8% of ^{10}B. As the role of the control rod in PWRs, changes in boric acid concentration can effectively regulate the rate of fission taking place in the reactor. However, due to fuel corrosion concerns, the pH around 7 of the coolant at 300°C is strongly recommended. For this reason, lithium hydroxide (LiOH) is also added in the primary coolant in order to achieve the desired pH. On the other hand, it can not be denied that the presence of boron and lithium in the primary coolant may cause complexness of water chemistry control in PWRs which will be explained in the following section Chap.1.4.B.

The secondary circuit of a PWR is composed of a main steam system and a condensate (or

feedwater) system. The hot reactor coolant flows from the reactor to the steam generator, through many tubes inside. The secondary coolant, or feedwater, flows around the outside of the tubes, where it picks up heat from the primary coolant. When the feedwater absorbs sufficient heat, it starts to boil and form steam. Then the steam is transferred to the main turbine so that it can be converted into electricity [5].

1.4.B Water Chemistry Control in the Primary Circuit

In PWRs, water chemistry control is extremely important because it has a great influence on corrosion issues which occur inside the reactor, either the primary or the secondary circuits. Dissolved corrosion products from the out-of-core region, the primary side of the steam generator tubes, may be deposited on the fuel cladding surfaces. Then, these activated corrosion products in the primary circuit will cause materials degradation in the reactor core, high-radiation fields on out-of-core surfaces, compromise fuel performance etc...

In order to avoid water radiolysis and to treat these corrosion issues, dissolved hydrogen has been imposed on the primary coolant initially. Therefore, it can reduce the ECP and raise pH in the primary circuit. A certain concentration of hydrogen (about 30 $cm^3.kg^{-1}$) is also required to suppress *water radiolysis* in the reactor core. Actually, it shares more or less the same principal reason for the addition of dissolved hydrogen in both PWRs and BWRs. However, in the primary coolant circuit, a steadily decreasing concentration of boric acid is used as a chemical shim throughout the fuel cycle which results in the use of lithium hydroxide to maintain the pH_T around 7. Thus, the balance between B and Li in order to keep an optimal pH_T is becoming another key factor for water chemistry control in PWRs. Following successful experience of BWRs, zinc injection has been adopted in the primary circuit of PWRs in several countries. In BWRS, zinc injection has proved to mitigate IGSCC. In PWRs, it may limit the concentration of ^{60}Co and delay the initiation of Primary Water Stress Corrosion Cracking (PWSCC) [18].

1.4.B.1 Dissolved Hydrogen

The primary coolant composed of a demineralised water with boric acid and lithium hydroxide, is under a radiation mixed up with:

- γ**-rays** from the fission reactions;
- **fast neutrons** from the fission reactions;
- a radiation of $^{10}\mathbf{B(n,\alpha)^7Li}$ produced in water by the thermal neutron capture reactions;

The proportion of these different types of radiations depends on the configuration of the reactor core and the concentration of boric acid. Furthermore, these radiations are the causes of chemical degradation of the water in the primary circuit. This is what is called **water radiolysis**. The products of water radiolysis can participate in corrosion process in the primary circuit of the reactor. In order to minimise the corrosion problem, the water has been deaerated to eliminate all trace of oxygen. Moreover, by adding molecular hydrogen dissolved into the water, the water decomposition is strongly

inhibited by a radical mechanism, and the production of oxygen will be slowed down. This will be discussed in the next chapter.

Other than inhibition of water radiolysis, the dissolved hydrogen is also used to decrease the redox potential of the PWR primary water in order to avoid being under an oxidising conditions. In France, the dissolved hydrogen in the primary PWR water is recommended to be 25 to 35 $cm^3.kg^{-1}$ (STP[2]), with the maximum values from 25 to 50 $cm^3.kg^{-1}$ (STP). The recommended amount of hydrogen corresponds to a concentration about 0.001 $mol.L^{-1}$. For PWRs, the quantity of water in the primary circuit is between 200 and 290 tonnes, thus the volume of hydrogen is between 5 to 10 m^3 at 20°C and 1 bar.

1.4.B.2 Balance of Li/B/pH$_T$

Recent work [18, 24–27] demonstrate that the effect of lithium, bore and pH on PWSCC is quite minimal on material susceptibility, comparing with stress state, temperature, pressure and other operational issues. Nevertheless, among the three parameters, at-temperature pH, pH$_T$ is the dominate which actually is adjusted by the concentration of both LiOH and boric acid.

A pH$_T$ between 6.9 and 7.4 was first recommended for the primary coolant in PWRs due to the fact that the temperature coefficients of solubility of magnetite and nickel ferrite are minimum at the range of these two pH values, and thus it can minimise the contamination of the circuit. The possibility of the deposit of corrosion products in the primary circuit is based on the solubilities of iron (magnetite) and nickel (nickel ferrite) which are strongly depend on pH, temperature, and redox potential. Thus, a maintained pH$_T$ in the range of [6.9, 7.4] is defined to reduce corrosion product release rates and continued to be used until now. Although, some details and specific precisions have been made to narrow the pH$_T$ range. Since the nickel ferrite is the prime constituent of CRUD, a preference of pH$_T \backsim$ 7.4 has been made little by little. General corrosion can be reduced on elevated pH$_T$ [28] and corrosion products release rates become less dependent on pH$_T$ as it approach to 7.4 [29]. Indeed, no significant adverse effect has been observed when the pH$_T$ increased to 7.3 in primary circuit of Comanche Peak PWR [30]. As a result, pH$_T$ in the ranges [7.1, 7.2], [7.3, 7.4] are becoming more and more popular. However, different voices on pH$_T$ has been brought up, a pH$_T$ even lower than 6.5 without any adverse effects has been observed in the most recent research [31]. After all, the discussion about pH$_T$ is still undergoing.

The effect of lithium is smaller than the pH$_T$ effect. Nonetheless, the concept of *coordinated of boron and lithium* has been developed form the very beginning. Originally, a limit of 2.2*ppm* of LiOH has been decided due to the Zircaloy corrosion concern. However, normally PWR fuel cycles start with a relatively high boric acid concentration, and reduce little by little until the end of the cycle. Thus, in order to maintain a constant pH$_T$, the concentration of LiOH needed to be gradually reduced in line with the boric acid reduction. Fig.1.5 shows that concentration range between lithium hydroxide and boron in order to obtain a constant pH$_{300°C}$ at 7.2.

The elevation of pH$_T$ actually demands an increase in lithium concentration on the condition that the concentration of boric acid stays constant. However, new laboratory data indicate that increasing

[2]**STP: S**tandard conditions for **T**emperature and **P**ressure are standard sets of conditions for experimental measurements established to allow comparisons to be made between different sets of data. In PWRs, the STP is normally referred to the standard of NIST, which means a temperature at 20°Cand an absolute pressure of 101.325 kPa (1 atm).

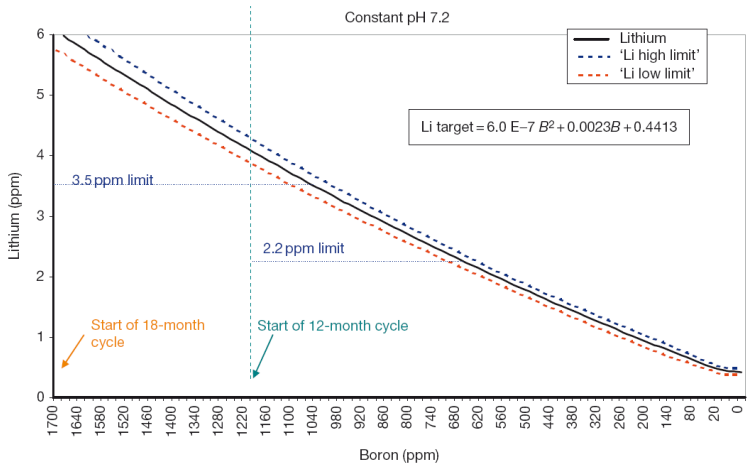

Figure 1.5: Concentration range of boric acid versus lithium hydroxide in order to maintain the $pH_{300°C}$ around 7.2 for different fuel cycle lengths [18].

lithium may lead to an acceleration of stress corrosion cracking on irradiated stainless steel [31]. As a matter of fact, the cracking rate can decrease with the hydrogen concentration, either lower or higher. It depends on the reactors themselves. For a relatively new reactors, such as these ones in France, in Japan and the new ones have just been constructed in the developing countries, they prefer a lower hydrogen concentration. On the opposite, a higher concentration of Li, between $3ppm$ and $3.5ppm$, becomes popular in USA for their long-time served reactors.

As the last parameter in the balance of $Li/B/pH_T$, boron is usually considered as the minor influence. Enriched Boric Acid (EBA) enables to give a desired pH_T with less lithium hydroxide. Hence, EBA has been employed in several PWRs. Nevertheless, boric acid in water can result in an aggressive environment that uniformly attacks the surface of the metal in PWRs.

In general, the balance of $Li/B/pH_T$ is flexible for different plants and different countries. Actually, the pH adjustment for minimising PWSCC has not been ensured and totally proved yet [32]. Thus, different strategies are established: like the elevated pH/lithium, like the use of EBA... Overall, monitoring pH in the primary circuit is considered as the priority in water chemistry control in PWRs.

1.4.B.3 Zinc Injection

Zinc injection in PWRs is actually following the successful experiences of BWRs. Like avoiding IGSCC in BWRs, zinc injection may delay the initiation of PWSCC in PWRs [30]. A recent VTT report [33] has shown the benefits of zinc injection: a significant decrease of SCC, no adverse effects on core performance, negligible effect on cladding integrity and mitigating the CRUD deposition in the core. Thus, zinc injection is nowadays treated as one of the key factors of primary coolant chemistry optimisation for corrosion mitigation and source term reduction in PWRs. Zinc injection in PWRs is widely used in USA and Germany from the late $1990s$, however in France, zinc injection is not so popular, it appears to be studied recently and might be adopted later.

1.4.C Water Chemistry Control in the Secondary Circuit

Water chemistry control in the secondary circuit is essentially important due to the fact that the corrosion damage of Steam Generators (SGs), such as impurities in boiling regions and sludge deposition on SG tubes, can be the cause of corrosion problems occur inside the SGs.

Water chemistry control in the secondary circuit is mainly based on three parts: pH, ECP and impurity controls. The method selected to protect SG tubes also needs to be achieved by the satisfactory of the balance-of-plant (BOP) components. For instance, Flow-assisted Corrosion (FAC) of carbon steel piping, tubing, heat exchanger internals and shells, and ammonia attack of copper and copper alloy and so on. Furthermore, FAC recirculating in the secondary circuit can affect the SG internal components. FAC can also cause wall thinning of carbon and low-alloy steel components. However, FAC depends a lot on pH_T and dissolved oxygen content in the secondary system, and hence it can be mitigated by water chemistry control.

Corrosion, Intergranular attack (IGA), SCC and pitting, all can be influenced by pH_T. An optimal pH_T around the BOP mitigates FAC and thus reduces tremendously the transport of corrosion products to the SG. In order to achieve this pH_T in the secondary circuit, products like ammonia (NH_4OH), ethanolamine (ETA), dimethylamine (DMA), 3-methoxypropylamine (MPA) have been used to control pH_T. In parallel, hydrazine and/or carbonhydrazide has been chosen as oxygen scavengers to control oxygen in PWR secondary feedwater. Keeping the system in a low concentration of oxygen means to maintain reducing conditions, which also to keep a low ECP in the system. Thus, SCC can be minimised in the SG. A poly acrylic acid (PAA) dispersant has also been used to decrease SG fouling. As a matter of fact, some impurity species accelerate corrosion inside SG tubing, such as sulfides, chlorides, they can increase the risk of IGA/SCC and pitting respectively. Afterwards, corrosion products deposited on the SGs tubes and hence sludge fouling of SG becomes more and more serious. It influences the materials performance, inhibits heat transfer, leads to thermal-hydraulic instabilities, etc. Thus, frequent chemical cleaning and SG maintenance are necessary to keep SG in a highly functional state. However, by using dispersant application may reduce the huge fee brought by these processes. Last but not least, very little soluble lead contribute dramatically to SCC of nickel alloy, thus lead assisted stress corrosion cracking (PbSCC) is another concern of corrosion issue of SG materials. Therefore, lead is completely prohibited in the PWR water.

1.5 Summary

The first chapter gives a short introduction to the LWRs, including BWRs and PWRs. However, the information about primary circuit of PWRs is referred as the most important concerning the thesis study, the followings are some important points about the primary circuit of PWRs should be mentioned again:

- **PWR solution:** Water used in a PWR, contains boric acid as a neutron poison to control the reactivity of nuclear fuel. The water also contains lithium hydroxide in order to adjust the pH to maintain around 7.2 at 300°C. Thus, this water will cause fewer corrosion problems.
- **Pressure:** Water in primary coolant circuit, a closed circuit, at a pressure of 155 **bar** in order

to avoid boiling;

- **Temperature:** Water of a PWR is around $300 - 320°C$.
- **Hydrogen:** Water is deaerated and contains hydrogen, $25 - 50$ cm^3. kg^{-1} (STP), for inhibiting decomposition caused by radiolysis.
- **Radiation:** Water is under radiation of γ, fast neutron, and $^{10}B(n,\alpha)^7Li$ produced in water by the thermal neutron capture reactions.

References

[1] World Nuclear News. Another drop in nuclear generation, May 2010.

[2] Key World energy Statistics 2007, 2008.

[3] Wikipedia. Nuclear power in france, http://en.wikipedia.org/wiki/nuclear power in france.

[4] Zoran V. STOSIC. Gen -III/III+ Reactors: Solving the Future Energy Supply Shortfall - The SWR - 1000 Option. In *Proceeding of the International Conference Nuclear energy for New Europe*, 2006.

[5] Reactor concepts manual - pressurized water reactor (pwr) systems,. Technical report, USNRC Technical Training Center.

[6] IAEA Nuclear energy Series. Integrity of Reactor pressure Vessels in Nuclear Power Plants: Assessment of Irradation Embrittlement Effects in Reactor Pressure Vessel Steels. Technical report, International Atomic Energy Agency, 2009.

[7] Design of the Reactor Core for Nuclear Power Plants.

[8] The History of Nuclear Energy. Technical report, U.S. Department of Energy, Office of Nuclera energy, Science and Technology.

[9] Nuclear Reactor Types - An Environment & Energy FactFile provided by IEE. Technical report, The Institution of Electricial Engineers, 2005.

[10] Wikipedia. Thermal-neutron reactor, http://en.wikipedia.org/wiki/Thermal-neutro reactor.

[11] Stephen M. Goldberg and Robert Rosner. Nuclear reactors: Generation to generation. Technical report, American Academy of Arts & Sciences, 2011.

[12] Wikipedia. Wylfa Nuclear Power Station, http://en.wikipedia.org/wiki/Wylfa Nuclear Power Station.

[13] Wikipedia. Generation II reactor, http://en.wikipedia.org/wiki/generation II reactor.

[14] Wikipedia. Generation III reactor, http://en.wikipedia.org/wiki/generation III reactor.

[15] Wikipedia. Generation IV reactor, http://en.wikipedia.org/wiki/generation IV reactor.

[16] Wikipedia. Boiling Water Reactor, http://en.wikipedia.org/wiki/Boiling water reactor.

[17] USNRC Technical Training Center. *Reactor Concepts Manual: Boiling Water Reactor (BWR) Systems.*

[18] R. Konings, editor. *Comprehensive Nuclear Materials.* Elsevier Science, 1*st* Edition edition, 2012.

[19] C.J. Wood. BWR Water Chemistry Guidelines - 2000 Revision. Technical report, EPRI, 2000.

[20] Garcia, S.; Wood, C. Recent advances in BWR water chemistry. In *In VGB NPC 08 Water Chemistry Conference, Berlin*, 2008.

[21] BWRVIP-190: BWR Vessel and Internals Project, BWR Water Chemistry Guidelines - 2008 Revision. Technical report, EPRI, 2008.

[22] Naoshi Usui, Nobuyuki Ota and Motomasa Fuse. BWR Water Chemistry Evaluation and Diagnosis System for Supporting Plant Operation. In *14th International Conference on the Properties of Water and Steam in Kyoto*, 2004.

[23] Wikipedia. Pressurized water reactor, http://en.wikipedia.org/wiki/Pressurized water reactor.

[24] Andresen, P.; Ahluwalia, A.; Hickling, J.; Wilson, J. Effects of PWR primary water chemistry on PWSCC of Ni alloys. In 13th International Conference onEnvironmental Degradation of Materials in Nuclear Power Systems, Whistler, Canada. 2007.

[25] Andresen, P.; Ahluwalia, A.; Wilson, J.; Hickling, J. Effects of dissolved H2 and Zn on PWSCC of Ni alloys. In *In VGB NPC 08 Water Chemistry Conference, Berlin*, 2008.

[26] Andresen P. L., Emigh P. W., Morra M. M. and Hickling J. Effects of PWR Primary Water Chemistry and Deaerated Water on SCC. In Allen T. R., King P. J. and Nelson L., editor, *Proceedings of the 12th International Conference on Envirommental Degradation of Materials in Nuclear Power System - Water Reactors*, pages 989–1008, 2005.

[27] Roman Celin, Franc Tehovnik. Degradation of a Ni-Cr-Fe alloy in a Pressurised-Water Nuclear Power Plant. *Materials and technology*, 45 (2):151–157, 2011.

[28] Fruzzetti, K.; Rochester, D.; Wilson, L.; Kreider, M.; Miller, A. Dispersant application for mitigation of steam generator fouling: Final results from the McGuire 2 long-term trial and an industry update and EPRI perspective for long-term use. In *In VGB NPC 08 Water Chemistry Conference, Berlin.*, 2008.

[29] Peter J. Millett, Christopher J. Wood. Recent Advances in Water Chemistry Control at US PWRs. In *Proceedings of 58th International Water Conference, Pittsburgh*, 2007.

[30] Stevens, J.; Bosma, J. Elevated RCS pH program at Comanche peak. In *In VGB NPC 08 Water Chemistry Conference, Berlin.*, 2008.

[31] Chemistry Update August 2012.

[32] K. Fruzzetti. Pressurized Water Reactor Primary Water Chemistry Guidlines, Volume 2, Revision 6. Technical report, EPRI, 2007.

[33] Iva Betova, Martin Bojinov, Petri Kinnunen, Timo Saario. Zn injectin in Pressurized Water Reactors - laboratory tests, field experience and modelling. Technical report, Technical Research Center of Finland (VTT), 2011.

Chapter 2

Water Radiolysis

Radiation chemistry deals with the chemical effects produced when materials are exposed to high-energy, ionising radiation. The most common types of radiation are those produced by the decay of radioactive nuclei (α, β and γ radiation), beams of accelerated charged particles (electrons, protons, helium nuclei, and heavier nuclei), and short-wavelength electromagnetic radiation ($x - ray$ or bremsstrahlung radiation).

Radiation-chemical change, or **Radiolysis** is typically produced by a mixture of reactive intermediates that includes ions, excited molecules and free radicals at a critical stage in the process. The high energies (in the keV or MeV range) available in radiation-chemical initiation are sufficient to raise any one of the molecules present to one of its possible ionised or excited states which may cause the complex radiation-chemical reactions mechanisms.

In this chapter, we will focus on the radiolysis of pure water which is followed by the radiolysis of PWR solution. Before these two paragraphs, a brief introduction of radiation sources will be presented.

2.1 The Interaction of Radiation with Matter

All radiation is detected through its interaction with matter. When a particle travels through a piece of material, it may interact with the nuclei or with the electrons present in the material. This probability depends on the thickness, the number of potential target particles (scattering centres) per volume unit and the interactions. The **cross section** is a convenient concept to describe the interaction of particles with matter. Higher cross section brings more interactions, that's why most nuclear reactors use materials have high neutron absorption cross section as neutron poisons. These particles: electrons, photons, protons, neutrons and so on, charged or non charged, first interact with the matter and then transfer energy to this medium and eventually stop by dissipating all of their energy.

There are two types of radiation, direct ionising and indirect ionising radiation for charged and uncharged particles, respectively. When charged particles, like α particles, β particles, electrons and protons, penetrate matter, they interact with the electrons and nuclei present in the material through the Coulombic force. They cause ionizations[1] and excitations[2] of atoms through Coulombic interactions. Ionisation and excitation are the most important processes for the majority of radiation types and interaction situation. On the other hand, indirect ionising of uncharged particles, like photons and neutrons, they can transfer energy to charged particles, nuclei and electrons through electromagnetic or nuclear interactions.

2.1.A Energy Loss via Interactions

When a particle is moving through a material, it interacts with the matter in different ways and loses energy during the interactions. Different particles have different processes of energy loss. For photons, energy may be totally lost via a single interaction. For neutrons, it is mainly due to nuclear interactions. These will be detailed in the following sections 2.1.C.1 and 2.1.C.4. For charged particles, the process involves multiple reactions which can be roughly divide into two different ways:

[1]**Ionisation:** An outer shell electron is removed from an atom in the medium and an ion pair, the free electron and the charged positively atom, is formed.

[2]**Excitation:** An electron within one of the orbits of an atom absorbs energy and is moved into a higher energy.

- Energy loss by *ionisation*;
- Energy loss due to *radiation*;

Before discussing these two processes, I will briefly recall the **scattering** process, which is a basis for energy transferring in particle physics.

2.1.A.1 Scattering

In general, scattering theory is a natural phenomenon. It happens in a lot of domains: physics, optics, acoustics, etc. Scattering also occurs in particle physics, for both quantum mechanics and quantum chemistry, it involves a lot of partial differential equations and Schrödinger's equation and so on [1]. However, these equations and calculations are not our initial interests, only a general introduction about scattering will be included in the following discussion.

Scattering occurs when a projectile is fired at a target, the projectile can be scattered or remain unscattered. The scattering problem is actually about the characteristics of both the scatterer, which is the incident particles and the medium, meaning the target. There are many kinds of scattering, among which the most discussed are elastic, inelastic and multiple scatterings.

Elastic Scattering Elastic scattering is a specific form of scattering because there is no energy loss during the process. It is often referred to *billiard ball* collisions under the condition that the electrons and nuclei of medium are considered to be initially free and at rest. The kinetic energy of the incident particle is shared between itself and the medium after the collision, thus momentum is always conserved. The maximum energy that can be transferred in a single collision occurs if the collision is head-on. Actually, not only the energy can be transferred during the collision, but also the direction can be changed. For example, most energy loss of a proton interaction is due to the collision with the electrons in the matter and most of the change of direction is due to the collisions with the nuclei. Normally for charged particles, after penetrating matter, a trail of excited atoms and free electrons from acquired energy in the collision, will be left behind.

Inelastic Scattering Inelastic scattering, on the contrary, is the kinetic energy of the incident particle which is not conserved. It is lost inside the medium, given to some other internal process and only part of the energy is continuously moving in the medium. Generally, scattering due to inelastic collision is inelastic scattering. Different from elastic scattering, it may break up the medium into new forms [2].

Multiple Scattering Other than elastic and inelastic scatterings, there is also multiple scattering which is actually defined as the change in direction of charged particles after the collision with the nuclei. It is also named as *direction straggling*. Normally, charged particles will lose their original direction after scattering over a very large angle in one radiation length. Among all, the most affected by multiple scattering is the electron interactions. For heavy charged particle like protons or α particles, they will stop before they have scattered over a large angle. Therefore, their path in the material will be a line in most cases. Oppositely, electrons can penetrate deeply in the material and their angles can be changed significatntly, thus their trajectories are normally curve.

2.1.A.2 Energy loss by ionization

The most classic way of describing energy loss by ionization is the **Bethe Formula**[3]. It describes the mean rate of energy loss $-dE$ in a distance dx by moderately relativistic charged particles. There are different versions of this formula found in different textbooks [3–6], the most complete form is given in Eq.2.1.

$$-\langle\frac{dE}{dx}\rangle = 4\pi N_A r_e^2 m_e c^2 z^2 \frac{Z}{A}\frac{1}{\beta^2}[\frac{1}{2}ln\frac{2m_e c^2\gamma^2\beta^2}{I^2}T^{max} - \beta^2 - -\frac{\delta(\beta\gamma)}{2}] \tag{2.1}$$

where:

N_A is Avogadro's number;

r_e is the classical electron radius;

m_e is the electron mass;

c is the velocity of light in vacuum;

z it the particle charge;

Z is the atomic number of absorber;

A is the atomic mass of absorber;

$\beta = \frac{v}{c}$, which is speed of the particle relative to c;

$\gamma = \frac{1}{\sqrt{1-(\frac{v}{c})^2}}$, Lorentz factor;

I is the mean excitation energy (potential);

T^{max} is the maximum of kinetic energy; and

$\delta(\beta\gamma)$ is the density effect correction to ionisation energy loss.

It gives a precision on the mean rate of energy loss for a $\beta\gamma$ between 0.1 and 1000, and for an intermediate-Z ($7 \leqslant Z \leqslant 100$) material with an accuracy of a few %. Furthermore, it indicates that the energy loss is independent of the mass of the incident particle but depends on the square of its charge. It depends both on the mass and the charge of the medium. It can also be considered as proportional to $1/\beta^2$ while the slowly varying logarithmic term is treated as a constant. Last but not least, for the particle with very low energy, the **Bethe formula** is no longer applicable, because the state of the charge varies continuously along its course by losing or recapturing electrons.

Despite the complication of the **Bethe formula**, many approximations have been made to simplify the original equation by considering the different valuer of $\beta\gamma$ [3, 5]. To simplify the explanation, when the valuer of $\beta\gamma$ is between $3 \Rightarrow 4$, it can obtain the the **minimum ionisation loss**. When the value is less than 3, thus energy loss falls as as $\beta^{-\frac{5}{3}}$, thus it is the **low velocity regime**. Oppositely, if the value is more than 4, there is the **relativistic rise**, energy loss rises indefinitely due to the **density effect** which might cause a saturation at a large value of $\beta\gamma$. High energy particles lose energy slowly due to ionisation, and thus they will leave **tracks** in the medium.

By using the **Bethe formula**, energy loss in air versus the kinetic energy for several different types of charged particles is illustrated in Fig.2.1. Energy loss decreases with increasing kinetic energy and

[3]In previous literature, it is often named the **Bethe-Bloch formula**.

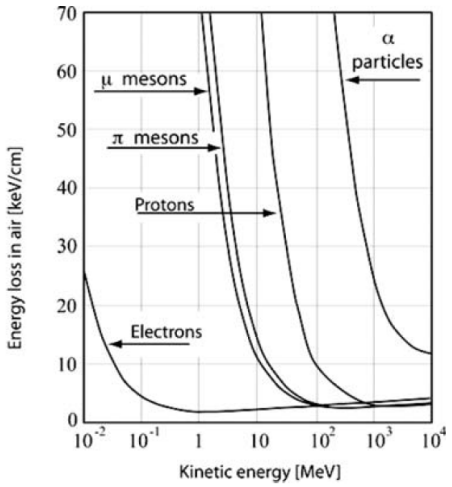

Figure 2.1: Energy loss in air versus kinetic energy for different charged particles. [3, 4].

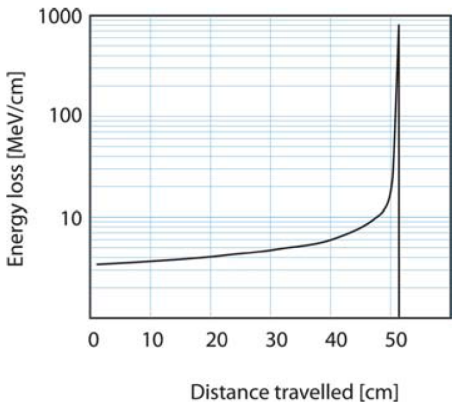

Figure 2.2: Energy loss of a 300MeV proton beam along its trajectory in water. [7].

gradually it arrives at a constant value which depends no more on energy. Except for α particles, the other particles share nearly the same value. For α particles, the energy loss is the greatest because of its low velocity compared with light.

Incident particles lose energy gradually on their way while traveling in the medium and eventually come to rest after losing their energy. The traveling distance is normally called the **range**. The range is defined as Eq.2.2, and it is not simply equal to the energy divided by the energy loss. Actually, if two different particles share the same velocity, the heavier one will travel further; and if they share the some initial kinetic energy, the lighter one travel further.

$$R = \int_{E_0}^{0} \frac{dE}{dE/dx} \tag{2.2}$$

The energy loss has a sudden increase towards the end of the range before it drops to zero, which is shown in the Fig.2.2 [7]. In literature, it is called as the **Bragg peak**. It clearly shows that most energy is deposited close to the end of its traveling path.

In addition, the energy loss can be considered as a statistical process: the particle starts with fixed energy E, and ends up with a spread of energies. This variability in energy values is referred as **energy loss straggling**[4]. Corollary to energy loss straggling, a spread of ranges can be observed in the end, so-called **range straggling**.

Finally, the concept of energy loss due to ionisation is not always true because many atoms may only be brought to an excited state and not ionised during the interaction. Fig.2.3 shows the process of energy loss step by step in a simplified distribution diagram. When the initial energy of the charged particle is strong enough, it can finally ionise the atoms and leave some of the electrons with sufficient energy themselves to excite or ionise atoms in the medium. These high-energy electrons are so-called δ electrons.

[4]In some literature, energy loss straggling is referred to energy straggling.

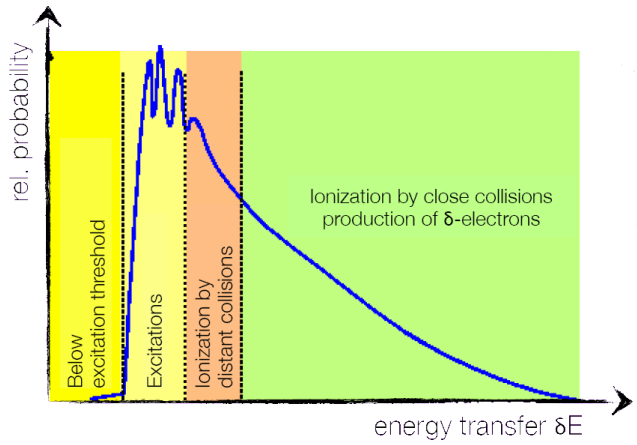

Figure 2.3: Simplified distribution diagram of energy loss in process during interactions.

2.1.A.3 Energy loss due to radiation

Energy loss of charged particles is also due to radiation, for example, the dominant mechanism of energy loss for high-energy electrons is electromagnetic radiation. There exists different interactions for energy loss due to radiation: **Bremsstrahlung**, **Cherenkov effect** and **transition radiation**. However, we will only focus on *Bremsstrahlung*, which is actually the most discussed.

Any charged particles undergoing acceleration will emit electromagnetic radiation. **Bremsstrahlung** is a unique form of it. For a charged particle penetrating a material, it emits radiation when it is accelerated or decelerated by the electric field of the material's atomic nuclei electrons, and therefore it will slow down and lose energy on its trajectory. This is so-called **Bremsstrahlung**. When a charged particle is lighter, the accelerations is greater.

In order to have a general idea on radiative energy loss, it is necessary to define the **radiation length**, X_0, it is parametrized by Y.S. Tsai [5, 6, 8, 9], Eq.2.3. In this equation, α is the fine structure constant; r_e, N_A, A and Z are the definition represented for the **Bethe formula** (Eq.2.1); the function f(Z) is an infinite sum, it could be represented as Eq.2.4 in general; and the values of L_{rad} and L'_{rad} are given in Tab.2.1.

$$\frac{1}{X_0} = 4\alpha r_e^2 \frac{N_A}{A}\{Z^2[L_{rad} - f(Z)] + ZL'_{rad}\} \tag{2.3}$$

$$F(Z) = \alpha^2 Z^2 [\frac{1}{1+\alpha^2 Z^2} + 0.20206 - 0.0369\alpha^2 Z^2 + 0.0083\alpha^4 Z^4 - 0.002\alpha^6 Z^6] \tag{2.4}$$

As the **Bethe formula** for energy loss by ionisation, the equation for energy loss due (dE) to bremsstrahlung per unit length (dx) can be written in Eq.2.5, in which the E means the reduced energy of the charged particle. It can be expressed by the initial energy E_0 and the thickness of the material x in Eq.2.6.

$$\left(\frac{dE}{dx}\right)_{bremsstrahlung} = \frac{E}{X_0} \tag{2.5}$$

$$E = E_0 e^{-x/X_0} \tag{2.6}$$

Because of the **Bremsstrahlung** effect, track length of charged particle becomes quite variable. If the particle radiates a photon, it can lose a significant fraction of its energy suddenly, and thus shorten its track length. Furthermore, the **Bremsstrahlung** effect takes place over a wide distance along the track of charged particles, and leads a large variability of its range.

2.1.A.4 Total Energy loss

The total energy loss of a charged particle can be simply defined as the sum of the loss via ionisation and radiation, 2.7.

$$\left(\frac{dE}{dx}\right)_{tot} = \left(\frac{dE}{dx}\right)_{Ion} + \left(\frac{dE}{dx}\right)_{Brems} \tag{2.7}$$

Nevertheless, for different types of particles, the dominate energy loss is different, shown is Eqs.2.8 and 2.9. It indicates that for a charged particle heavier than electrons, the energy loss is dominated by ionisation.

$$\left(\frac{dE}{dx}\right)^{electrons}_{bremsstrahlung} \gg \left(\frac{dE}{dx}\right)^{electrons}_{ionization} \tag{2.8}$$

$$\left(\frac{dE}{dx}\right)^{heavy\ particles}_{bremsstrahlung} \ll \left(\frac{dE}{dx}\right)^{heavy\ particles}_{ionization} \tag{2.9}$$

2.1.B Stopping Power and Linear Energy Transfer (LET)

2.1.B.1 Definition

When a charged particle penetrates a medium, it transfers its energy to the medium and thus slows down, eventually it dissipates all its energy and stops. From the angle of the charged particle, we emphasis the average linear rate of energy loss in a medium during the interactions. This has been discussed in the previous section. Oppositely, if we focus on the medium, thus a concept of **Stopping Power** of the material should been introduced. It is often referred as the **Linear Energy Transfer (LET)**, which is a measure of the rate of energy deposition or transferring in the medium. It is defined as the linear-rate of energy loss by an ionising particle crossing a material medium, and a

Z	Element	L_{rad}	L'_{rad}
1	H	5.31	6.144
2	He	4.79	5.621
3	Li	4.74	5.805
4	Be	4.71	5.924
$\geqslant 5$	others	$\ln(184Z^{-1/3})$	$\ln(1194Z^{-2/3})$

Table 2.1: L_{rad} and L'_{rad} values for calculating the radiation length in any element by using Eq.2.3. [5, 6]

rough average value calculated by dividing the total energy(E) of a particle by its path length(x), shown in the Eq. 2.10.

$$LET = -\frac{dE}{dx} \tag{2.10}$$

The official unit is J.m^{-1}, but more often keV.μm^{-1} is used. In general, at the same velocity, the particle with larger charge loses more energy per length unit, therefore, it will have a higher LET.

While this formula serves to indicate the order of magnitude of the **LET**, it ignores several important factors that must be reconsidered to obtain a more precise value. Like the fact that the rate of energy loss of an electron changes as it slows down so that the LET will vary at different positions along the track and so on. Thus, for high-energy charged particles, the **LET** is often calculated by the **Bethe** formula, Eq.2.1, discussed previously. Some average **LET** values in water for various radiation are given in Table 2.2, they are calculated by the program TRIM [10, 11]. The *primary* interaction of radiation with matter depends on the nature of the radiation. **LET** is a parameter to describe the radiation, but not sufficient to compare the effects of different radiations in water radiolysis.

Particles (energy)	LET (keV.μm^{-1})
^{60}Co γ rays (Compton electron, 1.17 MeV)	0.23
Electrons (2 MeV)	0.2
Protons (100 MeV)	0.65
α particles (5.3 MeV)	92
He^{2+} (1.5 MeV)	192
Li^{+} (0.85 MeV)	223.5
Carbon ions (25 MeV)	520

Table 2.2: Average values of LET for several different types of radiation in water [12–15]

2.1.B.2 Track Structure

The energy lost when a moving charged particle is slowed down in matter gives rise to a trail of excited and ionized atoms and molecules in the path of the particle. The result of the absorption of any type of ionizing radiation by matter is thus the formation of tracks of excited and ionised species. Therefore, tracks are formed by a set of heterogeneous zones containing highly reactive species localised around the path of energy deposition. These species normally will be the same in a particular material regardless of the type or energy of the radiation responsible. However, radiation of different types and energy will lose energy in matter at different rates, and consequently will form tracks that may be densely or sparsely populated with the active species. Track structure varies greatly depending on the characteristics of radiation, it can mainly be distinguished by two types: the photons and the electrons, **low LET**, and heavy charged particle **high LET**.

- **Track structure produced by low LET**

When the LET value is low, the energy deposition is distant from each other in general. Depending on the amount of energy deposited by radiation, those heterogeneous zones can be divided into three groups:

Spur: low energy deposition: E < 100 eV;

Blob: middle energy deposition: 100 eV < E < 500 eV;

Short tracks or branch tracks: high energy deposition: E > 5 keV;

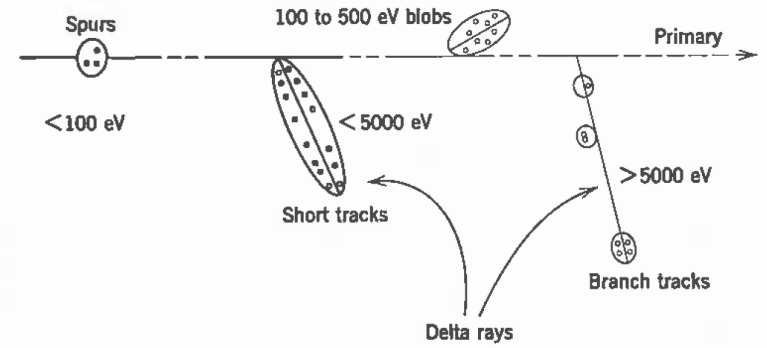

(a)

Figure 2.4: Distribution of ions and excited molecules in the track of a fast electron. [12]

Electrons ejected as a consequence of the ionisation produced by radiation may themselves be sufficiently energetic to produce further ionisation and excitation. If the energy of these secondary electrons is relatively low, less than 100eV, their range in liquid or solid materials will be short and any secondary ionizations that they produce will be situated close to the origin of the ionisation, giving a small cluster or **spur** of excited and ionised species. The average spur contains 2 to 3 ions pairs and excited species. Some of the secondary electrons will have sufficient energy to travel further from the site of the original ionisation and will form tracks of their own, branching from the primary track, such electrons are known as δ ray. For δ electrons in a middle energy range which is between 100 - 500 eV, they will generate a large spur described as a *blob*. For higher energy δ electrons from 500 eV to 5 keV, they are defined as **short tracks** or **branch tracks**. Fig.2.4 shows the distribution of ions and excited molecules in the track of a fast electron. The quantity of energy deposited determines whether an individual event will give rise to a *spur* or a larger group of ions and excited molecules: *blobs*, *short tracks* or *branch tracks*. Open circles represent positive ions, each of which will be associated with an electron and one or more excited molecules. The fraction of the energy deposited by electrons with energies in the MeV range that appears in short tracks and in spurs of different sizes.

- **Track structure produced by high LET**

Densely ionising radiation, like α particles, have a high LET. The number of interactions per unit length traveled is large because the velocity of the incident particle is small. Moreover, the energy depositions occur in a track more or less straight due to the angular deviations in an interaction which are inversely proportional to the mass of the particle. The spurs overlap and form a single cylindrical track. The track can be divided into two: the **core** and the **penumbra**. More than 50% of the initial energy is deposited in the *core* which is a small area so that the density of the species created is high. The rest of the energy is deposited in the *penumbra* by the secondary electrons also called δ rays. The

dimensions of the core and the penumbra vary depending on the velocity of the particle.

The concept of the **LET** is fundamental for understanding the interaction of radiation with matter. However, two particles with the same LET but different velocities do not produce tracks with the same dimensions, that influence the manner of species interacting with each other. Therefore, the effects of two radiation with the same LET may be different.

2.1.C Different types of radiation

There are mainly two types of radiation sources used in the study of radiation-chemical radiation. One is the classical radiation sources and the second is generators and accelerators. There exist various types of accelerators, like for electrons, and also accelerators such as Van de Graaff accelerator or cyclotron used to generate beams of positive ions. Nuclear reactors have also been used as radiation sources of neutron beams.

Most particles interact primarily with electrons. The coulomb interaction is long-ranged so the slowing down of the charged particles is most effective and is a continuous process. The electromagnetic interactions requires a collision of a photon and electron and leads to a discrete stopping process. Neutrons are different, they interact only with nuclei.

2.1.C.1 The Interaction of Photon Radiation

X-ray and γ rays are both high energy photons, with energy range from 1 to 100keV referred as X-ray and energy above as γ ray [3]. However, in most literature, any photon energy above 1keV is regarded as γ ray, which is focused on the discussion below. γ rays are electromagnetic radiation of nuclear origin with wavelength in the region of 3.10^{-11} m to 3.10^{-13} m which indicates approximately 40 keV to 4 MeV in energy. Normally, the interactions between photons and matters have small perturbations, a slight change in trajectory and number of incident particles remains basically unchanged. The intensity of the photon beam decreases exponentially with the placement of additional layers of shielding material, it can be defined with Eq.2.11, where I and I_0 are the intensities of photon beam with and without shielding material present, t is the thickness of shielding material present and μ is the **linear attenuation coefficient** which is dependent on the material itself.

$$I(t) = I_0 e^{-\mu t} \tag{2.11}$$

The interaction of photons with matter involves some distinct processes. For instance, coherent elastic scattering, photo-excitation, the photoelectric effect, the Compton effect, pair production and so on. The relative importance of each process depends on the photon energy and the atomic number of the stopping material. Nevertheless, among these different processes, the three most important mechanisms are shown in the Fig.2.5.

Photoelectric effect: Photoelectric effects dominate at low energies, <100keV. When the energy of the incident photon is above the work function or binding energy of an electron in the host atom, it can eject an atomic electron and meanwhile the photon has been completely absorbed by the atom

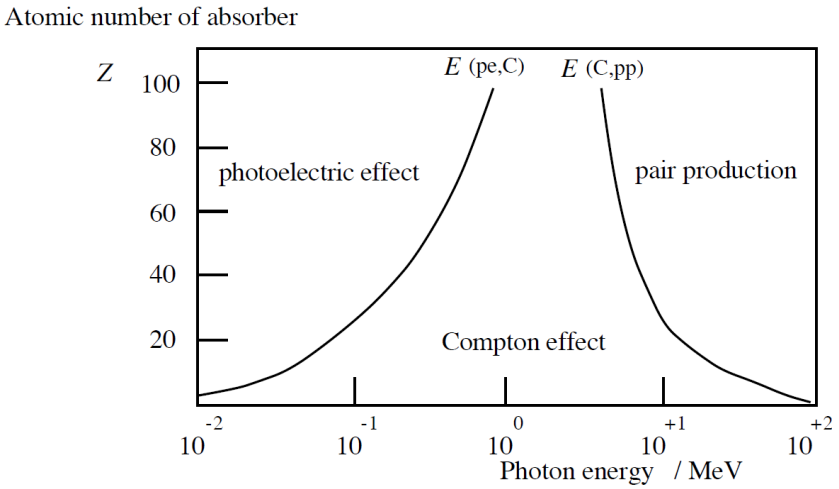

Figure 2.5: Effect of photon energy and atomic mass number of absorbing medium on dominant type of photon attenuation processes. [16].

and disappears. The energy form the injected photon is carried off by the ejected electron, it can be raised to a higher lever within the atom or can become a free photoelectron, described in Eq.2.12. Afterwards, this photoelectron will ionise and excite other atoms until it loses all its energy. The upside of this may explain the reason why photon radiation is classified as an indirect ionising radiation. The majority of the ionisation and excitation occurs during photon radiation and is not via the photon itself, but due to the photoelectron which are produced at the first ionisation caused by photon.

$$E_\gamma \rightsquigarrow e^- \tag{2.12}$$

Compton Scattering: Compton scattering dominates at medium energies, $\sim$ 1 MeV. It is an elastic collision between a photon and an electron. When the energy of a photon is well above electron binding energies, more likely, the photon will scatter off an electron and produce a photon degraded in energy and a recoil electron. The photon retains a portion of its original energy and continues moving in a new direction. Meanwhile, the electron ejected by the atom travels with the energy transferred to it from the photon minus the binding energy of its orbital shell. This process is illustrated in Eq.2.13, it contains both absorption and scattering components. However, if the atom takes up all the energy and the momentum transferred to the electron, this interaction will be called coherent Compton scattering or *Rayleigh scattering*. If the electron is ejected by the atom, the interaction is incoherent Compton scattering [3]. Generally, the probability of Compton scattering decreases with increasing photon energy and increasing atomic number (Z) of the medium. Moreover, concerning water radiolysis, which is a low atomic-number medium, Compton scattering is the predominant mode of photon interaction.

$$E_\gamma \rightsquigarrow E_\gamma^{'} + e^- \tag{2.13}$$

Pair production: Pair production dominates at high energies, > 1.024 MeV. When a photon has a mass at least 2 times larger than the mass of an electron[5] which means 1.024 MeV, it may create an electron and positron pair under the influence of the electromagnetic field of a nucleus. Eq.2.14 shows this process. Nevertheless, pair production only occurs under a strong electric field of nucleus, which means a much higher energy, like 5 or 10 MeV. Therefore, all the energy and momentum is taken up and conserved by the nucleus. In addition, the probability of pair production increases with atomic number (Z) of the medium and the photon energy. With *Bremsstrahlung* radiation, the electron and the positron produced will be projected in a forward direction relative to the incident photon. Afterwards, this electron-positron pair creates a large number of secondary γ-rays which will create continuously electron-positron pairs. This is called **electromagnetic showers**. The average energy of the photon has been decreased during each step of this process until it is totally absorbed or stopped.

$$E_\gamma \rightsquigarrow e^+ + e^- \tag{2.14}$$

For most cases of photon radiation, reactions can be shifted from high energies to low energies, thus it might involve some, maybe all of these processes. And unlike the other radiation types, the ranges of photon irradiations are normally indeterminate.

2.1.C.2 The Interaction of Electron Radiation

Electrons lose energy by exciting and ionising atoms along their trajectories. The interactions of electron radiation normally can be identified by two classes, elastic and inelastic scattering. The relative importance of these processes varies strongly with the energy of the incident electrons and sometimes also with the nature of the absorbing material.

If the electron passes through the medium without any scattering, they are a direct beam with no energy loss. During the elastic scattering, the electron is deflected form its path towards the core by Coulomb interaction with the positive potential inside the electron cloud which loses very little energy. Furthermore, if the electron is too close to the nucleus, it might be scattered back, which is called *backscattering*. Nevertheless, this is a rare case. There is also inelastic scattering where energy is transferred during the collision. It might generate several processes: inner-shell ionisation, *Bremsstrahlung* radiation, secondary electrons, etc [17]. At low energies, energy loss is mainly through elastic collision; at high energies, energy is lost predominantly by radiation emission. For electrons, it is negligible below 100 keV but increases rapidly with increasing energy, becoming the predominant mode of energy loss at an electron energy between 10 and 100 MeV. For example, *Bremsstrahlung* becomes a significant fraction of energy loss at high energy.

Electrons are more penetrable than proton and heavy charged particle radiation. However, due to the fact that the masses for both projectile and target are identical, they can scatter in any direction and lose large fractions of energy. Moreover, multiple scattering occurs subsequently thus the path of an electron is normally very erratic.

It is worth mentioning that when the energy is above a threshold, **Cherenkov** radiation is also possible for electron interactions. The *Cherenkov* effect is a light emission effect that occurs whenever

[5]The mass of an electron: 9.108^{-31}kg, also equals to 0.511 MeV in energy units.

a charged particle travels in a medium faster than the speed of light in that medium. For one thing, this effect will not cost a lot of energy loss compare with ionisation. However it only depends on the velocity of the particle. If the energy exceeds 264keV, electrons can show *Cherenkov* radiation in water.

2.1.C.3 The Interaction of Heavy Charged-Particle Radiation

Heavy charged particles, normally refer the particles like protons, α particle ($^4He^{2+}$), β particles. They interact with matter in the same way as electrons, but much strongly. It means a higher probability of interaction with the medium, producing large numbers of ions per unit length of their paths. Thus, they have a larger linear rate of energy loss and are less penetrating. For example, the ion density along the track of an α particle is several hundred times greater than that along the track of an electron of the same energy. On the other hand, the range through matter, which means a characteristic average traveling distance, normally depends on its initial kinetic energy. Furthermore, for both α particles and protons, the trajectories are approximately straight.

Among all the different particles, the way of interaction is more or less the same. However, α particles are often regarded as the most damaging radiation of internal deposition due to the fact that large amounts of energy are deposited within a very small distance of medium. Thus, only α particle will be explained in the following paragraph.

α particles can interact either with nuclei or orbital electrons in any absorbing medium. In fact, the scattering with nuclei may be deflect with no or very small exchange in energy or absorbing by nucleus, so-called **Rutherford scattering**[6]. However, it is negligible for α particles. On the contrary, ionisation, atomic or collective excitation are the process more important during the absorption of α particles. When an α particle comes close enough to an orbital electron of the medium, it can pull it out from orbit. This is the ionisation which costs the kinetic energy of the α particle. Thus, the α particle is slowed down. At the same time, when the α particle is not sufficient to trigger an ionisation with interaction, it can also lose its kinetic energy by exciting orbital electrons. The α particles have tendency to cause ionizations at an increasing rate when it is slowed, thus most energy is deposited at the end of its track, in the **Bragg** peak. In the end, the α particle collects two electrons and becomes a helium atom when it stops.

2.1.C.4 The Interaction of Neutrons Radiation

Neutron radiation is most commonly found in nuclear reactors which create significant neutron fluxes. Materials surrounding will be activated by capturing neutrons, it is normally an undesirable outcome. Concerning their interactions with matter, due to the fact that they have no charge, the ionisation via electromagnetic interaction with atomic electrons is negligible. Hence, it leaves only nuclear collision as an important source of dissipating energy. Neutrons have comparable masses to protons so that *billiard-ball* type collisions are possible during the interaction. This will give a large amount of scattering angles, thus the range is difficult to estimate. Nevertheless, neutrons can penetrate much

[6]**Rutherford scattering:** Rutherford scattering is based on the elastic deflection of charged particles in Coulomb field of an atomic nucleus.

greater thickness of material, and the consequences of neutron irradiation are not confined to the surface region of the absorber.

Like photon radiation, the intensity of the neutron beam decreases exponentially with the thickness of the material, it can be defined as Eq.2.15, where I and I_0 are intensities of neutron beam before and after passing through matter of thickness, t is the thickness and N is the atom density of the material, σ is nuclear cross-section which describes the attenuation of neutrons. It is pointed out that more interactions with neutrons will be possible if the material has a higher cross-section.

$$I(t) = I_0 e^{-N\sigma t} \tag{2.15}$$

Neutrons are generally categorised by their energy: high-energy neutrons, energy $>$ 1 GeV; fast neutrons, energy between 100 keV and 10 MeV; slow neutrons, energy $<$ 0.5 eV. The neutrons produced in a nuclear reactor are generally fast neutrons. The process of elimination of neutrons was introduced briefly in the previous chapter (Chapter Light Water Reactor). Nevertheless, it will be detailed as below.

At first, the neutrons undergo **thermalisation** via elastic and inelastic scattering form the absorber nuclei. The maximum energy loss for the neutrons is when it scatters a proton which share the same mass. Hence the energy loss is mainly due to the elastic scattering and until their energy is equal to the thermal energy of the surrounding environment. On the other hand, during the inelastic scattering the nucleus is left in an excited state which later decays by γ emission or some other type of radiation.

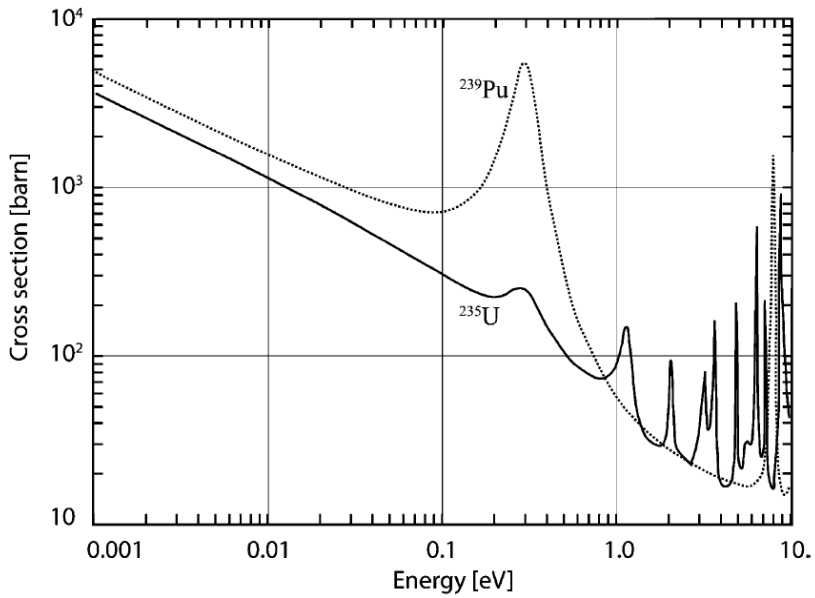

Figure 2.6: Fission cross section of ^{235}U and ^{239}Pu as a function of energy. [18]

Afterwards, the thermalised neutrons will be captured and absorbed by the nuclei and then eventually disappear. The cross section dependence of the neutron capture cross section in uranium and plutonium has been illustrated in Fig.2.6. It shows that at the lowest energies the cross sections increase monotonically with decreasing energy and become very large at thermal energies. Besides, sharp structure is observed at higher energies, which means the cross section shows a peak at a par-

ticular energy because of the capture of neutrons into specific nuclear energy levels populated in the reactions. There are several disintegration reactions types for neutron capturing [3], for example:

- **(n, γ)** with the emission of a photon;
- **(n, α)** with an α particle;
- **(n, p)** with a proton.

As mentioned before, thermalised neutrons are important for a nuclear reactor to stay at operational efficiency, and hence the absorption of thermalised neutrons need to be treated carefully. On one hand, they need to be eliminated for the safety concerns. On the other hand, they have to be preserved for efficient nuclear operation. The best choice for the materials are those who have high neutron capture cross sections, such as boron shown in Eq.1.1. The cross section of boron is quite high, σ=3838 barn. On the contrary, in order to avoid too much neutron loss, the neutron preservation is done by using materials with very small cross sections for neutron capture reactions, such as hydrogen atoms, shown in Eqs.2.16 and 2.17, or oxygen atoms, the σ=1.8×10^{-4} barn. These indicate that water contains hydrogen, light water is an effective materials for thermalising neutrons with minimum loss due to reactions. This might also explain the reason that light water is chosen as a moderator for LWRs.

$$1^n + 1^H \rightarrow 2^H \qquad \sigma = 0.322\ barn \tag{2.16}$$

$$1^n + 2^H \rightarrow 3^H \qquad \sigma = 5.7 \times 10^{-4}\ barn \tag{2.17}$$

2.2 Pure Water Radiolysis

Water radiolysis [12–14, 19–25] is the decomposition of water molecules when they are irradiated by ionising radiation. Water molecules are decomposed to form radiolysis products: ions, excited molecules and free radicals[7] are the first reactive species formed. While both ions and excited molecules can give stable chemical products directly, the free radicals are unstable with high reactivity. Therefore, most of them only exist during the intermediated formation, and eventually disappear in the water.

In general, the reaction of water radiolysis can be written as Eq.2.18. Due to ionizing radiation, the radiolysis of water produces: hydrated electrons, $H^\bullet$ atoms, $HO^\bullet$ and $HO_2^\bullet$ radicals, H_3O^+ and OH^- ions, H_2 (dihydrogen) and H_2O_2 (hydrogen peroxide) molecules. The global equation of water radiolysis is now well understood experimentally as well as theoretically [12–14, 19–22].

$$H_2O \xrightarrow{Ionizing\ \ Radiation} e_{aq}^-, H^\bullet, HO^\bullet, HO_2^\bullet, H_3O^+, OH^-, H_2O_2, H_2 \tag{2.18}$$

2.2.A Mechanism of Water Radiolysis

Ionising radiation produces ionisation and excitation by transferring energy to electrons present in water molecules. The energy is first absorbed, and then deposited into water molecules. During the

[7] In chemistry, a **free radical** also called a *radical*, which is an atom, molecule or ion with at least one unpaired electron.

initial interaction, inner-shell electrons may be excited and the absorbed energy is rapidly redistributed. Thus, chemically important ions and excited states are produced by loss or excitation of less-firmly bound electrons, such as the outer-shell electrons [12].

One of the recent models about the mechanism of water radiolysis was proposed by Sxiatla-Wojcik and Buxton [20], shown in Fig.2.7. It divides the water radiolysis mainly into three steps:

- the **physical stage**;
- the **physico-chemical stage**;
- the **chemical stage**.

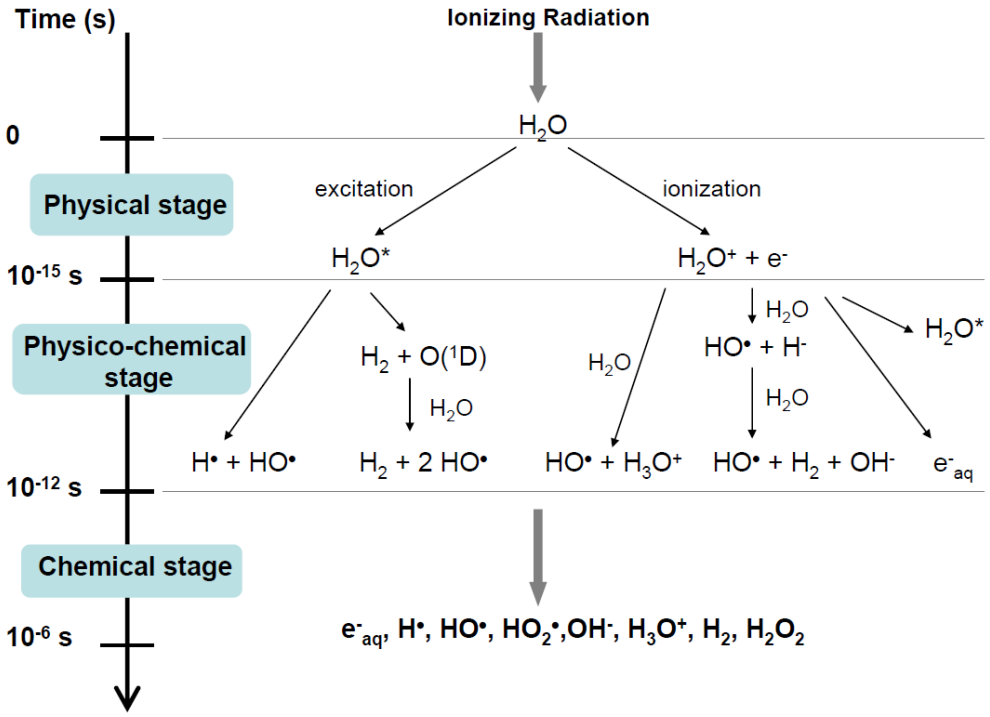

Figure 2.7: Schematic diagrams of water radiolysis [19].

As shown in the Fig.2.7, it illustrates the water decomposition as a function of time after the irradiation. Precisely, it shows the chemical reactions have been taken place during the first 1 μs after the radiation energy deposited into the water molecules.

2.2.A.1 The Physical Stage

The **physical stage** is the absorption of ionising radiation by water, which leads the ionisation and excitation of water molecules. Therefore, the incident particles and the electrons in water molecules are generated and both slowed down. It is the period that consists of energy deposition followed by fast relaxation processes. The physical stage is the first step of water radiolysis, which only lasts about 10^{-15} s[8], 1 fs, after the initial interaction.

[8]In some literature, they define the duration as 10^{-16} s, one tenth of a femtosecond.

The water molecule H_2O can either be ionised, by removing an electron, Eq.2.19:

$$H_2O \xrightarrow{Radiation} e^- + H_2O^+ \tag{2.19}$$

$$H_2O + e^- \rightarrow 2e^- + H_2O^+ \tag{2.20}$$

or be excited, by transferring an electron from a fundamental state to an excited state, Eq.2.21:

$$H_2O \xrightarrow{Radiation} H_2O^* \tag{2.21}$$

$$H_2O + e^- \rightarrow H_2O^* + e^- \tag{2.22}$$

Nevertheless, Eqs.2.20 & 2.22 are considered as the continuous reactions of water molecule and the ejected electron by Eq.2.19. At the end of this stage, the reactions have formed: excited water molecules $\mathbf{H_2O^*}$, ionised water molecules $\mathbf{H_2O^+}$ and sub-excitations electrons $\mathbf{e^-}$.

2.2.A.2 The physico-chemical stage

The **physico-chemical stage** is the second step of water radiolysis, from 10^{-15} to 10^{-12} s, in which a thermal equilibrium is established. During this period, the ionised and excited water molecules undergo transformations and thus they dissipate energy by transferring it to their neighbouring molecules and breaking bonds. In the mean time, the sub-excitations electrons become thermalised and then subsequently hydrated. There are many different processes in this stage and not all of them have been well characterised experimentally. However, some important processes are well detailed which will be represented in the following sections.

- **Excited water molecules $\mathbf{H_2O^*}$:**

Dissociative relaxation The dissociation of the excited water molecule H_2O^* produces the radicals $HO^\bullet$ and $H^\bullet$ by bond breaking, Eq.2.23. Two models have been described in the literature. One leads to dihydrogen molecule H_2 and $O(^1D)$ which can react quickly with water molecule and give the $OH^\bullet$ radical. In the second model, the $H^\bullet$ radical and $O(^3P)$ can be formed by the reaction below, but due to the weak quantity in the liquid water, this reaction is often negligible [26], That is the reason for its absence in the scheme of main reactions (Fig. 2.7). It is worth mentioning that $O(^1D)$ and $O(^3P)$ are the singlet and triplet state of the atomic oxygen respectively. It needs to be pointed out that the excited water molecule can return to its fundamental state without any dissociation, but only by losing heat. In the case of liquid water, the role of excited molecules is normally less important compared to the ionised ones [27].

$$H_2O^* \rightarrow HO^\bullet + H^\bullet \tag{2.23}$$

$$H_2O^* \rightarrow H_2 + O(^1D) \xrightarrow{H_2O} H_2 + 2OH^\bullet \ (or H_2O_2) \tag{2.24}$$

$$H_2O^* \rightarrow 2H^\bullet + O(^3P) \tag{2.25}$$

- **Ionized water molecules H_2O^+:**

Ion-molecule reaction The ion-molecule reaction can also be thought as transferring a proton to a neighbouring molecule. The ion H_2O^+ is not stable and it reacts very quickly with water molecules, Eq.2.26. This reaction is important because it leads to the production of $HO^\bullet$ radical and proton H_3O^+, which may have other role in further reactions [28].

$$H_2O^+ + H_2O \rightarrow HO^\bullet + H_3O^+ \tag{2.26}$$

- **Sub-excitation electrons e^-:**

Thermalisation and solavatation of sub-excitation electrons Most ejected electrons have low energy. However, some of them may have considerable energy during ionisation, in keV or even in MeV range. They can lose their energy through collisions with other molecules before the electron neutralises a positive ion. In other words, the electrons is reduced to thermal or near thermal energy before recombination occurs, Eq.2.27. Then it can interact with the surrounding water molecules and eventually becomes an **hydrated electron**, $\mathbf{e}^-_{aq}$, Eq.2.28. The energy of thermalization is about 0.0025 eV at 25 °C.

$$e^- \rightarrow e^-_{th} \tag{2.27}$$

$$e^-_{th} + n\ H_20 \rightarrow e^-_{aq} \tag{2.28}$$

Germinate recombination The germinate recombination process is an ion recombination. The energy is lost during molecular collisions and the molecule rapidly drops to its lowest excited state, Eq.2.29. During the ionisation of the water molecules, the potential is about 8 eV. The incident particle or the electromagnetic radiation can have a sufficient energy to eject an electron which can recombine with a neighbouring water molecule, a positive water ion, in order to give an excited water molecule.

$$e^- \rightarrow e^-_{th} + H_20^+ \rightarrow H_2O^* \tag{2.29}$$

Dissociative electron attachment (DEA) Before the thermalization, apart from the recombination process, the sub-excitation electrons can also react with a water molecule by giving the H_2, $HO^\bullet$

and OH^-, Eqs.2.30 & 2.31. This process is thus called *dissociative electron attachment*. It involves the resonant capture of e^- to a water molecule followed by the dissociation of the transient anion and by reaction of the hydride anion with another water molecule through a prompt proton transfer process [21]. The electron capture by this process may lead to a disproportionately high rate of decomposition [12].

$$e^- + H_2O \rightarrow HO^\bullet + H^- \tag{2.30}$$

$$H^- + H_2O \rightarrow H_2 + OH^- \tag{2.31}$$

After 1 ps of the energy deposition into water molecules, which is also the end of the physicochemical stage, the spatial distribution around the axis of the ionisation track includes e^-_{aq}, H_3O^+ and $HO^\bullet$ which are the species involving in the reactions for the next stage. The species H_2 and H_2O_2 are also created in this stage. All these species are referred as the **initial yields** of water radiolysis.

2.2.A.3 The chemical stage

The **chemical stage** is often considered as highly non-homogeneous, and hence in some literature, it is named as the non-homogeneous chemical stage. However, one thing can be sure that the chemical stage starts with a non-homogeneous state and ends homogeneously. It takes place between 10^{-12} and 10^{-6} s. The radical species react in the tracks and then diffuse in solution. They can thus react with each other and also with surrounding molecules in the solution, Eqs.2.32, 2.33 & 2.34.

$$HO^\bullet + HO^\bullet \rightarrow H_2O_2 \tag{2.32}$$

$$H^\bullet + H^\bullet \rightarrow H_2 \tag{2.33}$$

$$e^-_{aq} + e^-_{aq} \rightarrow H_2 + 2OH^- \tag{2.34}$$

In general, this stage can be divided into two: the heterogeneous and the homogeneous ones. At the heterogeneous chemical stage, normally extends from 10^{-11} to 10^{-8} s, the recombination reactions are favoured which lead to the formation of molecular products in a relative high concentration in small zones along the radiation track. Afterwards, the track of the particles expands because of the diffusion of radicals and their subsequent chemical reactions. Therefore, it brings the homogeneous state of the radicals and molecules to the solution at the end of the chemical stage.

1 μs after the particles pass through, the distribution of radiolyic species in water is considered homogeneous. The reactions occur after these three stage can generally be well described homogeneously while all the species have diffused evenly into the water. All the species have been produced after these three stages are call **primary products** of water radiolysis, already shown in the global equation, Eq.2.18.

Several remarks need to be pointed out:

- The oxygen is not a primary product of water radiolysis, it is formed in the stage of homogeneous chemistry which means after 10^{-6} s of energy deposition in the water [29].

- The radical superoxide, $OH_2^\bullet$, is presented like a primary product in the global equation, but actually it is formed in the heterogeneous stage and the mechanism of its formation is not clear yet. The most cited hypothesis is that it is formed by the reaction between $HO^\bullet$ radical and an oxygen atom at triplet state.

- The formation of molecular hydrogen H_2 is involved in two stages after the initial energy disposition: it can be produced by the Eqs. 2.33 & 2.34, in the chemical stage. In the earlier physicochemical stage, the formation of H_2 can be presented by the dissociation of excited water molecules, Eq.2.24 and the dissociative electron attachment, Eqs.2.30 & 2.31. Indeed, the dominant way of H_2 formation is the dissociative recombination process of the water cation and the non-hydrated electron during the physicochemical stage [30], not in the last stage.

- The production of H_2 has two different types of tracks along the radiation path, either are spherical spurs formed at more than 100 nm separations with low LET radiation, or are cylindrical track of connecting spurs with high LET radiation [22].

2.2.B Radiolytic Yields

2.2.B.1 Definition

The radiolytic yield, noted as **g(X)**, is defined as the number of species created or destroyed for 100 eV deposited energy. SI unit for the radiolytic yield is mol.J^{-1} which equals to 9.649×10^6 molecules/100 eV. It can measure the radicals and molecular products that escape from the **spurs** and **tracks**. Actually, there is a competition between the diffusion and the reaction of these species as the non-homogeneous concentration gradients relax. However, these yields are usually referred to as homogeneous or steady-state yields, and they are representative of the state of an electron track as found at about 10^{-7} s[9], after the passage of an ionising particle which has deposited energy in the system. It means that any reactions occurring within spurs and tracks have been completed [31].

The primary yields of both radical (e_{aq}^-, $H^\bullet$, $OH^\bullet$, $OH_2^\bullet$) and molecular (H_2, H_2O_2) products can be simply subdivided into two groups: the reducing radicals e^- and $H^\bullet$, and the oxidising products $OH^\bullet$, $HO_2^\bullet$ and H_2O_2. The molecular hydrogen is relatively inert and normally plays little part in the subsequent reactions [12].

To maintain a material balance, the relationship between the radical and molecular yields are written as the equations (Eqs.2.35, 2.36 and 2.37) below, in which g(-H_2O) is defined as the corresponding yield of decomposition of water at this stage.

Oxygen part:

$$g(-H_2O) = g(e_{aq}^-) + g(OH) + 2g(H_2O_2) + 2g(HO_2) + g(OH^-) \tag{2.35}$$

[9] In the literature, the duration is defined as 10^{-6} s [12, 19].

Hydrogen part:

$$g(-H_2O) = g(H_2) + g(e^-_{aq}) + g(H_2O_2) + \frac{1}{2}[g(H) + g(OH) + g(H^+) + g(OH^-) + g(HO_2)] \quad (2.36)$$

Charges conservation:

$$g(H^+) = g(e^-_{aq}) + g(OH^-) \quad (2.37)$$

With the three precise equations, we can establish the relation of all the primary products:

$$g(-H_2O) = g(OH) + 2g(H_2O_2) + 3g(HO_2) = g(H) + g(e^-_{aq}) + 2g(H_2) \quad (2.38)$$

The equation expressed in Eq.2.38 is often used in the determination of radiolytic yields. The first thing to point out is that all the radiolytic yields evolute with time, illustrated in Fig.2.8. It indicates that the radicals yields decrease while the molecular yields increase as a function of time. In other words, it means that the radicals recombine and form molecular products with time. Therefore, the radicals are difficult to detect after a short time of the radiation.

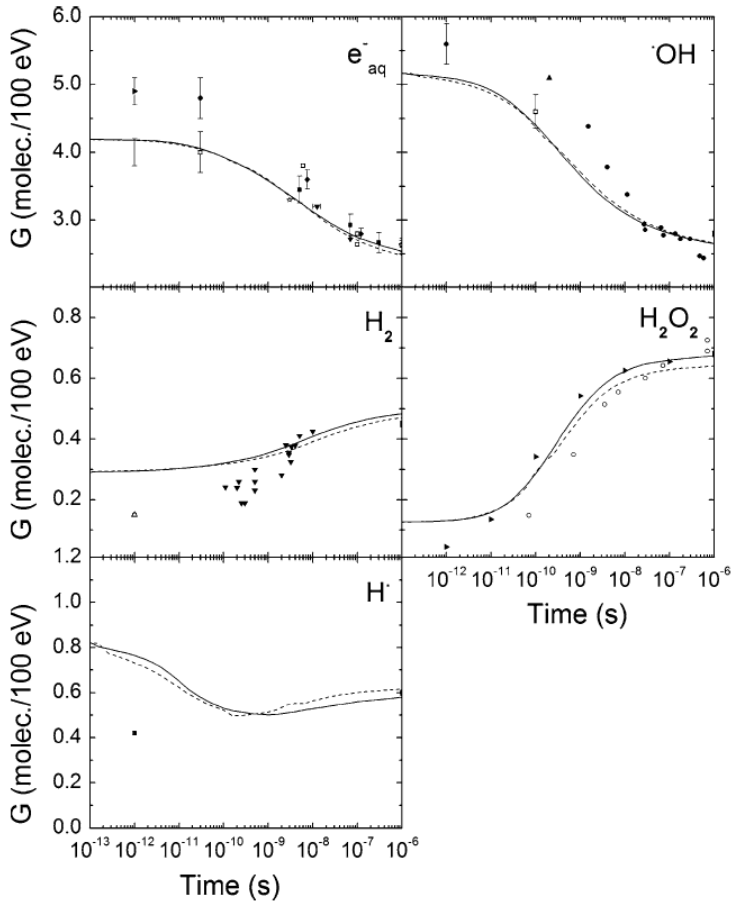

Figure 2.8: Time-dependent of primary yields; $H^\bullet$, $HO^\bullet$, H_2, H_2O_2 and e^-_{aq} produced by low LET radiation tracks of proton (300 MeV, LET $\sim$ 0.3 keV/μm) at neutral pH and 25°C. Broken line: IONLYS-IRT calculation; solid line: SBS calculation; spline: Monte-Carlo simulation results [32].

In general, the radiation types do not have a huge influence on the radiolytic yields, especially

for low LET radiations. Nevertheless, for LET $>$ 10 keV/μm, g($H^\bullet$) increases as the incident ion velocity increases [33]. The radiolytic yields still depend on a lot of parameters: the characteristics of irradiation, such as LET and dose rate; the characteristics of water itself, like temperature, pressure and pH.

2.2.B.2 Influence of LET

The Linear Energy Transfer **LET** of incident radiation can significantly change the values of primary radiolytic yields. The radiation tracks can be very differently due to the LET, low LET gives isolated spurs and high LET gives cylindrical tracks. Therefore, different tracks cause different diffusion models for the primary yields [34–36]. The radicals $H^\bullet$ and $HO^\bullet$ in cylindrical tracks are easier to combine with each other because they are closer in distance and more concentrated than in spurs, then result in form more molecular products. On the contrary, spurs are favoured to form more radical products. In short, with the increase of LET, the yields of radical products (e^-_{aq}, $H^\bullet$, $HO^\bullet$) decrease while the molecular yields (H_2O_2 and H_2) increase, as shown in Fig.2.9. However, for $H^\bullet$ yields, it reaches a maximum value around 6-10 keV/μm and then decreases with LET [32, 33, 37] at neutral pH and 25°C. The yields of O_2, not shown in the figure, actually, increase significantly with LET at the similar conditions, [38].

Source	LET (keV/μm)	g(-H_2O)	g(e^-_{aq})	g(OH)	g(H)	g(H_2)	g(H_2O_2)	g(HO_2)
^{60}Co γ-ray [39]	0.23	4.08	2.63	2.72	0.55	0.45	0.68	0.008
H^+ [39]	12.3	3.46	1.48	1.78	0.62	0.68	0.84	-
Fast neutron [40]	40	3.19	0.93	1.09	0.50	0.88	0.99	0.04
He^{2+} [39]	108	2.84	0.54	0.54	0.27	1.11	1.08	0.07
^{10}B(N, α)^{7}Li [41–43]	220	3.9	0.33	0.30	0.10	1.8	1.67	0.13

Table 2.3: Primary yields (molecules/100 eV) of water radiolysis for different types of radiations at room temperature: evolution of primary yields versus LET.

Tab.2.3 shows the values of primary yields of different LET radiations. It is worth noting that at low LET, the value of $HO_2^\bullet$ is actually too little to be taken into account, thus it can be neglected for the determination of the radiolytic yields. Overall, the G-values for neutral water at room temperature under low LET radiation conditions have been well established [12, 39]. They are the basis for further studies.

2.2.B.3 Influence of dose rate

Dose rate is defined as the dose received per unit time, it is often expressed in Gy/s. It can be thought as the intensity of radiation. The influence of dose rate is similar to the LET effect. High dose rate results in high concentration of radicals produced by the irradiation, and thus the radical-radical reactions are favoured [44]. In short, with the increase of dose rate, the radicals yields decreases while the molecular yields increase [14]. In consequence, the water decomposition is promoted, as illustrated in Fig.2.10 [45].

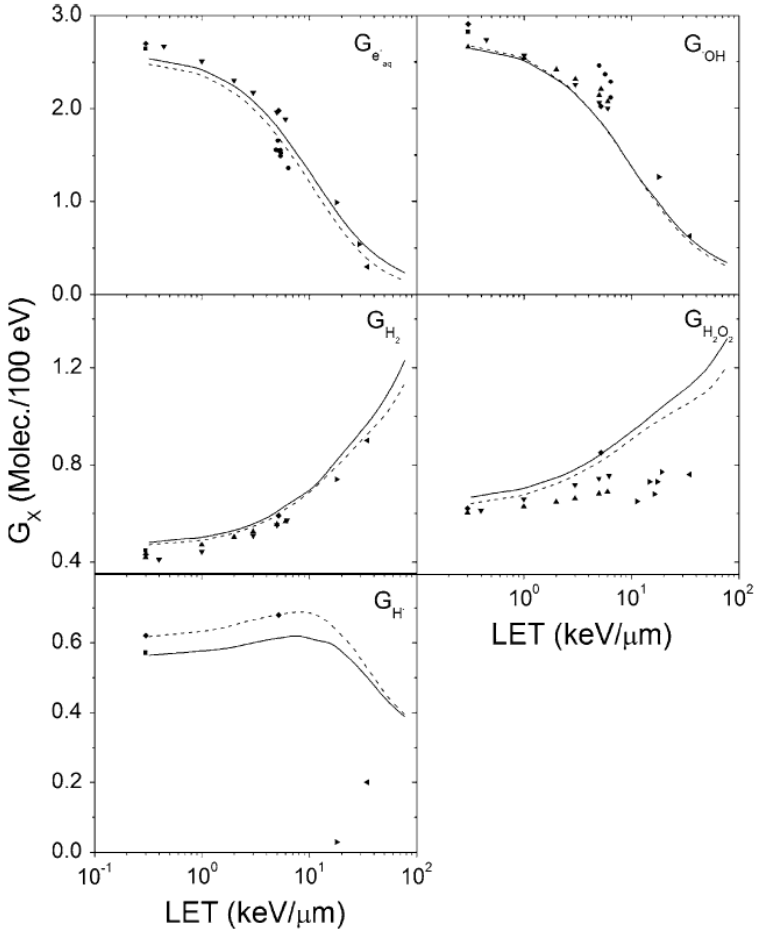

Figure 2.9: Primary yields of $H^\bullet$, $HO^\bullet$, H_2, H_2O_2 and e^-_{aq} in neutral liquid water irradiated by proton (300-0.1 MeV, LET $\sim$ 0.3-85 keV/μm) at 25°C. Broken line: IONLYS-IRT calculation; solid line: SBS calculation; spline: Monte-Carlo simulation results [32].

2.2.B.4 Influence of pH

The pH influence has been studied for a long time, as Draganić and Draganić conclude, which I quote: "*There is no strong dependence of the primary yields on pH, although the situation at extreme pH's is not yet quite clear.*" [47]. Therefore, we consider that the radiolytic yields are not affected by the pH between 4 and 9 [13, 14, 48, 49]. Furthermore, even for the time less than 10^{-6} s after energy deposition, pH can also be regarded as no large influence on the radiolytic yields ranging form 1 to 13 [50].

More precisely, Fig.2.11 illustrates the radiolytic yields as a function of pH up to 7. To get a better understanding, the polynomials indicated in Tab.2.4 shows the constant reaction rate of some important reaction concerning about pH. At pH equals to 4, the rate constant of Eq.2.39 is 2.1×10^{10} $M^{-1}s^{-1}$ and $[H^+]$=10^{-4}, which implies the time scales of this reaction is about 5×10^{-7} s. It is quite close to 10^{-6} s, which is the end of spur expansion. Therefore, for a higher pH which means a lower $[H^+]$, the primary yields are not affected. Oppositely, for a higher $[H^+] \geqslant 10^{-4}$ M, it brings more $H^\bullet$ due to Eq.2.39. In the competition between e^-_{aq} and $H^\bullet$, they both react with $HO^\bullet$, Eqs.2.40 & 2.41, and the reaction Eq.2.40 is more efficient than Eq.2.41. This can explain that at pH $\leqslant$ 4, the value of

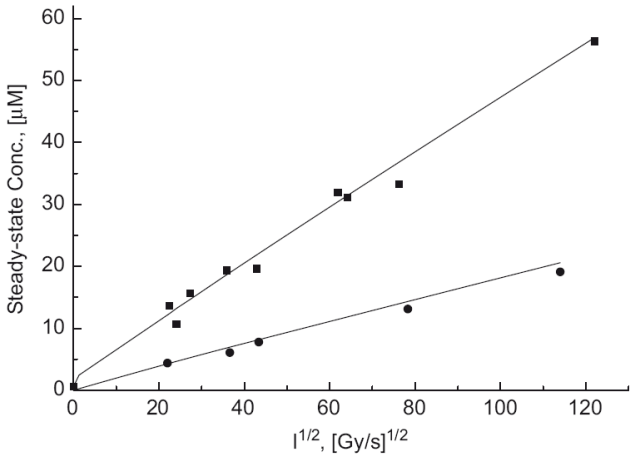

Figure 2.10: Steady-state concentration of oxide species as function of the square root of dose rate. ■: $[H_2O_2]+2[O_2]$; •: $[H_2O_2]$. [45, 46].

yields e^-_{aq} and $H^\bullet$ increase while g($HO^\bullet$) decrease as the pH decreases. Another reason for the decrease of $HO^\bullet$ is due to Eq.2.42, they recombine with each other and to form H_2O_2. It brings the increase of the yields H_2O_2 with the decrease of pH. The gradually decrease of H_2 yields with pH form 4 to 0 is due to the reaction rate of Eq.2.44 is much smaller than Eq.2.43 [32, 51].

Reaction (Eq n°)		Constant reaction rate k L.mol^{-1}.s^{-1}	Estimated at 25°C L.mol^{-1}.s^{-1}
$e^-_{aq} + H^+ \rightleftharpoons H^\bullet$	(2.39)	$10^{(39.127-3.888\times10^4/T+2.054\times10^7/T^2-4.899\times10^9/T^3+4.376\times10^{11}/T^4)}$	2.1×10^{10}
$HO^\bullet + e^-_{aq} \rightarrow OH^-$	(2.40)	$10^{(13.123-1.023\times10^3/T+7.634\times10^4/T^2)}$	3.5×10^{10}
$HO^\bullet + H^\bullet \rightarrow H_2O$	(2.41)	$4.26 \times 10^{11}e^{-1091/T}$	1.1×10^{10}
$OH^\bullet + OH^\bullet \rightarrow H_2O_2$	(2.42)	$10^{(8.054+2.193\times10^3/T-7.395\times10^5/T^2+6.870\times10^7/T^3)}$	4.8×10^9
$e^-_{aq}+H^\bullet(+H_2O) \rightarrow H_2+OH^-$	(2.43)	$1.14 \times 10^{13}e^{-1795.7/T}$	2.76×10^{10}
$H^\bullet + H^\bullet \rightarrow H_2$	(2.44)	$2.70 \times 10^{12}e^{-1867.5/T}$	5.1×10^9

Table 2.4: Table of reaction rate constant over the temperature range $20 - 350$°C, and the g-Value estimated at 25°C, based on information available in 2008. [52].

On the other hand, when pH is higher than 9, the primary yields are also affected. However, for alkaline solutions, the evolution of the primary yields is still not very clear yet. However, under basic condition, they are most influenced by the radical $O^{\bullet-}$. The most cited explanation is that the yields of H_2O_2 and e^-_{aq} + $H^\bullet$ decrease while g($HO^\bullet$) increase as the pH increase from 12 to 14 [48, 53, 54]. However, there is an inverse explanation of the primary yields due to the selection of the constant reaction rate of the radical $O^{\bullet-}$. The table below, Tab.2.5, shows the primary yields of water radiolysis at different pH value at room temperature in general.

2.2.B.5 Influence of temperature

The temperature of the water is one of the most important parameters on primary radiolytic yields. Many parameters are affected by temperature, for example, reaction constant rate, diffusion coefficient,

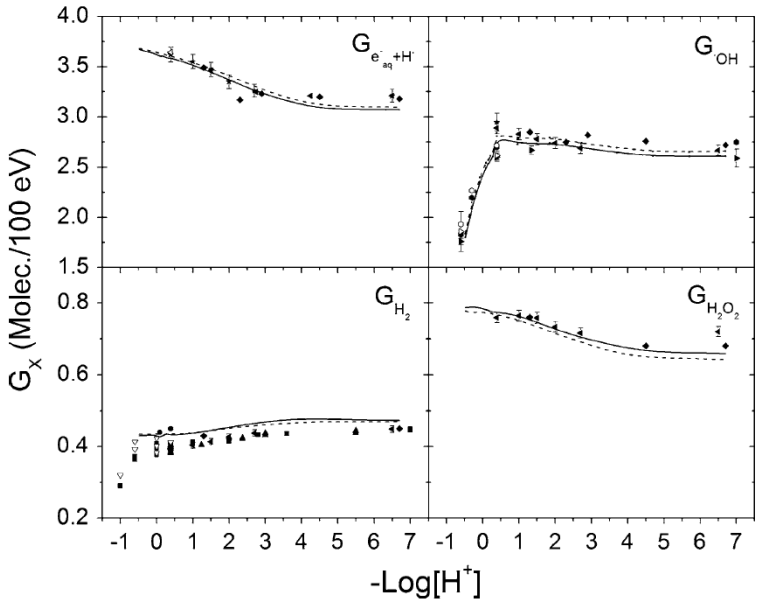

Figure 2.11: Primary yields of $HO^{\bullet}$, H_2O_2, H_2 and reducing species (e^-_{aq}+$H^{\bullet}$) versus -Log[H^+] for the radiolysis of air-free aqueous slufuric solution at 25°C with 300 MeV protons. Broken line: IONLYS-IRT calculation; solid line: SBS calculation; spline: Monte-Carlo simulation results [32].

pH	g(H^+)	g(OH^-)	g(e^-_{aq})	g($H^{\bullet}$)	g(H_2)	g($HO^{\bullet}$)	g(H_2O_2)
0-2	3.45	0.4	3.05	0.6	0.45	2.95	0.8
4-9	3.4	0.7	2.7	0.6	0.45	2.8	0.7
12-13	3.6	0.55	3.05	0.55	0.4	2.9	0.75

Table 2.5: Primary yields (molecules/100 eV) of water radiolysis for at different pH value at room temperature [46].

and Onsager radius[10] [55]. The primary yields are significantly influenced by these parameters. Many studies have been done [20, 33, 56–59], including the most cited literature by Elliot *et al.* [52, 60]. Many experiments have been performed to measure the primary radiolytic yields at various temperatures, and they also collected data from all over the world. Therefore, their values are normally regarded as the most complete [52]. The reaction constant rate has been calculated as a function of temperature (Tab.2.4). Figs.2.12 (a) & (b) illustrate a simulation of g-values for the primary species formed by water radiolysis as a function of temperature: (a) uses the data for γ or electron radiation, both can be regarded as low LET radiation, and (b) shows the data collected from fast neutron radiation which implies for high LET radiation.

For low LET radiation, most primary yields increase with the increase of temperature in different ways, except for H_2O_2 which actually decreases. The diffusion coefficients and the constant reaction rates both strongly depend on the temperature, and thus the diffusion rate and reaction rate increase sharply with temperature. At high temperatures, the diffusion rates for all the radicals are higher than the recombination rates, and results in the augmentation of the radical yields. Normally, the increase of radicals yields leads to the decrease of the molecular yields, H_2 and H_2O_2. However, in the

[10]**Onsager Radius:** the distance at which the energy of the Coulomb interaction in dielectric continuum becomes equal to thermal energy k_BT.

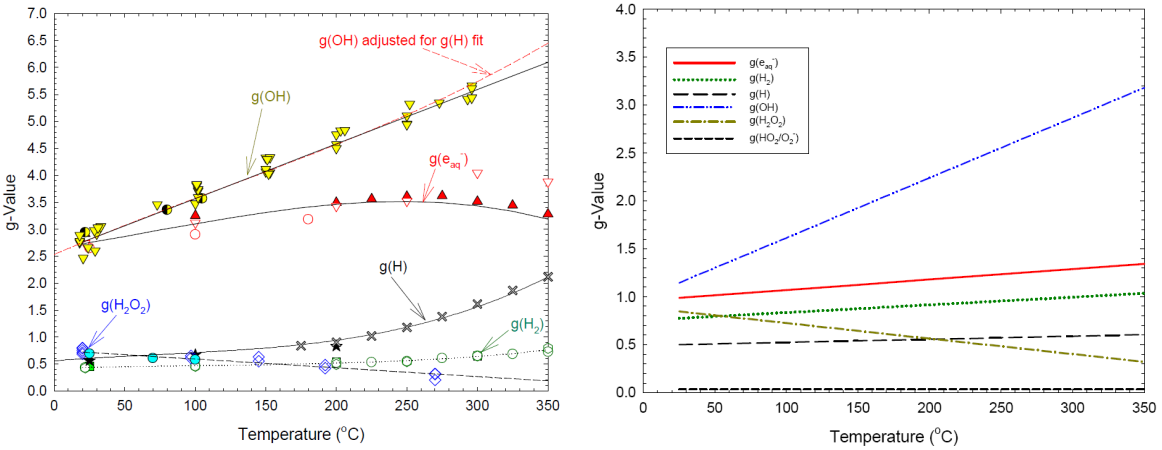

(a) (b)

Figure 2.12: The g-values for the primary species formed in reaction 2.18 as a function of temperature: (a) low LET radiation; (b) high LET radiation (fast neutron radiation for natural uranium fuel). [52].

.

case of H_2, it also increases with temperature. One explanation is considered as the formation of H_2 during the physicochemical stage, Eqs.2.24 & 2.31. There exists other explanations and arguments which are ongoing. The diminution of H_2O_2 yields is the consequence that the radicals are escaped from recombination.

For high LET radiation, as a function of temperature, the yields of $g(e_{aq}^-)$, $g(HO^\bullet)$ and $g(H_2)$ increase, $g(H^\bullet)$ and $g(HO_2^\bullet/O_2)$ stay nearly constant, while $g(H_2O_2)$ decreases. Tab.2.6 lists polynomial function of LET for every primary yield in order to give a relationship between temperature dependence and LET. It clearly shows that with the increase of LET, the temperature dependences of $g(e_{aq}^-)$, $g(H^\bullet)$ and $g(HO^\bullet)$ decrease while the one of $g(H_2)$ increases. Therefore, it results in slight difference of temperature dependence between low and high LET. In the same time, $g(H_2O_2)$ is actually not sensitive with LET, it actually decreases in almost the same tendency with the temperature in both high and low LET [52, 61].

In general, by comparing the two figures, it seems that the g-values of primary yields vary more significantly in low LET. The temperature dependences of these g-values decrease with increasing LET [62]. It might also link to the different tracks produced by low and high LETs. The isolated spurs of low LET are favoured for diffusion while the cylindrical tracks of high LET promote recombination.

Parameter	Function
$d(g(e_{aq}^-))/d(\text{temperature})$	$1.92 \times 10^3 - 2.56 \times 10^{-5}$LET
$d(g(H_2))/d(\text{temperature})$	$7.59 \times 10^{-4} + 1.32 \times 10^{-6}$LET
$d(g(H^\bullet))/d(\text{temperature})$	$6.70 \times 10^{-4} - 1.08 \times 10^{-5}$LET
$d(g(HO^\bullet))/d(\text{temperature})$	$7.34 \times 10^{-3} + 3.37 \times 10^{-5}$LET
$d(g(H_2O_2))/d(\text{temperature})$	-1.62×10^{-3}
$d(g(HO_2/O_2))/d(\text{temperature})$	No temperature dependence

Table 2.6: The temperature dependency of each primary yields as a function of track-averaged LET [52].

Last but not least, the influence of temperature may be more pronounced on the physicochemical stage rather than on the later radical diffusion stage [63].

2.2.B.6 Influence of pressure

In the $1960's$, a lot of research about pressure influence was done. Hentz *et al.* [64–69] figured out that the primary yields in water raidolysis are independent of pressure until 6.34 kbar. It is worth mentioning that pressure may play an important role in other solutions or in another phase (gas phase [70, 71]).

The primary yields vary with many parameters, among them the most important is the LET linked to the irradiation. Afterwards, they are influenced by the temperature, which is linked to the nature of water itself. Under some extreme conditions, like very high pressure, very acid or basic pH, may also influence the primary yields.

To sum up, irradiation of pure water leads to buildup of a steady-state concentration of hydrogen peroxide in solution, and the continual formation of hydrogen and oxygen. In a simply way, we may just consider that the radiation decomposes the water into hydrogen and oxygen.

Water radiolysis occurs in many situations, especially in nuclear reactors. It is also a key factor to nuclear corrosion phenomena. However, only pure water radiolysis is not enough to understand the radiolysis which occurs inside of nuclear reactors. The water used in nuclear reactors, either light water or heavy water, they both have a specific chemical conditioning. Therefore, the radiolysis process is more complex than in pure water. The following section will show the PWR water radiolysis, which is the main interest this thesis study.

2.3 PWR Water Radiolysis

The light water used in PWR is deaerated pure water with addition of dissolved hydrogen, boric acid and lithium hydroxide. The process of radiolysis is modified by these components. Meanwhile, the radiolytic yields are also affected.

2.3.A Radiolysis in the Presence of H_2, H_2O_2 and O_2

2.3.A.1 Reducing - A Chain Reaction: H_2

The study of the influence of the three stable products H_2, H_2O_2 and O_2 of radiolyisis reactions on the water decomposition can be traced back to the $1950's$. Allen *et al.* [72] and Hochanadel [73] have established a basic mechanism for the forward and backward reactions between H_2 and H_2O_2, moreover the production of O_2. Both O_2 and H_2O_2 accelerate the water decomposition while H_2 is always regarded as an inhibitor of radiolysis. That is the reason why H_2 is added into the PWR water. Its role is to decompose the H_2O_2 and thus to suppress the production of O_2. There is a chain reaction involved in radiolysis process: dissolved hydrogen captures an oxidising species $HO^\bullet$ and transfers into a reducing species $H^\bullet$, then the $H^\bullet$ reacts with rapidly with H_2O_2 and re-form $HO^\bullet$, listed in Tab.2.7, Eqs.2.48 & 2.49. Finally a global reaction is given in Eq.2.57, [13, 74].

Reactions (Eq. n°)		k [46] L.mol^{-1}.s^{-1}	k estimated at 25°C [52] L.mol^{-1}.s^{-1}	E_a [46] kJ.mol^{-1}	E_a [52] kJ.mol^{-1}
$HO^\bullet + H^\bullet \rightarrow H_2O$	(2.45)	7.0×10^9 [75]	1.1×10^{10}		9.1
$HO^\bullet + HO^\bullet \rightarrow H_2O_2$	(2.46)	5.3×10^9	4.8×10^9	8.0	
$H^\bullet + H^\bullet \rightarrow H_2$	(2.47)	7.9×10^9	5.1×10^9	12.6	15.5
$HO^\bullet + H_2 \rightarrow H_2O + H^\bullet$	(2.48)	3.74×10^7		18.0	
$H^\bullet + H_2O_2 \rightarrow HO^\bullet + H_2O$	(2.49)	3.44×10^7 [75]	3.6×10^7	13.6	21.2
$HO^\bullet + H_2O_2 \rightarrow HO_2^\bullet + H_2O$	(2.50)	3.8×10^7	2.9×10^7	14.0	13.8
$HO_2^\bullet \rightleftharpoons H^+ + O_2^-$	(2.51)	7×10^5	pK=4.8	12.6	
$HO_2^\bullet + HO_2^\bullet \rightarrow H_2O_2 + O_2$	(2.52)	8.1×10^5	8.4×10^5	24.7	6.6
$HO_2^\bullet + O_2^- \rightarrow HO_2^- + O_2$	(2.53)	9.5×10^7	$\sim$ 1×10^8	8.8	8.1
$O_2 + H^\bullet \rightarrow HO_2^\bullet$	(2.54)	2.0×10^{10}	1.13×10^{10}	12.6	15.2
$O_2 + e_{aq}^- \rightarrow O_2^-$	(2.55)	1.94×10^{10}	2.3×10^{10}	13.0	11.6
$H_2O_2 + e_{aq}^- \rightarrow HO^\bullet + HO^-$	(2.56)	1.14×10^{10}	1.4×10^{10}	15.1	15.7

Table 2.7: Table of reactions, constant reaction rates k (L.mol^{-1}.s^{-1}) and activation energies E_a (kJ.mol^{-1}) [46, 52, 75].

$$H_2 + H_2O_2 \rightarrow 2H_2O \tag{2.57}$$

The chain reaction can retain effective as long as enough HO$^\bullet$ and H$^\bullet$ presented. In other words, all the species reacting/recombining with H$^\bullet$ and HO$^\bullet$ make the process less efficient, for instance reaction Eq.2.54 in Tab.2.7. Furthermore, it also reveals that the process can be stabilised due to the effective recombination, such as Eqs.2.45, 2.46 and 2.47, listed in the same table.

2.3.A.2 Oxidising - Inhibitors of Chain Reaction: H_2O_2 and O_2

The hydrogen peroxide H_2O_2 on one hand can react with H$^\bullet$ in the chain reaction, Eq.2.49, on the other hand it can also react with the radical HO$^\bullet$ to inhibit the chain reaction and produce the radical $HO_2^\bullet$, Eq.2.50 in Tab.2.7. The recombination of $HO_2^\bullet$ can either form H_2O_2 and O_2, or oxidise the O_2^- to O_2. (Eqs.2.51, 2.52 and 2.53 Tab.2.7. Then, the global reaction of H_2O_2 and HO$^\bullet$ can be written as Eq.2.58. That is the reason H_2O_2 are often regarded as the precursor of O_2.

$$2HO^\bullet + H_2O_2 \rightarrow 2H_2O + O_2 \tag{2.58}$$

The oxygen molecule O_2 can also directly participe in the radiolysis process. O_2 react with H$^\bullet$ or e_{aq}^- and reduced to be $HO_2^\bullet$ and O_2^- respectively (Eqs.2.54 & 2.55 in Tab.2.7) and then eventually form H_2O_2 or re-form O_2 in result (Eqs.2.52 & 2.53, same table).

Normally, once there is O_2 present in the water, they will be reduced by e_{aq}^- and H$^\bullet$ immediately. Considering about the constant reaction rate of Eq.2.54 and 2.55 for O_2, which are much larger than those of Eq.2.48 and 2.49 for H_2. O_2 can be referred as the chain reaction *killer*, it will certainly

accelerate water decomposition. So long as the concentration of O_2 stay very low, the H_2O_2 produced during the radiolysis can be consumed by Eq.2.49 (Tab.2.7). Therefore, the decomposition of water can be avoided. Oppositely, when the concentration of O_2 is too high, they will join in the competition with H_2 for $HO^\bullet$. As explained, the reactions of O_2 are much more efficient than H_2 thus even a little bit of O_2 can totally block the role of dissolve hydrogen. In consequence, the chain reaction of H_2O_2 and O_2 is stopped and water decomposition takes place.

Latest, Ershov *et al.* have established a model of radiolysis of water and aqueous solution of H_2, H_2O_2 and O_2 [46]. It includes almost all the relevant experimental results. As illustrated in Fig.2.13, (a) indicates that with higher $[H_2O_2]$ in the solution, more O_2 is going to be formed. Moreover, the rate of H_2O_2 decomposition also depends on Eq.2.55 and 2.56 (Tab.2.7); (b) on the other hand, shows the efficiency of H_2O_2 decomposition decreases with its initial concentration in the water.

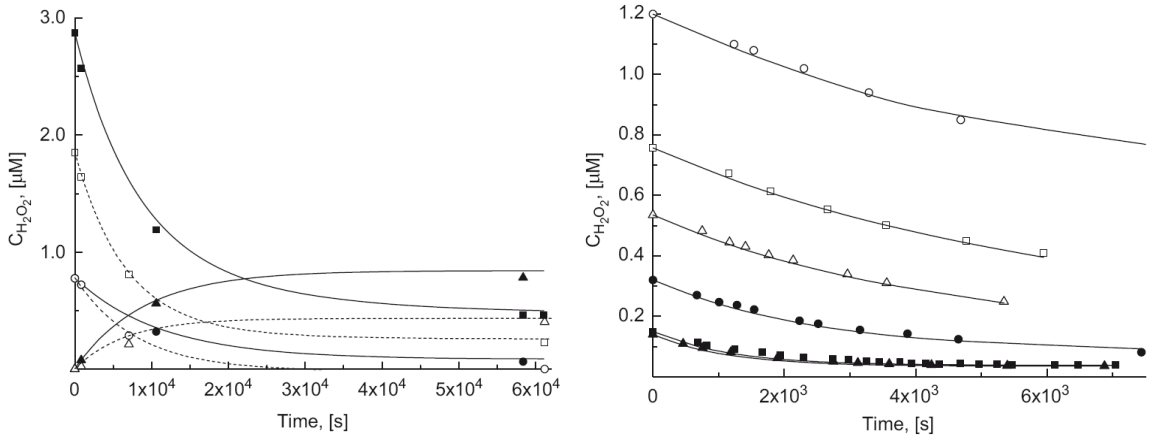

(a) (b)

Figure 2.13: (a) γ ray effect on solutions containing H_2 and excess H_2O_2, constant dose rate = 0.77 Gy.s^{-1}, constant $[H_2] = 7.8 \times 10^{-4}$ M: ■ for high $[H_2O_2]$ & □ for low $[H_2O_2]$; ○ high $[H_2]$ & ● low $[H_2]$; ▲ for high $[O_2]$ & △ for low $[O_2]$; calculation curve of $[H_2O_2]$ in decreasing order: straight line, dot line [46, 73]; (b) Decomposition of neutral deareated aqueous solution, constant dose rate = 0.2 Gy.s^{-1} $[H_2O_2]$ in a decrease order: ○, □, △ ●, ■, ▲, [46, 76].

.

2.3.B Critical Hydrogen Concentration (CHC)

In PWRs, the water is deareated to eliminate O_2 and a certain quantity of H_2 is added, as introduced in Chapter 1. However, dissolved hydrogen has its inconvenience: bringing stress corrosion problem, increasing the maintenance fee etc... Therefore, a concept of critical hydrogen concentration (**CHC**) need to be brought into conversation, which has become a hot topic. Early studies [77] has already shown that 1 cc/kg of H_2 is more than enough to reduce hydrogen peroxide generated by raidolysis.

Recently, Bartels *et al.* [78–81] have done a lot of research on finding the value of CHC, it is first relevant with the types of reactors, the core design, the parameters of PWR water and etc. In general, the normal-industry level of dissolved hydrogen for operating PWR varies from 25 to 40 cm^3 (STP).kg^{-1}, depending on different countries. Still these values are largely above the CHC, the most recent modelling in the AECL reactor [81] says that the CHC is approximately 0.5 cm^3 (STP).kg^{-1} for

a typical PWR conditions. This value seemed quite low, whereas the modelling value should be lower if there are no ammonia impurities problems. Actually, under PWR conditions, rather than factors mentioned before, the only major factor for CHC is the sensitivity of the constant rate of reaction Eq.2.48 (Tab.2.7) at high temperature. The steady state H_2 concentration in pure water is almost completely determined by the equilibrium of this reaction [78]. Despite the fact that these research are under the PWR condition, some of these conclusions are obtained without the presence of boric acid which can lead to $^{10}B(n,\alpha)^7Li$ reactions. In this case, the value of CHC may be increased due to the fact that no radicals produced in α radiation [81].

Nevertheless, Takiguchi *et al.* [82, 83] also found the optimal dissolved hydrogen value was below 0.5 $cm^3(STP).kg^{-1}$ in the out-of-core region in the INCA loop. However, the approximate dissolved hydrogen threshold for in-core region was at least twice higher than the out-of-core value.

The study of CHC starts from the mid-1990$'s$ and still goes on today, it is not only important in the point view of suppress radiolysis with minimum amount of H_2 which can bring an economic benefits, but also in the aspect of avoiding the corrosion problems trigged or accelerated by the excess H_2.

2.3.C Radiolysis in the Presence of Bore and Lithium

Before talking about the effect of ^{10}B, the influence of LET needs to be discussed. As explained in the previous section, low LET like γ-ray gives more radicals products than molecular ones and favours the recombination of the chain reaction. In short, there will be no water decomposition with low LET. Reversely, high LET leads to a higher concentration of H_2O_2 and thus limits the chain reaction and produces O_2 [84–86]. Therefore, the water decomposition is more likely occurring with high LET. $^{10}B(n,\alpha)^7Li$ happens to be one of high LET radiation.

In PWRs, the global LET actually depends on the ratio between high ($^{10}B(n,\alpha)^7Li$) and low (γ-ray) LET radiation. In different parts of PWRs, like the in-core and out-of-core, the LET is different. Without any doubt, the concentration of ^{10}B directly affects on the local ratio of $^{10}B(n,\alpha)^7Li/\gamma$. The ratio increases with the concentration of ^{10}B, thus the global LET also increase and tends to high LET radiation. In consequence, the augmentation of $[^{10}B]$ results in higher probability of water decomposition. Fig.2.14 illustrates this influence of $[^{10}B]$ on the radiolytic yields of H_2O_2 and O_2 [87, 88], which seem to be linked with the temperature:

- At room temperature, (30°C), it appears to have a threshold about 0.13 $mol.L^{-1}$. Above this threshold, both H_2O_2 and O_2 increase sharply with the concentration of ^{10}B.
- In the middle temperature, (100°C), this threshold is shifted towards a higher concentration, approximately 0.19 $mol.L^{-1}$.
- At high temperature, (200°C), there is no visible threshold shown in the Fig.2.14. It implies that more ^{10}B can be added into PWR water without bringing the water decomposition as temperature increases. The reason might be explained in three aspects:
    1. The radical yields increases with temperature as mentioned before, and hence the recombination reactions are favoured.

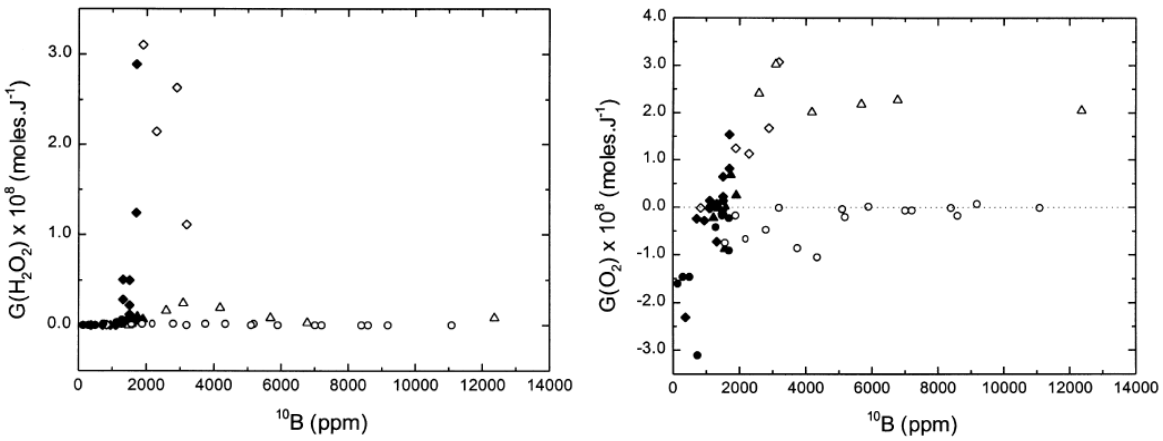

(a) (b)

Figure 2.14: The effect of ^{10}B concentration on water radiolysis: (a) $g(H_2O_2)$ vs. [^{10}B]; (b) $g(O_2)$ vs. [^{10}B]. 30°CNBA (◊), 30°C EBA (♦) ; 100°C NBA (▲), 100°C EBA △; 200°C NBA (●), 200°C EBA (○). NBA (open symbols): Natural Boric Acid, contains 19.8% of ^{10}B; EBA (solid symbols): Enriched Boric Acid, contains 99.5% of ^{10}B [87].

2. The kinetics of the chain reaction are favoured over those of forming oxidising species H_2O_2 and O_2. The reason will be explained in the section of temperature influence.
3. The hydrogen solubility increases with temperature, thus more H_2 at high temperature, more chain reaction taking place and less water decomposition.

No specific effect of enriched boric acid (EBA) on water radiolysis has been observed. At the same concentration, EBA and NBA show the same behaviours. Therefore, EBA can be safely used for replacing NBA in PWRs as far as the concern of radiolysis.

Actually, the presence of ^{7}LiOH causes more water decomposition, as shown in Fig.2.15. The explanation of this phenomenon is not very clear yet. The main role of ^{7}LiOH is to adjust and maintain the pH at 7 for PWR water. But, as shown previously, this variation of pH will not affect on the water decomposition, and hence the pH effect should not be the cause of the increase brought by ^{7}LiOH. Li^+ does not seem to react with the radicals normally. Briefly, a negative influence on PWR water radiolysis is brought by the presence of ^{7}LiOH, although further studies need to be done.

2.3.D Influence of Other Parameters on Radiolytic Yields

Under PWR conditions, other than the influence of H_2, ^{10}B and ^{7}LiOH, the radiolytic yields can also be affected by a lot of parameters before of after steady-state. However, like the influence of LET has already been detailed in the previous section 2.3.C, and the influence of dose rate does not seem different between pure and PWR waters, then they will not be discussed in the following sections.

2.3.D.1 Influence of Temperature

According the temperature effect on pure water, the radicals yields increase while the molecular yields decrease as a function of temperature. Consequently, the recombination reactions are promoted. In the

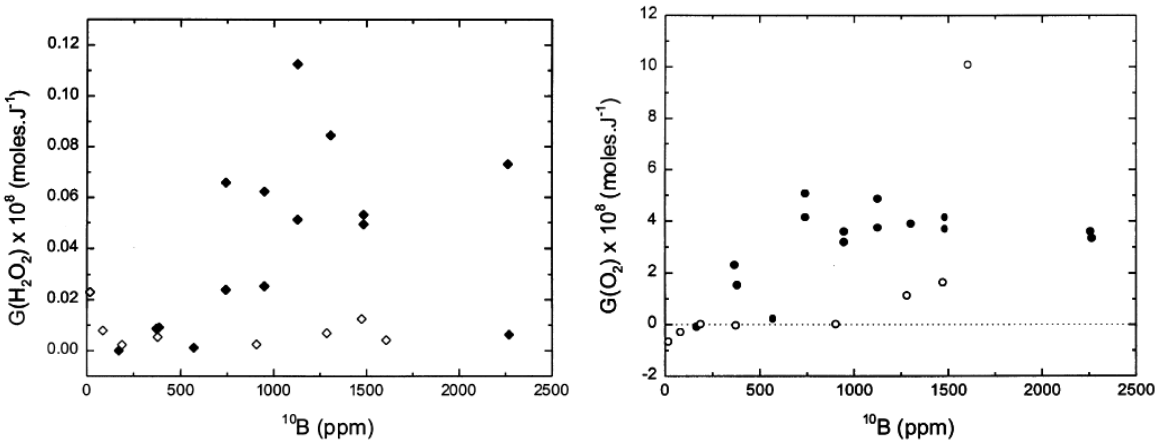

(a) (b)

Figure 2.15: The effect of ^{7}LiOH on water radiolysis at 200°C: (a) g(H_2O_2) vs. [^{10}B]; (b) g(O_2) vs. [^{10}B]. Solid symbols: solution contains ^{7}LiOH, calculated by MULTEQ® to achieve a pH = 7 at 200°C; Open symbols: blank solution without ^{7}LiOH [87].

case of PWR water, with the increase of temperature, the chain reaction of H_2 is preferred to others. One explanation is linked to the activation energy $\mathbf{E}_a$[11]. It can be expressed by the **Arrhenius Equation** as written in Eq.2.59, in which, k is the constant reaction rate, E_a means the activation energy, R is the ideal gas constant and A is the frequency factor (or attempt frequency) of the reaction.

$$ln(k) = -\frac{E_a}{RT} + ln(A) \tag{2.59}$$

As indicated in Tab.2.7, the values of E_a for the chain reaction, Eqs.2.48 & 2.49, are higher than Eqs.2.45, 2.46 and 2.47, which are the chain *stoppers*. Nevertheless, the increase of E_a is less significant than the augmentation of the radicals with the raise of temperature. On the other hand, as mentioned in Ch.2.3.C, the solubility of H_2 increases with temperature and results in favour of the chain reaction. Therefore, it seems that the effect of temperature may slow down the PWR water decomposition.

2.3.D.2 Influence of pH

Fig.2.16 illustrates the pH of PWR water with temperature. At 300°C the pH is about 7, and the pH behaviour of PWR water is actually following the one of boric acid. Below this temperature, the pH seems to reach a minimum of the curve at 150°C [89, 90].

Fig.2.17 has portrayed the variation of steady-state concentration of H_2O_2 and O_2 as a function of pH [46, 91]. Briefly, it describes:

- The concentration of H_2O_2 increases sharply with the decrease of pH from 4 to 0. For a higher pH, it seems to have no effects on the H_2O_2;
- The concentration of O_2 is not affected by the pH from 4 to 8. Then in the two extreme zones, it increases with the pH. As a result, in the alkaline environment, the concentration of O_2 is much higher than it of acid zone.

[11] $\mathbf{E}_a$: the energy needs to be overcome in order to achieve a chemical reaction.

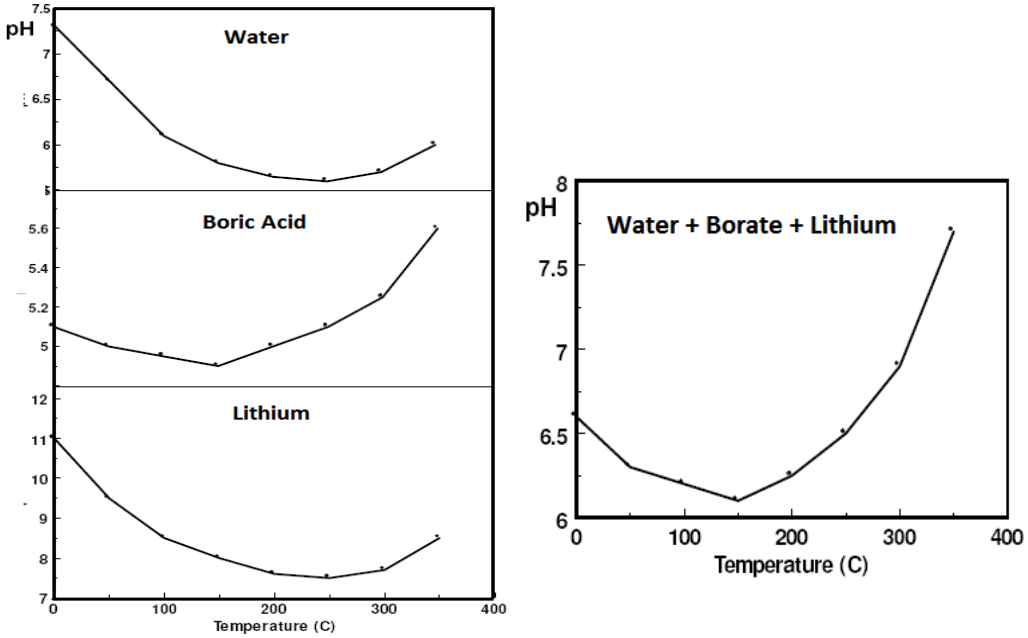

(a) (b)

Figure 2.16: The effect of boric acid and lithium on pH as a function of temperature: (a) water, boric acid and lithium respectively; (b) PWR water by including the three elements [89].

Generally, regardless the temperature, the pH of PWR water stays in the range form 6 to 8 approximately. Thus, the pH ($4 \leqslant pH \leqslant 10$) appears to have no specific effect on PWR water decomposition. However, either in acidic or in basic environment, the pH can still affect the water decomposition, especially for the molecular products, H_2O_2, O_2 and H_2.

The variation of steady-state concentration of H_2O_2 and O_2 from pH is strongly depend on the reaction between e^-_{aq} and a proton, H_3O^+, as shown in Eq.2.60, $k = 2.3 \times 10^{10}$ L.mol^{-1}.s^{-1}. Both e^-_{aq} and $H^\bullet$ reduce H_2O_2 and O_2, written in Eqs.2.61, and thus inhibit the water decomposition. The constant reaction rate decreases while the pH increases [92], Eq.2.60 is thus less efficient. Higher pH, the less $H^\bullet$ is produced.

$$e^-_{aq} + H_3O^+ \rightarrow H^\bullet + H_2O \tag{2.60}$$

As the constant reaction rates indicated for Eqs.2.61, H_2O_2 prefers to react with e^-_{aq} over $H^\bullet$. For the O_2, there is no difference since the k values are practically the same. With the increase of pH, H_2O_2 appears to be more competitive for e^-_{aq} and $H^\bullet$, and thus to be reduced [46].

$$\begin{aligned} e^-_{aq} + H_2O_2 &\rightarrow O_2^- \qquad k = 1.14 \times 10^{10} L.mol^{-1}.s^{-1} \\ e^-_{aq} + O_2 &\rightarrow OH^- + HO^\bullet \qquad k = 1.94 \times 10^{10} L.mol^{-1}.s^{-1} \\ H^\bullet + H_2O_2 &\rightarrow H_2O + HO^\bullet \qquad k = 3.44 \times 10^{7} L.mol^{-1}.s^{-1} \\ H^\bullet + O_2 &\rightarrow OH_2^- \qquad k = 2.0 \times 10^{10} L.mol^{-1}.s^{-1} \end{aligned} \tag{2.61}$$

In a highly alkaline medium, Matheson *et al.* [93] found the evidence of the reaction Eq.2.62. Thereby, the decrease of $H^\bullet$ while the increase of e^-_{aq} leads to the same conclusion as before.

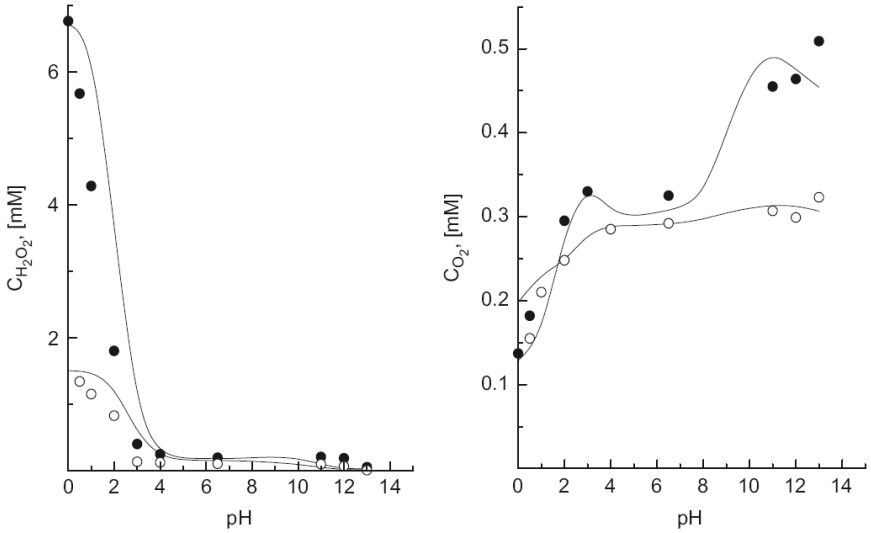

Figure 2.17: The concentration of H_2O_2 and O_2 versus pH at room temperature under different dose rates: • = 4.72 Gy.s^{-1}; ∘ = 0.42 Gy.s^{-1} [46, 91].

$$OH^-_{aq} + H^\bullet \rightarrow e^-_{aq} + H_2O \tag{2.62}$$

The acid-base equilibria reactions are listed in Tab.2.8 [52]. They play an important role in homogeneous chemistry.

Equilibrium Reaction (Eq n°)		pK$_a$ at 20°C	pK$_a$ at 150°C	pK$_a$ at 300°C
$HO_2^\bullet \rightleftharpoons H^+ + O_2^-$	(2.63)	4.83	4.91	6.57
$H_2O \rightleftharpoons H^+ + OH^-$	(2.64)	15.92	13.43	13.24
$H_2O_2 \rightleftharpoons H^+ + HO_2^-$	(2.65)	11.84	10.29	10.35
$HO^\bullet \rightleftharpoons H^+ + O^-$	(2.66)	11.84	10.29	10.35
$H^\bullet \rightleftharpoons H^+ + OH^-$	(2.67)	9.74	6.92	6.64
$H^\bullet + H_2O \rightleftharpoons H_2 + HO^\bullet$	(2.68)	12.17	7.95	5.57

Table 2.8: Table of acid-base equilibria reactions and their acid dissociation constant in minus logarithmic form, pK_a values, at different temperature [52].

The radical $HO_2^\bullet$ in Eqs.2.52 & 2.53 (in Tab.2.7) can both form oxidising species H_2O_2 and O_2. The constant reaction rate $k_{Eq.2.52}$ is at least 200 times smaller than $k_{Eq.2.53}$. At pH = 4.8, the acid-base equation Eq.2.52 comes to equilibrium, thus the reaction rate of Eq.2.53 comes to the maximum. With the increase of pH, not only the constant reaction rate reduces, but also the equilibrium of Eq.2.52 towards right side. As a result, more O_2^- accumulates in the solution, which can react with $HO^\bullet$, Eq.2.69, then decreasing the probability of the chain reaction. In this point of view, the increase of pH brings a negative effect on PWR water radiolysis.

$$(Eq.2.52) \qquad HO_2^\bullet + HO_2^\bullet \rightarrow H_2O_2 + O_2$$

$$(Eq.2.53) \qquad HO_2^\bullet + O_2^- \rightarrow HO_2^- + O_2$$

$$HO^\bullet + O_2^- \rightarrow O_2 + OH^- \tag{2.69}$$

Besides, under basic environment, the radical $HO^\bullet$ and transient species like O_2^- and O_3^-, play a major role in the radiation chemical transformations and in the determination of the steady-state concentration of molecular products H_2, O_2 and H_2O_2, as listed in Eqs.2.70 [46, 89].

$$\begin{aligned} HO^\bullet + OH^- &\rightarrow O^- + H_2O \qquad k = 1.3 \times 10^{10} L.mol^{-1}.s^{-1} \\ O^- + H_2O_2 &\rightarrow O_2^- + H_2O \qquad k = 5.0 \times 10^{8} L.mol^{-1}.s^{-1} \\ O^- + H_2 &\rightarrow H^\bullet OH^- \qquad k = 8.0 \times 10^{7} L.mol^{-1}.s^{-1} \\ O^- + O_2 &\rightarrow O_3^- \qquad k = 3.6 \times 10^{9} L.mol^{-1}.s^{-1} \\ O_3^- + HO^\bullet &\rightarrow O_2 + HO_2^- \qquad k = 8.5 \times 10^{9} L.mol^{-1}.s^{-1} \end{aligned} \tag{2.70}$$

Otherwise, in an acid environment, with the decrease of pH, the recombination of $H^\bullet$ is promoted over e_{aq}^- [35], thus the concentration of O_2 decreases while the one of H_2O_2 increases.

In brief, higher pH brings higher concentration of O_2, lower pH results in more H_2O_2. However, in the range of pH from 4 to 10, the steady-state concentration of H_2O_2 and O_2 are not affected.

2.3.D.3 Influence of Pressure

As told, pressure has no effect on the primary yields until 6.34 kbar on pure water radiolysis [64–69]. It is still true under PWR conditions. However the constant reaction rate may be affected by the pressure if there is a change in activation volume during the *transition state*. **Transition State Theory** (**TST**) completes the Arrhenius rate law and explains the reaction rates of elementary chemical reactions [94].

$$ln(k) = ln(k_0) - \left(\frac{\Delta V^\ddagger}{RT}\right) P \tag{2.71}$$

In Eq.2.71, k and k_0 are the constant reaction rate at the pressure P and the atmospheric pressure P_0 respectively, R and T are the ideal gas constant and the absolute temperature in Kelvin, $V^\ddagger$ is actually the activation volume, normally in $ml.mol^{-1}$. The volume of activation is defined as the difference between the partial molar volumes of the transition state and the sums of the partial volumes of the reactants at the same temperature and pressure according **TST**. In practice, the $V^\ddagger$ may also be a function of pressure, thus the situation becomes more complicated. Briefly, the variation of k depends on $\Delta V^\ddagger$ and the pressure itself if it is high enough. In most water radiolysis reactions, $\Delta V^\ddagger$ dose not vary much. Therefore, the variation of constant reaction rate can be neglected unless the pressure is too high [13].

2.3.D.4 Influence of Impurities

Under PWR conditions, impurities in the water provokes serious problems like the deposition of CRUD on the tubing and so on. For PWR waters, the most studied impurity without any doubt is iron [95].

Iron impurities: Fe^{2+}, Fe^{3+} Generally, only ferrous ions can be released from the metal surface. However, they can be oxidised into ferric ions by water itself or oxidising radiolysis products, such as $HO^{\bullet}$, $HO_2^{\bullet}$, O_2^- and H_2O_2, written in Eqs.2.72 [87, 95].

$$\begin{aligned} 2Fe^{2+} + 2H^+ + \tfrac{1}{2}O_2 &\rightarrow 2Fe^{3+}_{aq} + H_2O \\ Fe^{2+} + HO^{\bullet} &\rightarrow Fe^{3+} + OH^- \\ Fe^{2+} + HO_2^{\bullet} &\rightarrow Fe^{3+} + OH_2^- \\ Fe^{2+} + O_2^- &\rightarrow Fe^{3+} + H_2O_2 + 2OH^- \\ 2Fe^{2+} + H_2O_2 &\rightarrow 2Fe^{3+} + OH_2^- \end{aligned} \tag{2.72}$$

Oppositely, ferric ions can also be reduced by $H^{\bullet}$, e^-_{aq} and so on, shown in Eqs.2.73 [87, 95].

$$\begin{aligned} Fe^{3+} + H^{\bullet} &\rightarrow Fe^{2+} + H^+ \\ Fe^{3+} + e^-_{aq} &\rightarrow Fe^{2+} \end{aligned} \tag{2.73}$$

Fig.2.18 shows the influence of $Fe(NO_3)_3$ on H_2O_2 and O_2 yields at room temperature. An increase of H_2O_2 can be observed due to the presence of ferric ions. Actually, Fe^{3+} and (Fe^{2+}) acts as scavengers of the radicals and result in less water recombination reactions. In a word, the presence of iron impurities leads to more radiolysis products at high boron concentration, and thus it is not a desirable phenomenon for PWR waters. Indeed, this conclusion is dragged out without considering the temperature influence on the solubility, though the solubility of ferric oxide appears not to depend on temperature between $250 - 350°C$ [96].

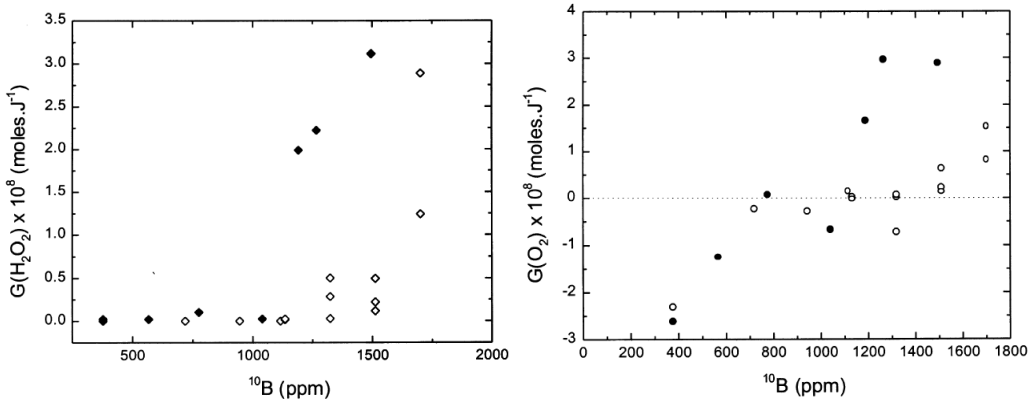

(a) (b)

Figure 2.18: The effect of $Fe(NO_3)_3$ at 30°C on water radiolysis: (a) $G(H_2O_2)$ vs. [^{10}B]; (b) $G(O_2)$ vs. [^{10}B]. Solid points: • and ♦ for 2ppm $Fe(NO_3)_3$; open points: ○ and ◇ for blank solution [87].

Zinc impurities : Zn^{2+}, Zn^+ Zinc is added in PWR water to suppress the radioactivity build-up on metallic surfaces due to cobalt-60 accumulation. Zn is not an impurity, it is actually an added element, though the concentration is quite low, few ppb.

Many studies [13, 87, 97, 98] have demonstrated in different ways that no negative effect of Zn on the radiolysis of the PWR water. Zn^{2+} can react with e^-_{aq} and be reduced to Zn^+. Also, it is hardly oxidised by other substances, thus Zn^{3+} is seemed not possible in the radiolysis water. On the

other hand, Zn^+ can react with the molecular products H_2O_2 and the radical $HO^\bullet$, which is somehow a diffusion controlled reaction. In consequence, Zn^+ may be oxidised back to Zn^{2+} or form other products. Briefly, in the point of view of water radiolysis, the presence of Zn have no major influence.

$$\begin{gathered} Zn^{2+} + e^-_{aq} \rightarrow Zn^+ \\ Zn^+ + H_2O_2 \rightarrow Zn^{2+} + HO^\bullet + OH^- \\ Zn^+ + OH^\bullet \rightarrow Zn^{2+} + OH^- \end{gathered} \tag{2.74}$$

Nitrate and nitrite impurities: NO_3^-, NO_2^- The influence of both nitrate and nitrite are still debatable, though it tends to be desirable for water radiolysis [99–101]. Even with a low concentration, they can react with the radicals formed during water radiolysis, such as e^-_{aq}, $HO^\bullet$ and $^\bullet O^-$, as Eqs.2.75 listed below. The competition between nitrate and nitrite for the radicals result in increasing the concentration of H_2 and H_2O_2.

$$\begin{gathered} e^-_{aq} + NO_3^- \rightarrow^\bullet NO_3^{2-} + H_2O \rightarrow^\bullet NO_2 + 2OH^- \\ {}^\bullet O^- + NO_3^- \rightarrow^\bullet NO_3^{2-} + H_2O \rightarrow^\bullet NO_2 + 2OH^- + O_2 \\ e^-_{aq} + NO_2^- \rightarrow^\bullet NO_2^{2-} + H_2O \rightarrow^\bullet NO + 2OH^- \\ HO^\bullet + NO_2^- \rightarrow^\bullet NO_2^{2-} + OH^- \\ 2^\bullet NO_2 + H_2O \rightarrow NO_3^- + NO_2^- + 2H^+ \end{gathered} \tag{2.75}$$

NO_3^- reacts more efficient with e^-_{aq} than NO_2^-. Nevertheless, the consequence is that the concentration of H_2O_2 is increased. Besides, NO_2^- can act as a good scavenger for $HO^\bullet$ which is important for the chain reaction of H_2 to suppress the radiolysis [102]. Furthermore, as long as the intermediate product $2^\bullet NO_2$ exists in the solution, which may also be directly excited by radiation, the net conversion between NO_3^- and NO_2^- will be continuous. Therefore, even with little NO_3^- and NO_2^- presence, the influence can be significant.

When the steady-state is achieved, the presence of nitrogen species depends on pH value, either as NO_3^- or in form of NO_3^-. Nitrate is the dominant species as pH $\lessapprox$ 10 while nitrite takes the leading at higher pH value.

Other impurities: Other than the impurities mentioned before, the existence of copper, Cl^-, SO_4^{2-} and so on should be brought into conversation too. Indeed, no one kind of impurity has been proved to have beneficial effect. Regardless the aspect of corrosion problem, even in the point view of water radiolysis, impurities accelerate PWR water decomposition, except for Zn which appears to have no effect.

Indeed, the presence of impurities copper [13, 103, 104] leads to more serious problem for water decomposition. As expressed in Eqs.2.76, Cu^{2+} and Cu^+ react with oxidising species and form O_2 and H_2O_2 in one hand, on the other hand they are also good scavenger for $HO^\bullet$ and $H^\bullet$, thus inhibit the chain reaction.

$$\begin{gathered} Cu^{2+} + O_2^- \rightarrow Cu^+ + O_2 \\ Cu^+ + O_2^- + (2H_2O) \rightarrow Cu^{2+} + H_2O_2 + 2OH^- \\ Cu^+ + HO^\bullet \rightarrow Cu^{2+} + OH^- \\ Cu^{2+} + H^\bullet \rightarrow Cu^+ \end{gathered} \tag{2.76}$$

Moreover, the copper ions may act as catalysis and accelerate the decomposition of H_2O_2 into O_2. In brief, the presence of copper is not favoured in PWR water, no matter what concentration.

Other impurities, like Cl^-, SO_4^{2-} will not be detailed here. However, their effects seems to be more serious for corrosion than for radiolysis [13].

2.4 Summary

In this chapter, three aspects of radiation chemistry have been detailed, the interaction of radiation with matter and water radiolysis, including pure and PWR water.

During the interaction of radiation with matter, the energy loss leads to ionisation and radiation. The concept of LET is the most common method to describe a source of radiation. The ways of interaction with matter, the LETs and the tracks left in the medium are different, depending on the different types of interactions.

Water radiolysis happens within 1μs after the energy deposition in the water and afterwards the water is regarded as a homogenous state. Therefore, the primary yields, both radical and molecular products, refer to homogenous and steady-state yields. They can be influenced by many parameters, the most dominant factors are the LET of radiation and the water temperature.

Concerning PWR water decomposition, which can be simply thought as the pure water radiolysis with presence of H_2, $B(OH)_3$ and LiOH. However, the radiolysis process becomes more complex. In one hand, dissolved hydrogen can join in the reaction from the beginning to the end. On the other hand, the presence of ^{10}B can directly affect on LET and cause more water decomposition. And ^{7}LiOH also accelerates PWR water decomposition, but the reason is still not clear yet. Nevertheless, the high temperature of PWR water may slow down the water decomposition.

Generally, the radiation damages the materials and through the production of oxidising species, the radiolysis causes corrosion problem, which are two serious factors to limit the PWR life extension.

References

[1] Erik Koelink. Scattering Theory wi4211 Advanced Topics in Analysis. Technical report, TUDelft, 2006.

[2] Scattering, course of University of Oxford, Physics Department, WEB, http://www.physics.ox.ac.uk/documents/PUS/dis/scattering.htm.

[3] S. Tavernier. *Experimental Techniques in Nuclear and Particle Physics*. Springer; 2010 edition, 2010.

[4] C. Leroy, P. Rancoita. *Principals of Radiation Interaction in Matter and Detection*. World Scientific Publishing Company, 2 edtion edition, February, 2009 February 2009.

[5] Wiliam Frass. Passage of Particles Through Matter. Technical report, Oxford Physics, 2009.

[6] J. Beringer et al. (Particle Data Grourp). Review of particle physics. *Phys. Rev. D*, 86, 2012.

[7] National Institute of Standards and Technology, Physical reference data, httm://physics.nist.gov/PhysRefData/content.html.

[8] Y. Tsai. Pair production and bremsstrahlung of charged leptons. *Rev. Mod. Phys.*, Vol.46, 815 (1974), Vol.49, 421 (1977).

[9] C. Amsler et al . Review of Particle Physics. *Physics Letters B*, 667:1 – 6, 2008. Review of Particle Physics.

[10] U. Littmark J.F. Ziegler, J. Biersack. *The Stopping and Range of Ions in Matter*. Pergamon Press, 1985.

[11] James F. Ziegler, M.D. Ziegler, and J.P. Biersack. Srim the stopping and range of ions in matter (2010). *Nuclear Instruments and Methods in Physics Research Section B: Beam Interactions with Materials and Atoms*, 268:1818–1823, 2010. 19th International Conference on Ion Beam Analysis.

[12] J.W.T. Spinks and R.J. Woods. *An introduction to radiation chemistry*. Wiley, 1990.

[13] PASTINA Barbara. *Etude sur la radiolyse de l'eau en relation avec le circuit primaire de refroidissement des réacteurs nucléaires á eau sous pression.* PhD thesis, Universite de Paris-SUD U.F.R. Scientifique d'Orsay, 1997.

[14] TRUPIN-WASSELIN Virginie. *Processus primaries en chimie sous rayonnement. Influence du Transfert d'Energie Linéique sur la radiolyse de l'eau.* PhD thesis, Universite de Paris-SUD U.F.R. Scientifique d'Orsay, 2000.

[15] Ferradini, Christiane and Jay-Gerin, Jean-Paul. *Canadian Journal of Chemistry*, 77(9):1542–1575, 1999.

[16] Yoneho Tabata, Yasuo Ito. *CRC Handbook of radiation chemistry.* CRC Pr, 1991.

[17] Frank Krumeich. Properties of Electrons, their Interactions with matter and Applicaitons in Electron Microscopy. Technical report, Laboratory of Inorganic Chemistry.

[18] Nuclear Data Center tables, Brookhaven national laboratory, available from the WEB at http://www.nndc.bnl.gov/.

[19] Le Caër S. Water Radiolysis: Influence of Oxide Surfaces on H_2 Production under Ionizing Radiation. *Water*, 3(1):235–253, 2011.

[20] Swiatla-Wojcik, Dorota and Buxton, George V. Modeling of radiation spur processes in water at temperatures up to 300 °C. *The Journal of Physical Chemistry*, 99(29):11464–11471, 1995.

[21] V. Cobut and J.-P. Jay-Gerin and Y. Frongillo and J.P. Patau. On the dissociative electron attachment as a potential source of molecular hydrogen in irradiated liquid water. *Radiation Physics and Chemistry*, 47(2):247 – 250, 1996.

[22] Xing L. Yan and Ryutaro Hino, editor. *Nuclear Hydrogen Production Handbook (Green Chemistry and Chemical Engineering)*. CRC Press, 1 edition edition, March 2011.

[23] Nikola and Getoff. Radiation chemistry and the environment. *Radiation Physics and Chemistry*, 54(4):377 – 384, 1999.

[24] D. M. Bartels, M. T. Craw, Ping Han, and A. D. Trifunac. Hydrogen/deuterium isotope effects in water radiolysis. 1. the mechanism of chemically induced dynamic electron polarization generation in spurs. *The Journal of Physical Chemistry*, 93(6):2412–2421, 1989.

[25] Frongillo Y, Fraser M J, Cobut V, Goulet T, Jay-Gerin J P and Patau J P. Evolution of the species produced by slowing down of fast protons in liquid water: simulation based on the independent reaction times approximation. *J. Chim. Phys.*, 96:93–102, 1996.

[26] Weldon G. Brown and Edwin J. Hart. Effect of ph on oxygen(3p) atom formation in .gamma.-ray irradiated aqueous solutions. *The Journal of Physical Chemistry*, 82(24):2539–2542, 1978.

[27] V. Cobut, Y. Frongillo, J.-P. Patau, T. Goulet, M.-J. Fraser and J.-P. Jay-Gerin. Monte carlo simulation of fast electron and proton tracks in liquid water - I. physical and physicochemical aspects. *Radiation Physics and Chemistry*, 51(3):229 – 243, 1998.

[28] Ping Han and D.M. Bartels. H/D isotope Effects in Water Radiolysis. 4. The mechanism of $(H)_{aq} \rightleftharpoons (e^-)_{aq}$ Interconverison. *J. Phys. Chem.*, 96:4899–4906, 1992.

[29] G H Olivera, C Caraby, P Jardin, A cassimi, L Adoui and B Gervais. Multiple ionization in the earlier stage of water radiolysis. *Phys. Med. Biol.*, 43:2347–2360, 1998.

[30] LaVerne, Jay A. and Pimblott, S. M. New Mechanism for H_2 Formation in Water. *The Journal of Physical Chemistry A*, 104(44):9820–9822, 2000.

[31] LaVerne, Jay A. and Pimblott, Simon M. Scavenger and time dependences of radicals and molecular products in the electron radiolysis of water: examination of experiments and models. *The Journal of Physical Chemistry*, 95(8):3196–3206, 1991.

[32] Ianik Plante. A Monte-Carlo step-by-step simulation code of the non-homogeneous chemistry of the radiolysis of water and aqueous solutions - Part II: calculation of radiolytic yields under different conditions of LET, pH, and temperature. *Radiat Environ Biophys*, 50:405–415, 2011.

[33] Jintana Meesungnoen, Jean-Paul Jay-Gerin, Abdelali Filali-Mouhim, samlee Mankhetkorn. Monte-Carlo calculation of the primary $H^\bullet$ atom yield in liquid water radiolysis: effet of radiaiton type and temperature. *Chemical Physics Letters*, 335:458–464, 2001.

[34] Aryeh H. Samuel and John L. Magee. Theory of Radiation Chemistry. II. Track Effects in Radiolysis of Water. *The Journal of Chemical Physics*, 21(6):1080–1087, 1953.

[35] Schwarz H. A. Application of the Spur Diffusion Model to the Radiation Chemistry of Aqueous Solutions. *The Journal of Chemical Physics*, 73(6):1928–1937, 1969.

[36] Appleby A. and Schwarz H. A. Radical and Molecular Yields in Water Irradiated by γ Rays and Heavy Ions. *The Journal of Chemical Physics*, 73(6):1937–1941, 1969.

[37] LaVerne, Jay A. Track Effects of Heavy Ions in Liquid Water. *Radiation Research*, 153:487–496, 2000.

[38] B. Gervais and M. Beuve and G.H. Olivera and M.E. Galassi. Numerical simulation of multiple ionization and high LET effects in liquid water radiolysis. *Radiation Physics and Chemistry*, 75(4):493 – 513, 2006.

[39] Michael A.J. Rodgers Farhataziz. *Radiation chemistry: principles and applications.* VCH Publishers, 1987.

[40] Burns W. G. and Moore P. B. Water radiolysis and its effect upon in-reactor zircaloy corrosion. *Radiat. Eff.*, 30:233–242, 1976.

[41] Yokohata A. and Tsuda S. A slovated electron formed the water by the irradiation of the recoil particles of $^{10}B(n,\alpha)^{7}Li$ and $Li(n,\alpha)T$. *Bull. chem. Soc. Jap.*, 47:2869–2870, 1974.

[42] J. A. La Verne. The production of OH radiacals in the radiolysis of water with He ions. *Radiat. Res.*, 118:201–210, 1989.

[43] Miller N. Radical yield measurement in irradiated aqueous solutions II. Radical yields with 10.9-MeV Deuterons, 21.3-MeV and 3.4-MeV alpha particles, and $^{10}B(n, \alpha)^{7}Li$ recoil radiations. *Rad. Res.*, 9:633–646, 1958.

[44] Ned E. Bibler. Dose Rate Effects in the Steady and pulse Radiolysis of Liquid Chloroform. *The Journal of Chemical Physics*, 75(16):2436– 2442, 1971.

[45] Schwarz H. A. A Determination of Some Rate Constants for the Radical Process in the Radiation Chemistry of Water. *J. Phys. Chem.*, 66:255–262, 1962.

[46] B.G. Ershov and A.V. Gordeev. A model for radiolysis of water and aqueous solutions of H_2, H_2O_2 and O_2. *Radiation Physics and Chemistry*, 77(8):928 – 935, 2008.

[47] Zorica D. Draganić Ivan G. Draganić. *The Radiation Chemistry of Water*. 1971.

[48] Christiane Ferradini and Jean-Paul Jay-Gerin. The Effect of pH on Water Radiolysis: A Still Open Question - A Minireview. *Res. Chem. Intermed.*, 26 (No.6):549–565, 2000.

[49] Swiatla-Wojcik, Dorota. Computation of the effect of pH on spur chemistry in water radiolysis at elevated temperatures. *NUKLEONIKA*, 53(Supplement 1):31–37, 2008.

[50] Vincent Cobut and Catherine Corbel and Jean Paul Patau. Influence of the pH on molecular hydrogen primary yields in He_2^+ ion tracks in liquid water. A Monte Carlo study. *Radiation Physics and Chemistry*, 72:207 – 215, 2005. <ce:title>Christiane Ferradini Memorial Issue</ce:title>.

[51] Narongchai Autsavapromporn, Jintana Meesungnoen, Ianik Plante, and Jean-Paul Jay-Gerin. Monte Carlo simulation sutdy of the effects of acidity and LET on the primary free-radical and molecular yields of water radiolysis - Application to the Fricke dosimeter. *Canadian Journal of Chemistry*, 85:214–229, 2007.

[52] A.J. Elliot and D.M. Bartels. The Reaction set, rate sonstants and g-Values for the Simulation of the Radiolysis of Light Water over the Range 20°C to 350°C Based on Information Available in 2008. Technical report, Atomic energy of Canada Limited, 2009.

[53] Roth, Olivia and LaVerne, Jay A. Effect of pH on H_2O_2Production in the Radiolysis of Water. *The Journal of Physical Chemistry A*, 115(5):700–708, 2011.

[54] Trupin V., Frongillo Y., Baldacchino G., Le Parc D. et Hikel B. Détermination de constantes de vitesse de réactions de recombinaison de radicaux. *J. Chem. Phys.*, 96:30–34, 1999.

[55] Plante I. A Monte-Carlo step-by-step simulation code of the non-homogeneous chemistry of the radiolysis of water and aqueous solution. Part I: theoreticla framework and implementation. *Radiat Environ Biophys*, 2011.

[56] Herve du Penhoat M. A. and Meesungnoen J. and Goulet T. and Filali-Mouhim A., mankhetkorn S. and Jay-Gerin J. P. Linear-energy-transfer effects on the radiolysis of liquid water at temperatures up to 300°C- a Monte-Carlo study. *Chemical Physics Letters*, 341:135 – 143, 2001.

[57] Herve du Penhoat M. A., Goulet T., Frongillo Y., Fraser M. J., Bernat P., and Jay-Gerin J. P. Radiolysis of Liquid Water at Temperatures up to 300°C: A Monte Carlo Simulation Study. *The Journal of Physical Chemistry A*, 104(50):11757–11770, 2000.

[58] Stefanic, Igor and LaVerne, Jay A. Temperature Dependence of the Hydrogen Peroxide Production in the γ-Radiolysis of Water. *The Journal of Physical Chemistry A*, 106(2):447–452, 2002.

[59] David M. Bartels. Comment on the possible role of the reaction $H^{\bullet} + H_2O \rightarrow H_2{+}OH$ in the radiolysis of water at high temperatures. *Radiation Physics and Chemistry*, 78(3):191 – 194, 2009.

[60] A . J. Elliot, M. P. Chenier et D . C Ouellette. Temperature dependence of g values of H20 and D20 irradiated with low linear energy transfer radiation. *J . Chem. Soc. Faraday Trans.*, Vol. 89:1193–1197, 1993.

[61] Eillot A. J., Chenier M. P., Ouellette D. C. and Koslowsky V. T. Temperature Dependence of g-Values for Aqueous Solutions Irradiated with 23 MeV $^2H^+$ and 157 MeV $^7Li^{3+}$ Ions Beams. *J. Phys. Chem.*, 100:9014–9020, 1996.

[62] Dorota Swiatla-Wojcik and George V. Buxton. Modelling of linear energy transfer effects on track core processes in the radiolysis of water up to 300 °C. *J. Chem. Soc., Faraday Trans.*, 94(15):2135–2141, 1998.

[63] Hochanadel C. J. and Ghormley J. A. Effect of temperature on the decomposition of water by gamma rays. *Radiation Research*, 16:653–660, 1962.

[64] Robert R. Hentz, Farhataziz, David J. Milner and Milton Burton. γ Radiolysis of Liquids at High Pressures. I. Aqueous Solutions of Ferrous Sulfate. *J. Phys. Chem.*, 46(8):2995–3000, 1967.

[65] Robert R. Hentz, Farhataziz, David J. Milner and Milton Burton. γ Radiolysis of Liquids at High Pressures. III. Aqueous Solutions of Sodium Bicarbonate. *J. Chim. Phys.*, 47(2):374–377, 1967.

[66] Robert R. Hentz, Farhataziz, and David J. Milner. γ Radiolysis of Liquids at High Pressures. IV. Primary Yields in Neutral Aqueous Solutions. *J. Phys. Chem.*, 47:4856–4867, 1967.

[67] Robert R. Hentz, Farhataziz, and David J. Milner. γ Radiolysis of liquids at High Pressures. V. Reaction of the Hydrated Electron with Water. *J. Phys. Chem.*, 47(12):5381–5384, 1967.

[68] Robert R. Hentz and Glarence G. Johnson Jr. γ Radiolysis of liquids at High Pressures. VII. Oxidation of Iodide Ion by Hydrogen Atoms in Aqueous Solutions. *J. Phys. Chem.*, 51(3):1236–1241, 1969.

[69] Robert R. Hentz and Ronald J. Knight. γ Radiolysis of liquids at High Pressures. VIII. Primary Yields at 8.7 kbar and Reactions of the Hydrated Electron with H_2O and H_3O^+. *J. Phys. Chem.*, 52(5):2456–2459, 1970.

[70] P. Ausloos, R. Gorden, Jr., and S.G. Lias. Effect of Pressure in the Radiolysis and Photolysis of Methane. *J. Phys. Chem.*, 40(7):1854–1860, 1964.

[71] Sava Lukac. *Radiolysis of N-Pentane in the Gas Phase.* PhD thesis, Ecole Polytechnique Federale de lausanne, 1978.

[72] Allen, A. O. and Hochanadel, C. J. and Ghormley, J. A. and Davis, T. W. Decomposition of Water and Aqueous Solutions under Mixed Fast Neutron and γ-Radiation. *The Journal of Physical Chemistry*, 56(5):575–586, 1952.

[73] Hochanadel C. J. Effects of Cobalt γ-Radiation on Water and Aqueous Solutions. *J. Phys. Chem.*, 56:587–594, 1952.

[74] Chien C. Lin. *Radiochemistry in Nuclear Power Reactors.* The National Academies Press, 1996.

[75] Alam M. S., Kelm M., Rao B. S. M., Janata E. Reaction of $H^{\bullet}$ with H_2O_2 as observed by optical absorption of perhydroxyl radicals or aliphatic alcohol radicals and of $^{\bullet}OH$ with H_2O_2. A pulse radiolysis study. *Radiation Physics and Chemistry*, 71:1087–1093, 2004.

[76] Hayon E. Radiolysis of Air-Free Aqueous solutions of Hydrogen Peroxide. *Trans. Faraday Soc. I*, 60:1059–1067, 1967.

[77] Garbett K., Henshaw J., Sims H. E. Hydrogen and oxygen behaviour in PWR primary coolant. 85. In *Water Chemistry in Nuclear Reactor System 8, British Nuclear Energy Society.*, 2000.

[78] Kotchaphan Kanjana and Kyle S. Haygarth and Weiqiang Wu and David M. Bartels. Laboratory studies in search of the critical hydrogen concentration. *Radiation Physics and Chemistry*, 82:25 – 34, 2013.

[79] Janik, Dorota and Janik, Ireneusz and Bartels, David M. Neutron and $\beta\gamma$ Radiolysis of Water up to Supercritical Conditions. 1. $\beta\gamma$ Yields for H2, $H^{\bullet}$ Atom, and Hydrated Electron. *The Journal of Physical Chemistry A*, 111(32):7777–7786, 2007. PMID: 17645317.

[80] Haygarth, Kyle and Bartels, David M. Neutron and β/γ Radiolysis of Water up to Supercritical Conditions. 2. SF6 as a Scavenger for Hydrated Electron. *The Journal of Physical Chemistry A*, 114(28):7479–7484, 2010.

[81] David M. Bartels, Jim Henshaw, Howard E. Sims. Modeling the critical hydrogen concentration in the AECL test reactor. *Radiation Physics and Chemistry*, 82:16–24, 2013.

[82] Takiguchi Hideki, Ullberg Mats and Uchida shunsuke. Optimization of Dissolved Hydrogen Concentraion for Control of Primary Coolant Radiolysis in Pressurized Water Reactors. *Journal of NUCLEAR SCIENCE and TECHNOLOGY*, 41(5):601–609, 2004.

[83] TAKIGUCHI Hideki, TAKAMATSU Hiroshi, UCHIDA Shunsuke , ISHIGURE Kenkichi, NAKAGAMI Motonori and MATSUI Makoto . Water Chemistry Data Acquisition, Processing, Evaluation and Diagnostic Systems in Light Water Reactors. *Journal of NUCLEAR SCIENCE and TECHNOLOGY*, 41 (2):214 – 225, 2004.

[84] Allen, A. O. *The radiation chemistry of water and aqueous soluitons.* Princeton, N. J., Van Nostrand, 1961.

[85] Pastina, Barbara and LaVerne, Jay A. Hydrogen Peroxide Production in the Radiolysis of Water with Heavy Ions. *The Journal of Physical Chemistry A*, 103(11):1592–1597, 1999.

[86] Pastina, Barbara and LaVerne, Jay A. Effect of Molecular Hydrogen on Hydrogen Peroxide in Water Radiolysis. *The Journal of Physical Chemistry A*, 105(40):9316–9322, 2001.

[87] B. Pastina, J. Isabey and B. Hickel. The influence of water chemistry on the radiolysis of the primary coolant water in pressurized water reactors. *Journal of Nuclear Materials*, 264:309–318, 1998.

[88] B. Pastina, J. Isabey and B. Hickel. Water radiolysis: the influence of some relevant parameters in PWR nuclear reactors. *Water Chemistry of Nuclear Reactor Systems 7.*, pages 153–155, 1996.

[89] Mahmoud N. S., El-Fawal M. M. and Gadalla A. A. Assessment of Cooling Water Chemistry on the Safety of Water Cooled Power Reactors. *Nature and Science*, 9(9):27–34, 2011.

[90] AREVA. Primary coolant chemistry: Fundamental aspects & improvements/ optimizations. In *Fundamentals & Developments*, Nov. 2008.

[91] Kabakchi S. A., Shubin V. N., Dolin P.I. Effect of pH on the stationary concentration of radiolysis products of aqueous solution of oxygen. *High Energ. Chem.*, 1(2):148–153, 1967.

[92] Bielski B. H. J., Cabelli E., Arudi A.L. Reactivity of HO_2/O_2^- Radicals in Aqueous Solution. *J. Phys. Chem. Ref. Data*, 14(4):1041–1100, 1985.

[93] Matheson M. S. and Rabani J. Pulse Radiolysis of Aqueous Hydrogen Solutions. I. Rate Constants for Reaction of e_{aq}^- with Itself and Other Trasients. II. The Interconvertibility of e_{aq}^- and H. *The Journal of Chemical Physics*, 69(4):1324–1335, 1965.

[94] Pinede J.R.E.T. and Schwartz S. D. Prottein dynamics and catalysis: the problems of transition state theory and the subtlety of dynamic control. *Phil. Trans. R. Soc. B*, 361:1433–1438, 2006.

[95] Allen A. O. and Rothschild W. G. Studies in the Radiolysis of Ferrous Sulfate Solutions. Effect of Oxygen Concentration in 0.8 N Sulfuric Acid. *Radiation Research*, 7:591–602, 1957.

[96] You D. Bilan des mesures de solubilité des ferrites mixtes, private communication. Technical report, CEA, 1998.

[97] Domae M., Chitose N., Zuo Z., Katasumura Y. Pulse radiolysis study on redox reactions of zinc (II). *Radiation Physics and Chemistry*, 56:315–322, 1999.

[98] Buxton G.V., Sellers R. M. and McCracken D. R. Pulse Radiolysis Study of Monovalent Cadmium, Cobalt, Nickel and Zinc in Aqueous Soltuion. *J. Chem. Soc., Faraday Trans. 1*, 76:1464–1476, 1972.

[99] Hyder M. L. The Radiolysis of Aqueous Nitrate Solutions. *The Journal of Physical Chemistry*, 69(6):1858–1865, 1965.

[100] Yakabuskie P. A., Joseph J. M., Stuart C. R. and Wren C. Long-Term γ-Radiolysis Kinetics of NO_3^- and NO_2^- Solutions. *The Journal of Physical Chemistry A*, 115:4270–4278, 2011.

[101] Cunningham J. Radiation Chemistry of Ionic Solids. IV. Modifying Nitrate Radiolysis in Crystals by Compression. *The Journal of Physical Chemistry*, 70(1):30–39, 1966.

[102] Hiroki, Akihiro and Pimblott, Simon M. and LaVerne, Jay A. Hydrogen Peroxide Production in the Radiolysis of Water with High Radical Scavenger Concentrations. *The Journal of Physical Chemistry A*, 106:9352–9358, 2002.

[103] Schwarz H. A. The Effect of Solutes on the Molecular Yields in the Radiolysis of Aqueous Solutions. *J. Am. Chem. Soc.*, 77(19):4960–4964, 1955.

[104] Bernhardt P. V. and Lawrance G. A. Pulse radiolysis of mono-and binuclear copper (II) marcrocyclic complexes. *Polyhedron*, 10(12):1373–1377, 1991.

Chapter 3

Corrosion issues of 316L under Primary PWR Conditions

Stainless steel 316L is one of the most widely used materials in the industry. In the case of PWRs, stainless steel, such as 304 and 316L are largely employed, for the internal core, for the pressure boundary pipings and etc. Their good mechanical properties and corrosion resistance serve very well for the extreme conditions of PWRs.

However, corrosion-related materials failures, particularly stress corrosion cracking, is one of the major issues concerning the ageing of PWRs. Irradiation can create point defects like vacancies, interstitials, dislocations, and result in significant changes in microstructure and mechanical properties. In addition, irradiation may also alert resistance to stress corrosion cracking. The specific corrosion cracking, IASCC (Irradiation-Assisted Stress Cracking Corrosion) alone with other types may occur in the PWRs, IGSCC (Inter-granular Stress Corrosion Cracking) and PWSCC (Primary Water Stress Corrosion Cracking), can totally affect and damage the nuclear materials, including the stainless steels.

Our study is in based on stainless steel 316L under primary PWR conditions, thus this chapter is focused on its oxide film, and the two specific style of the most common stress corrosion cracking, IGSCC: the water chemistry related corrosion, PWSCC, and the radiation-related corrosion, IASCC. In some cases, not only high temperature, but also room temperature have been studied in order to get a complete understanding of the corrosion issue.

3.1 The Oxide on 316L Formed under Primary PWR Water

Stainless steel 316, is an iron-based alloy containing at least 16% chromium and 10% nickel. The chemical compositions are indicated in Tab.3.1. The added molybdenum element to 316 gives a higher resistance to pitting and crevice corrosion and also to stress corrosion cracking in chloride environments compared to 304 which does not contain molybdenum. 316L refers to a low carbon content ($< 0.03\%$) and is a material suitable for welding which is not the case for the 316 with higher carbon content. On the other hand, 316L offers an excellent toughness, higher creep, stress to rupture and tensile strength at elevated temperatures, Tab.3.2.has listed some mechanical and physical properties.

	Cr	Ni	Mo	Mn	Si	N	P	C	S	Fe
Min.	16.0	10.0	2.0	-	-	-	-	-	-	balance
Max.	18.0	14.0	3.0	2.0	0.75	0.10	0.045	0.03	0.03	balance

Table 3.1: Composition ranges for 316L stainless steels, (%mass.).

Density (kg/m^3)	Elastic Modulus (GPa)	Thermal Conductivity (W/m.K)	Elec Resistivity (nΩ.m)	Tensile Stress (MPa) min	Yield Stress 0.2% Proof (MPa) min
8×10^3	193	16.3 (at 100°C) 21.5 (at 500°C)	740	485	170

Table 3.2: Some mechanical and physical properties for 316L stainless steel.

Without any doubt, the excellent corrosion resistance of 316L is due to the oxide layer formed on its surface, which will be detailed in the following section.

3.1.A Double-Layer Structure Oxide

During the last thirty years, many works have been done in order to understand the mechanism of oxide formed on austenitic stainless steel under high temperature in aqueous solution [1–6]. Gradually, the influence of different chemical conditions have also been studied, such as lithium, dissolve hydrogen and so on [7, 8].

The latest studies [7–10] show that the oxide formed on 316L under PWR conditions is identified as a **double-layer structure**, called inner and outer layers. They are two spinel oxide layers, an iron-based outer layer on top of a chromite-based inner layer. The inner layer is often regarded as the protective layer while the outer layer is not so protective [2].

3.1.A.1 Composition

According to the studies, the compositions of the oxide film formed on stainless steel 316L may be changed, as demonstrated by different papers [6–10]. This is due to the fact that the mechanism of the corrosion process is sensitive to the environment. A small change in the corrosion environment may cause a change in the oxide layer.

Nevertheless, a proposition for both inner and outer layer has been made, spinel oxide $\mathbf{AB_2O_4}$. **A** refers to a divalent cation and **B** represent a trivalent cation, where A = Ni(II) and Fe(II), B = Fe(III) and Cr(III). For both layers, Ni and Cr maintain the same valence, Ni(II) and Cr(III), whereas Fe may have both valence, (II) and (III) [4–7, 11].

Indeed, the dominant component for either inner or outer layer is different.

- Outer layer is mainly magnetite, Fe_3O_4 and AB_2O_4 in which Fe(III) is the main constituent for **B** and Fe(II) also takes the majority parts over Ni(II) for **A**. In result, the AB_2O_4 can be written as $(Ni_{1-x}Fe_x)(Fe_yCr_{1-y})_2O_4$, where x and y are certainly much larger than 0.5, especially for y, which may very well equals 1.

- Inner layer is mostly chromite, Cr_2O_3 [7, 12, 13] and AB_2O_4 in which Cr(III) is the main constituent for **B**. Concerning **A**, Fe(II) still holds the dominant position against Ni(II). Thereby, it can also be written as $(Ni_{1-x}Fe_x)(Fe_yCr_{1-y})_2O_4$, where $x > 0.5$ while $y < 0.25$.

Briefly, it has been considered for a long time that the outer layer is more or less like $NiFe_2O_4$ and $FeCr_2O_4$ for the inner layer. Da Cunha Belo *et al.* [7] divided the oxide film formed on 316L under primary PWR conditions into three regions, the outermost is $Ni_{0.75}Fe_{2.25}O_4$ spinel oxide, the intermediated is both $Ni_{0.75}Fe_{2.25}O_4$ and Fe_3O_4 spinel oxide, and the innermost is the chromium-rich oxide.

Last but not least, Terachi *et al.* have identified a nickel enrichment at the metal/oxide interface of 316 under simulated PWR primary conditions, as shown in Fig.3.1 (a), (b) and (c). The nickel enrichment at the metal/oxide interface is somehow more than twice that of its bulk concentration in the matrix [14]. This phenomenon is also observed before in nickel-based alloys [15], there the mechanism or the explanation is based on the diffusion of chromium to form a chromium-rich oxide and thus the chromium depleted area is below this layer. Consequently, nickel enriches at oxide/ metal interface.

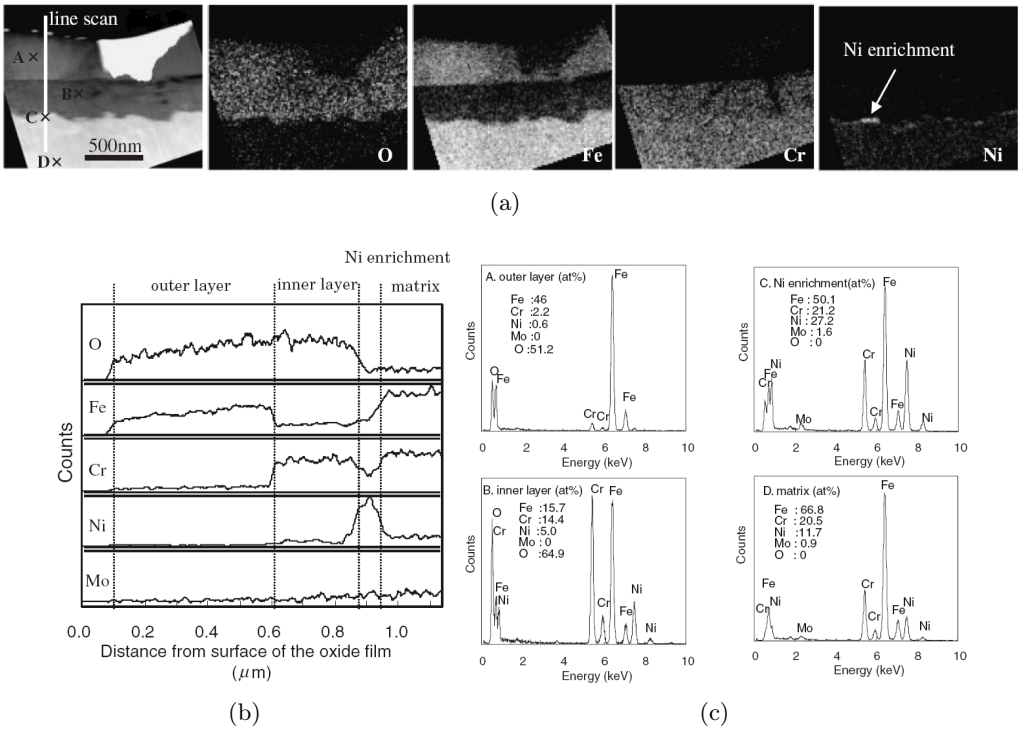

Figure 3.1: TEM/EDS analysis of an oxide film formed on 316L under simulated PWR primary water at 320°C for approximately 500 hours : (a) TEM elemental maps of oxygen, iron, chromium, and nickel; (b) EDS line scan (shown in (a) leftmost figure) profiles penetrates the oxide film; (c) EDS analysis for chemical composition of the oxide and the matrix (A, B, C and D shown in (a) leftmost figure) [14].

.

3.1.A.2 Structures

The structure of the oxide formed on the 316L stainless steel under primary PWR conditions is a spinel structure, which can be proved by a XRD analysis shown in Fig.3.2. No peak of hydroxide or corundum was observed, and hence the oxide film consisted only of the spinel structures.

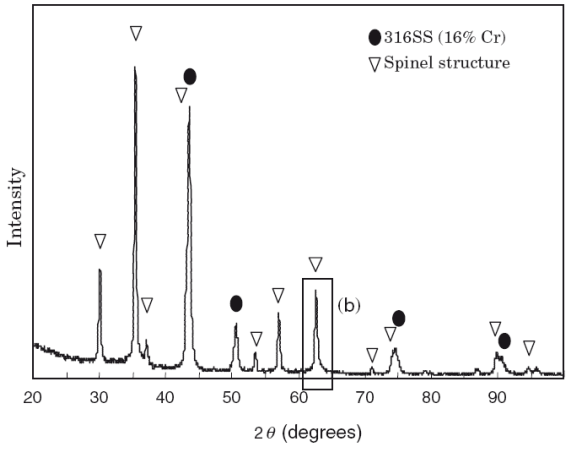

Figure 3.2: XRD analysis of 316L formed under PWR simulated conditions, 320°C, 380 hours [10].

3.1.A.3 Morphology

The morphologies of the oxide film formed on 316L austenitic stainless steel under primary PWR conditions have also been investigated for a long time [4, 8]. The iron-rich outer oxide, formed on top of the original alloy and grows outwards in the solution; while the Cr-rich inner oxide is growing into the original alloy surface.

The outer layer is considered porous and loosely adherent, it is mainly in the form of crystals or crystallites depending on the size. Generally, they show a well-defined polyhedral shapes. However the sizes and the densities are related to plenty of parameters: content of Cr, corrosion process, etc. In general, the crystal size varies from hundreds of nanometers to several micrometers. The inner oxide is a non-porous, tightly adherent layer, considered as a compact structure [5]. This thin inner chromium-rich layer plays an important role on the passivity of stainless steel. It is often regarded as the *protective layer*.

The equivalent thickness of the oxide film of 316L formed under primary PWR conditions is normally from 200 to 500 nm, whereas the passive film formed on it at ambient temperature is only a few nanometers [11]. It depends on the temperature of the environment and also the duration spent at this temperature.

As represented by Terachi *et al.* [10], a TEM/EDS analysis, Fig.3.3, on the cross-section of the oxide film on 316L under simulated PWR primary conditions. It illustrates the double layer structure oxide film:

- Fig.3.3 (a) clearly shows the difference in crystal size between outer and inner layer: the outer layer has big polyhedral shape particles while the inner layer is actually formed by extreme fine particles.
- Fig.3.3 (b) indicates that the oxide film formed is a spinel oxide: the spot pattern for outer layer (upper figure) and the ring pattern for inner layer (lower figure). They both match spinel pattern, however the different sizes of particles cause the divergence in the pattern.
- Fig.3.3 (d) gives the EDS analysis on a selected zone (indicated in (a), a zoom image in (c)) for estimating the chemical compositions: more chromium-rich oxide formed in the inner layer and the outer layer is mainly iron-rich.

In summary, we consider that the outer oxide layer is iron-rich and discontinuous; the inner layer is continuous and rich in chromium oxide, as depicted in Fig.3.4, which shows a simplified schematic view of the oxide film formed on 316L under simulated PWR primary conditions.

3.1.B The Mechanism of Oxide Formation

3.1.B.1 Formation of the Outer Layer

Lister *et al.* [2] have proposed and established a mechanism model of the oxide formation on austenitic stainless steel. More precisely, it focused on the outer layer formation. It relates the formation of the oxide layer to the corrosion products release. Among Fe, Ni and Cr, Fe is the easiest cation which can

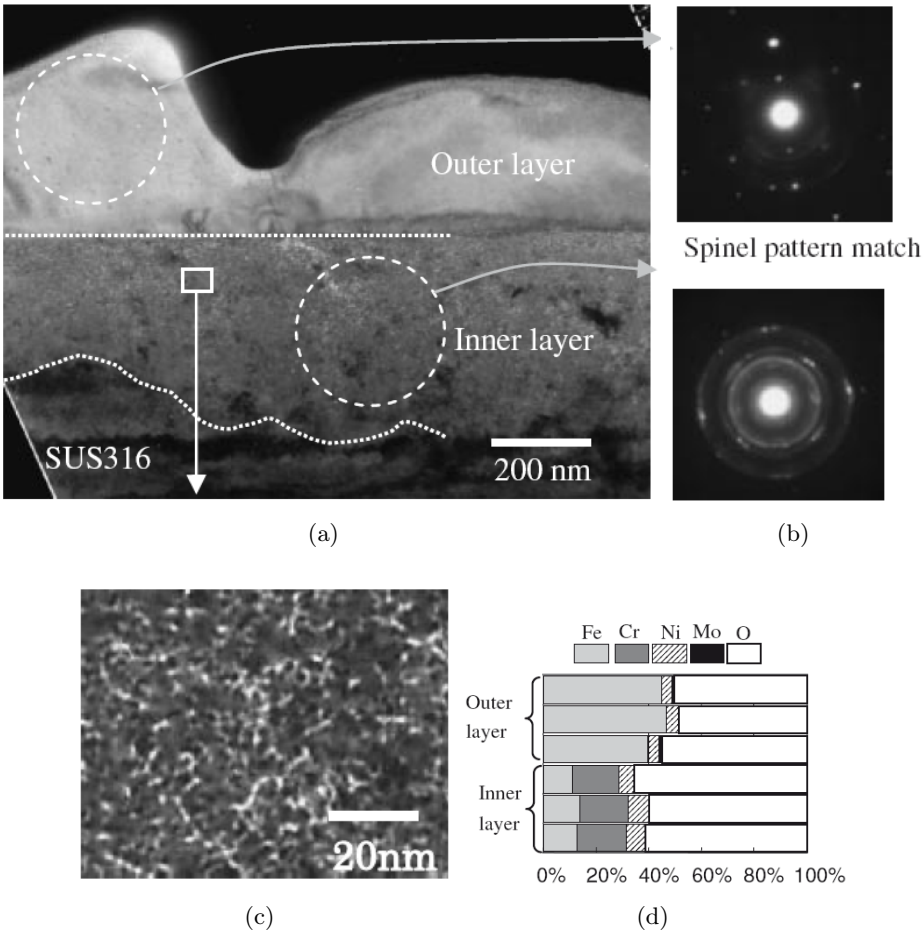

Figure 3.3: TEM and EDS analysis of 316L formed under PWR simulated condition, 320°C, 380 hours : (a) TEM image of both layers; (b) Electron diffraction pattern; (c) A zoom TEM image in inner layer; (d) Estimated chemical composition [10].

.

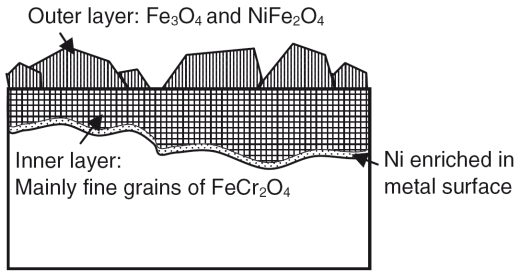

Figure 3.4: Simplified diagrammatic sketch of cross section of the oxide film on 316L austenitic stainless steel under simulated PWR primary water [10].

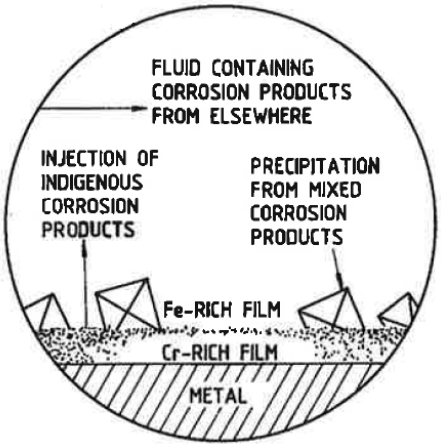

Figure 3.5: Schematic diagram of the mechanism model from Lister *et al.* [2].

diffuse through the oxide and be released into solution [16]. Therefore, the model proposed by Lister has ruled out the Ni and Cr release under consideration. The release of iron can be divided into three directions:

- release to the water;
- take part in the precipitation/re-deposition process of the iron-rich outer layer;
- diffuse through and be fixed in the chromium-rich oxide at the metal-oxide interface;

According to Lister, the outer layer can not be formed in corrosion product free water. Moreover, once the inner layer of chromium rich layer has been well established, the outer layer may be suppressed [2]. On the contrary, if the water is saturated with corrosion products, the scale of iron and nickel oxide in the outer layer will become important. Evidence has been found for the Nickel alloy 690, the dissolution or iron and nickel from the alloy prevails even at the very beginning stage of corrosion [17]. Similar results for 316L stainless steel are pronounced [18], the presence of the outer layer can be found in a extremely short duration after exposed to the environment.

The re-deposition process of the outer layer has been explained by Berge [19]. It is considered that the growth of magnetite crystallite on the surface is actually from the decomposition of ferrous hydroxide in aqueous solution at high temperature, through the **Schikorr Reaction** Eq.3.1.

$$3Fe(OH)_2 \rightleftarrows Fe_3O_4 + H_2 + 2H_2O \tag{3.1}$$

It formally describes the conversion of the Fe(II) hydroxide into Fe(II, III) oxide, whereas $Fe(OH)_2$ appears to be unstable above 85°C [20]. Though under PWR primary water, the existence of nickel hydroxide have both been found [21–23]. Therefore, through the same type reaction of Schikorr reaction, the spinel oxide nickel ferrite can be formed with magnetite as precipitates on the outer layer during the re-deposition process [24].

3.1.B.2 Formation of the Inner Layer

Recently, with the observation of nickel enrichment in the oxide/metal interface [14, 25], Lozano-Perez *et al.* [25] have explained the oxidation process for the inner layer into three steps:

1. chromium oxide starts to be formed when oxygen diffuses in and iron diffuses out while nickel stays static, the growth of inner and outer oxide layer inward and outward, respectively;
2. chromium oxide grows and pushes away nickel when the atomic concentration of oxygen reaches above 20%, and result in accumulation of nickel at the oxide/metal interface;
3. when the atomic concentration of oxygen is about 30%, nearly no nickel remains in the oxide while chromium oxide keeps growing.

It implies the oxidation of the inner layer is initially incomplete until it pushes aways all the nickel from the inner oxide and then forms a *real* chromium oxide.

In addition, Perrin *et al.* [26] have explained the growth of the inner oxide layer is due to oxygen diffusion along the grain boundary of the oxide.

In conclusion, the formation of the oxide layers can be divided into two parts: the re-deposition process of the iron oxide for the outer layer; and oxidation process of the chromium for the inner layer. The diffusion of oxygen along the grain boundaries of the oxides may play a significant role in the kinetics of the process. It may be emphasised that this mechanism is mainly observed in high temperature oxidation. It is completely different from the formation of the oxide layer on stainless steel at room temperature which is well described by the Point Defect Model.

3.1.B.3 Point Defect Model

The **Point Defect Model** (PDM) was proposed and has been well developed by MacDonald [27, 28]. It recognizes both the growth of the barrier oxide layer into the metal via the generation of oxygen vacancies at the metal/film interface and the dissolution of the barrier layer at the film/solution interface.

As verbalised in Fig.3.6(a), the PDM model bases on bilayer passive film formed on the metal surfaces, which is highly disordered. The outer porous precipitated film may incorporate with anions and/or cations in the solution. Between the inner passive film and substrate alloy, the transmission of ions is also possible, and may even pass through the barrier layer. Simple cation vacancies are produced at the film/solution interface, then are consumed at the metal/film interface. Anion vacancies are formed at the metal/film interface and consumed at the film/solution interface.

Further explanation of PDM has been delineated in Fig.3.6(b), it separates the process into three cases:

- The cation vacancy can be produced via Mott-Schottky pair reaction and may also be autocatalytic generated. If the annihilation reaction is not capable of consuming all the cation vacancies arriving at the metal/film interface, they will condense and eventually lead to the local detachment of the film.

- The regeneration of isolated oxygen vacancies may be caused by the submergence of cation vacancies into film. Besides, the anion-catalysed generation of cation vacancies at the film/solution interface can also penetrate into the film. As a result, vacancy condensation occurs at the metal/film interface.

- The oxygen and cation vacancies may remain on the surface and finally coalesce to destroy the lattice at the film/solution interface.

Combining these processes, a layout of different stages of pit nucleation is represented in Fig.3.6(c). At steady-state, a balance is established between the film formation at the metal/film interface and the dissolution at the film/solution interface. With the condensation of vacancies, the film will gradually detached locally from the metal. When the film ruptures, more metal dissolves into solution. Afterwards, the competition occurs between the re-passivation and stable pit growth.

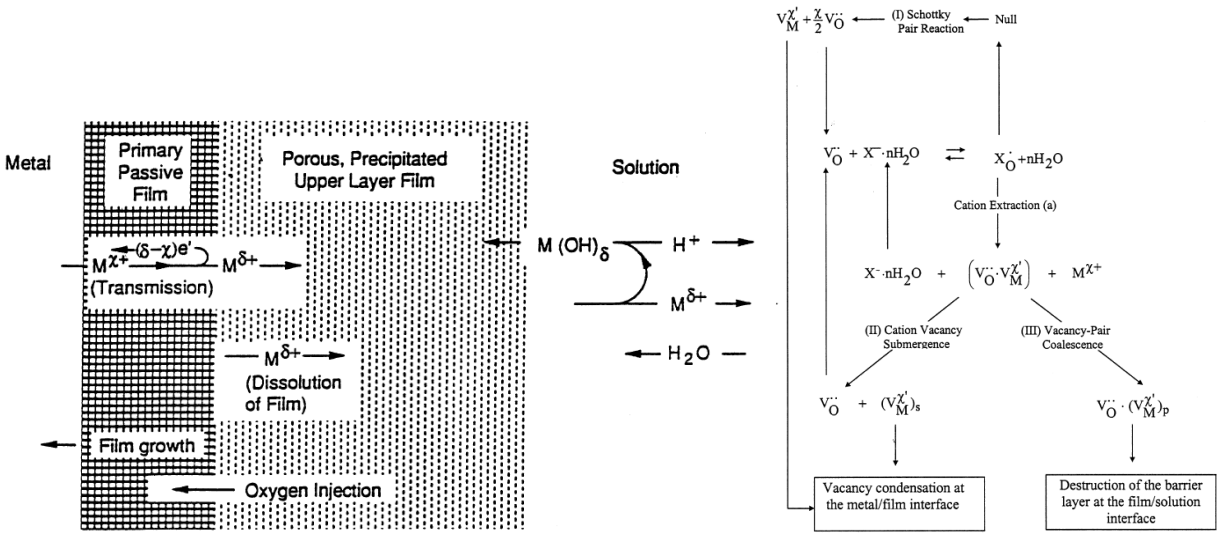

(a) (b)

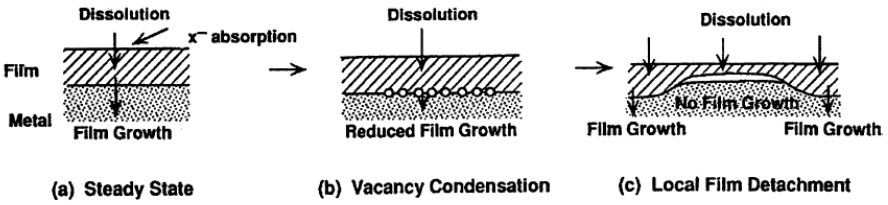

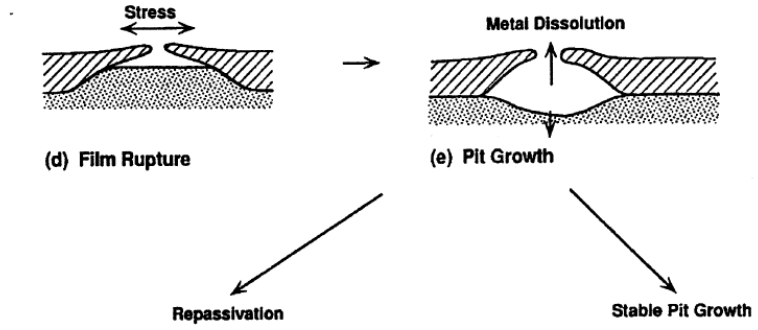

(c)

Figure 3.6: Schematic sketch of **Point Defect Model**: (a) process of bilayer passive film formation on the metal surfaces; (b) proposed reactions leading to cation vacancy condensation at the metal/film, film/solution interfaces and eventually the passivity breakdown; (c) cartoon outlining various stages of pit nucleation according the PDM [27].

A recent study of MacDonald [29] has demonstrated that the potential drop across the metal/film interface decreases linearly with increasing film thickness. And this potential drop is actually responsible for the oxygen vacancy formation reaction. In other words, the thinner the film, the easier oxygen vacancy formation occurs. However, this conclusion is dragged out when the oxygen vacancies are the dominant defect within the film.

In conclusion, the PDM describes metal/film/solution system under a steady state. Point defects like oxygen, cation, anion vacancies and interstitial cations can be generated, transported and consumed under the influence of concentration and potential gradient in the oxide and its boundaries with metal and solution.

3.1.B.4 Corrosion Kinetics

The thickness of the oxide layer and average crystallite size increase with exposure time to the primary PWR water environment [4].

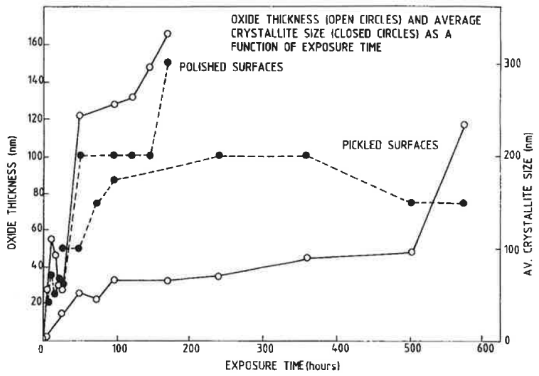

Figure 3.7: Oxide thickness (○) and average crystallite size (●) as a function of exposure time: upper zone polished surface; lower zone pickled zone [4].

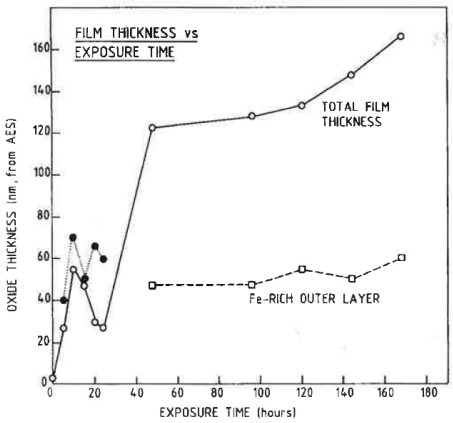

Figure 3.8: Oxide thickness versus exposure time (polished surface), crystallite size has been taken into account after 24 hours in same scales for thickness [4].

Fig.3.7 & Fig.3.8 show the increase of thickness and average crystallite size of 304 with exposure time under high temperature coolant. Due to the similarity of composition between 304 and 316, the conclusion obtained on 304 can also be adapted to 316L. In the first 10 hours, the initial nucleation and growth of both outer and inner layers take place very rapidly. As a result, both thickness and crystallites size increase sharply and reach a first maximum. Between 10 to 24 hours, the dissolution and the growth of the outer oxide film compete with each other, thus the curve somewhat decreases. From 24 to 48 hours, the thickness and crystallite sizes increase sharply again. Afterwards, the increase of nucleation and growth of the oxide film is stabilised. At this time, the overall growth of the oxide can be considered as a dynamic balance between precipitation and dissolution.

Tapping *et al.* [4] have estimated an expression for the corrosion rate, Eq.3.2 where d is the equivalent thickness of the oxide, k_p is the appropriate rate constant, t is the duration of exposure and $n = 0.53$:

$$d = k_p t^n \tag{3.2}$$

Since the value of n was close to 0.5, Tapping *et al.* considered that the growth kinetic of the oxide film has a parabolic character. Thereby, Terachi *et al.* [10] have used the parabolic equation, as written in Eq.3.3, in which d and t have the same definitions, whilst k_p is the parabolic rate constant.

$$d^2 = 2k_p t \tag{3.3}$$

Indeed, this equation corresponds to a growth mechanism with a rate limited by diffusion. The formation of the outer layer is considered as a re-deposition process of iron, nickel and chromium dissolved in solution due to general corrosion of stainless steels. It grows with outward diffusion of metal. Reversely, the inner layer is a protective, mostly chromium oxide, formed spontaneously on the metal surface. It grows with inward diffusion of oxygen.

3.1.C The Electronic Properties of Oxide Film

The oxide film formed on the austenitic stainless steel is often regarded as semiconductor under primary PWR conditions.. Many studies have been done in this domain and hence the electronic properties have been well described [3, 7, 13, 30–32].

The characterisation of electronic properties, also called semiconducting properties, can be interpreted by capacitance measurements (Mott-Schottky approach) and photoelectrochemical measurements [30].

3.1.C.1 Capacitance mesurements (Mott-Schottky approach)

The capacitance behaviour of a passive film-electrolyte interface is similar to the one of a semiconductor-electrolyte interface, and the semiconductor-electrolyte interface is equivalent to that of a semiconductor-metal Schottky junction. The effect of the applied electrochemical potential **U** on capacitance value is described by the **Mott-Schottky** equation [33]:

$$\frac{1}{C^2} = \frac{1}{C_H^2} + \frac{1}{C_{SC}^2} = \frac{2}{\varepsilon\varepsilon_0 q N_q}\left(U - U_{FB} - \frac{kT}{q}\right) \tag{3.4}$$

The measured capacitance includes two parts: C_{SC}, space charge capacitance, is related to the applied potential (**U**) through the classical Mott-Schottky equation; the other is C_H, the contribution of the Helmholtz layer capacitance, which can not be neglected if the passive film is considered as heavily doped. In Eq.3.4, N_q is the density for donor and acceptor, ε the dielectric constant of the passive film, ε_0 the vacuum permitivity, q the elementary charge (-e for electrons and +e for holes), k the Boltzmann constant, T the absolute temperature and U_{FB} the flat band potential. From the slope and the intercept given by the plot between C^{-2} and U, the doping density and the flat band can both be determined, respectively. Furthermore, the characteristics of the semiconductor can also be obtained.

Noting that for the study of electronic properties, **U** is usually used as the applied potential while in most corrosion studies, **E** is always regarded as the corrosion potential.

3.1.C.2 Photoelectrochemical measurements

The photoelectrochemical behaviour of the oxide film is examined by determining the photocurrent, generated under illumination, as a function of the incident light energy [7, 13]. The Gärtner model [34] is the most used calculation together with some simplifications [35], such as neglecting the contribution to the photocurrent of the hole-electron pair formed in the bulk region. Therefore, the quantum efficiency η, the ratio between the photocurrent (I_{ph}) and the incident photon flux Φ_0 can be expressed by the Eq.3.5:

$$\eta = \frac{I_{ph}}{\Phi_0} = qAw\frac{(h\nu - E_g)^n}{h\nu} \tag{3.5}$$

where A is a constant, q the elementary charge, w the space charge layer thickness, E_g the band gap energy and $h\nu$ the photon energy. The value of n depends on the type of transition between the valence band and the conduction band. It is actually corresponds to indirect transitions in crystallised solids and to non-direct transitions in amorphous materials. In the case of passive films, the value of n is linked to indirect transitions in crystalline band structure model, and the most appropriate value is equal to 2 obtained by the analysis of the photocurrent spectra.

It has been pointed out that the photocurrent spectra depends on the oxidation time [36]. The increase oxidation duration can cause a higher disordered structure of the oxide and results in a decrease of photocurrent.

3.1.C.3 The Electronic Structures

Fig.3.9 shows the basic electronic properties of the oxide film formed on 316L in a high temperature environment, (a) is for the capacitance measurement and (b) is for the photoelectrochemical behaviour, they describe:

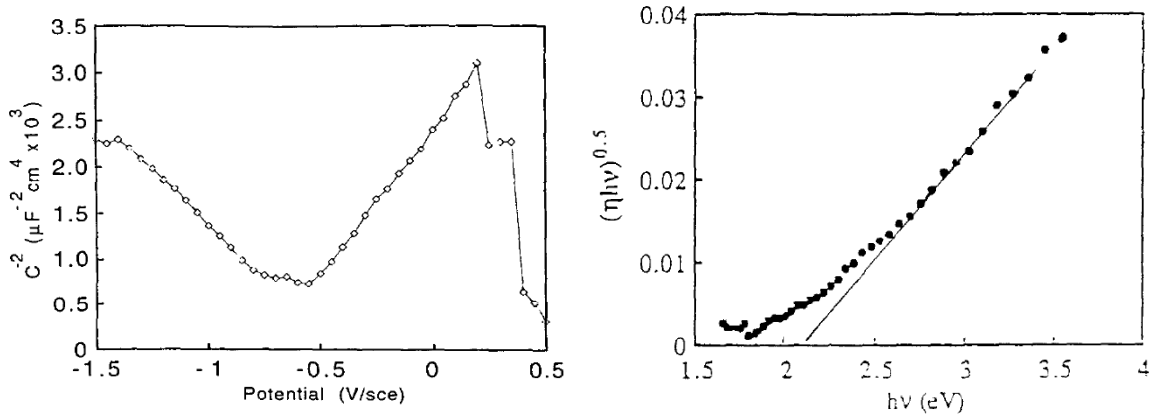

(a) (b)

Figure 3.9: Electronic characteristic of the oxide film formed on 316L austenitic stainless steel after 2000 hours exposure at 350°C under a simulated primary PWR environment : (a) Plot of $1/C^2$ (Mott Schottky plot) as a function of applied potential U, at 1580 Hz; (b) Plot of $(\eta h\nu)^{0.5}$ versus the incident light energy $h\nu$ [7].

- Fig.3.9(a): The positive slope in the region above −0.5 V indicates n-type semiconductiong properties; otherwise, the negative slope in the region below this potential meaning p-type semiconducting properties. Linking the two types of spinel oxide to the electronic properties, it has been demonstrated by Hakiki *et al.* [12] that the inner Cr-rich layer is p-type and outer Fe-rich layer on the other hand is n-type. They have well described the capacitance behaviour:

  1. the oxide film can take up ions and electrons from the metallic substrate, and cause a space charge region raised up at the metal/oxide film interface;
  2. the oxide film can produce a second space charge region on contact with the electrolyte.

  Therefore, this electronic structure is often regarded as a classical heterojunction [33]. The existence of both positive and negative slopes in the capacitance plot demonstrates the double structure of the oxide film formed on the 316L stainless steel. At about 0 V, another change can be noticed, which is considered as an important feature of the Mott-Schottky plot. It implies the existence of a second donor level for the n-type, formed by Fe^{2+} ions placed in the octahedral sites of the unit cell of the spinel oxide.

- Fig.3.9(b): The band gap energy obtained from the intercept of the straight line with the photon energy axis, which is about 2.3 eV for the passive film at room temperature, 2 eV for the thick passive film formed at high temperature. This slight difference here may mostly due to the higher iron oxide content [7]. The best fit for the band gap energy is a Fe-Cr oxide, $FeCr_2O_4$, however its theoretical value is actually 3.0 eV [37]. It is explained that the decrease may due to the presence of Fe(II) in the $FeCr_2O_4$ [38].

Furthermore, the n-type Fe-rich oxide and the p-type Cr-rich oxide are represented as inverse and normal spinel oxides, respectively. They are not immiscible, thus a significant difference can be noticed between inner and outer layer [5].

Based on the thesis study of Marchetti-Sillans [24], it was demonstrated that Cr_2O_3 and $Ni_{1-x}Fe_xCr_2O_4$ formed under primary PWR conditions are n-type semiconductors.

As mentioned, the electronic structure of oxide film can be regarded as a p-n heterojunction. It is composed of a p-type Cr-rich oxide at the metal/film interface and a n-type Fe-rich oxide at the oxide/electrolyte interface. Fig.3.10 represents this electronic structure in two cases, one is for applied **U** less than flat band potential, the other is the inverse case:

- $\mathbf{U} < \mathbf{U}_{\mathrm{FB}}$: Inner chromium rich layer is served as Schottky barrier showing the p-type semiconductivity, which means the inner layer is in a dominant position while outer iron rich layer is in a condition of accumulation ohmic contact;

- $\mathbf{U} > \mathbf{U}_{\mathrm{FB}}$: Outer iron rich layer take the dominant, thus the oxide act as the n-type semiconductor whilst inner layer is in the condition of accumulation ohmic contact.

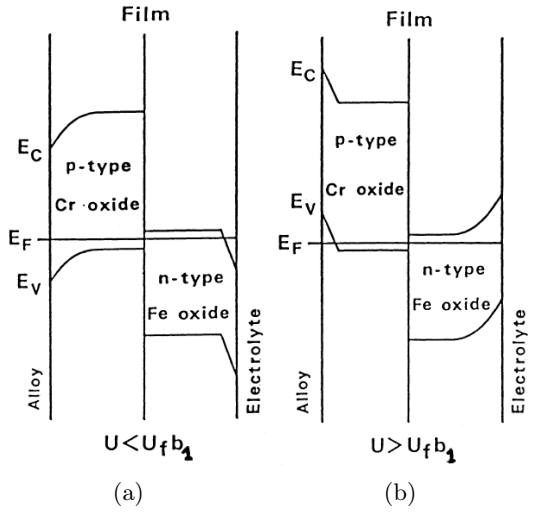

Figure 3.10: Schematic sketch of the electronic structure model of oxide film formed on 316L: (a) U $<$ U_{FB} (≈ -0.5 V); (b) U $>$ U_{FB} (≈ -0.5 V) [13].

.

3.1.C.4 Difference between Thick and Thin Passive Films

Considering the semiconducting properties of oxide film, one often distinguishes either the passive film as thick or thin, even though they show very similar electrochemical behaviours, as portrayed in Fig.3.11. For the same alloy, the passive oxide film is thicker when it is formed at high temperature than at room temperature under the same environment. In general, chromium oxide is often referred as the passive film for stainless steel.

One explanation for the difference between these passive oxide film is linked to their carrier concentration, or doping density, in which thin passive film formed at room temperature is much higher than the thicker one formed at higher temperature like in primary PWR conditions [13].

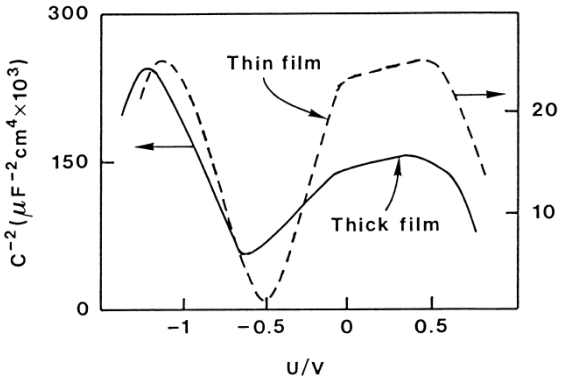

Figure 3.11: Plot of $1/C^2$ as a function of applied potential U on stainless steel: an thick passive film formed at high temperature in aqueous environment; a thin passive film formed at 0.6 V/SCE in borate buffer solution at room temperature [13].

Another explanation [31] relates this difference to the iron ions transport process through the inner chromium layer from the alloy. For oxide film, both Fe^{2+} can transport over tetrahedral and octahedral sites in the inner spinel oxide. However, when Cr content is high, which is the case for thin

passive film, chromium will certainly occupy most of the sites in the spinel and leave the transport of iron only through the grain boundaries. Nevertheless, the oxygen transport is always favoured by both passive films.

In addition, the transport of iron ions also links with the conductivity in the inner layer. The hopping conduction in the octahedral sites caused by Fe^{2+} may turning back the normal band conduction with a high content Cr in the spinel. These may explain the slight difference in semiconducting behaviours between the thick and thin passive films.

Briefly, studying the electronic structure is a good way to get a better understanding of the oxide film formed on the alloy. In our case, the oxide film formed on austenitic stainless steel 316L under primary PWR conditions reveals semiconducting properties, reflected as a p-n heterojunction.

3.1.D Influence of Different Parameters on The Oxide

Many parameters can influence the oxide film formed on 316L under PWR primary conditions. Some of them have direct effect on the oxide film, others may affect the electrochemical behaviour formerly and then influence the oxide film afterwards.

However, the basic double layer structure, the main composition and the basic electronic structure for both inner and outer layer will not change tremendously.

3.1.D.1 Influence of Boron and Lithium

The presence of boron and lithium in the primary PWR water are well-known for their role in neutron capture and adjusting pH, respectively. Concerning the oxide film formed on the 316, their influences are not so noticeable.

Boron The presence of boron dose not affect the oxide formed on stainless steel such as 316L [39]. As shown in Fig.3.12 [10], the oxide structure were considered as the same for both [B]=500 ppm and [B]=2300 ppm, which can lead to a different pH for both cases. Nevertheless, a NanoSIMS analysis [40] has otherwise demonstrated the boron tends to accumulate in the Cr-rich oxide, next to the interface of inner and outer layer. The absence of boron traces in other analysis [25] may be explained by the preparation process which can somewhat influence the outer part of oxide layer. Indeed, their extremely low concentration in the oxide film may also be another explanation.

Lithium The presence of lithium atoms on the oxide of stainless steel on the other hand has been proven by using the technique of Atom-Probe Tomography (APT) [25]. In Fig.3.13, the rose points represent the lithium atom detected by APT: they can be traced throughout the oxide to the oxide-metal interface. The presence of Li atom can be correlated to the CrO_2, as demonstrated in Fig.3.13 (d), nevertheless the concentration of Li was quite low, 200ppm. It was considered that Li atoms incorporate into the Cr-rich oxide and it may be explained by the changes in oxide conductivity when varying the Li content in the water [41].

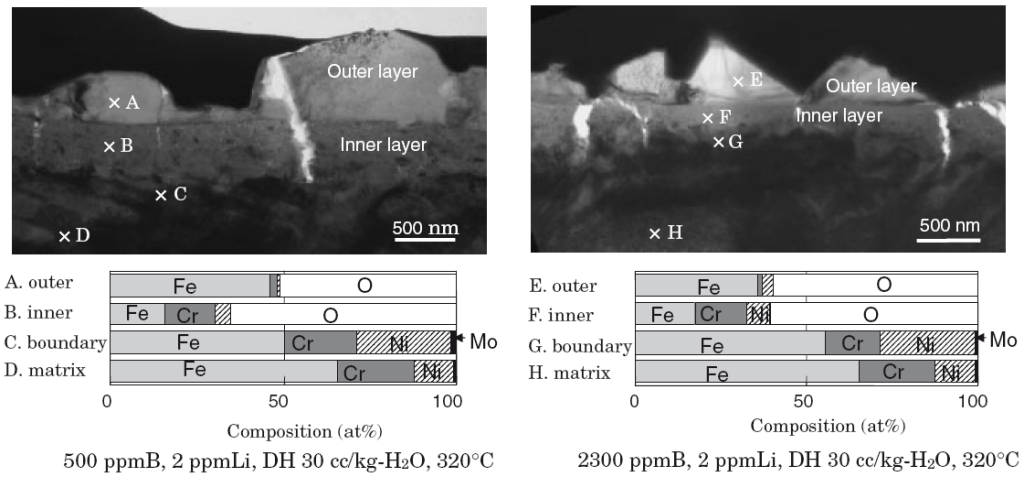

Figure 3.12: TEM images and EDS analysis on oxide film formed on 316 stainless steel under primary PWR water with 2 ppm Lithium and 30 cc/kg dissolved hydrogen at 320°C: [B] = 500 ppm (left) and [B] = 2300 ppm (right), [10].

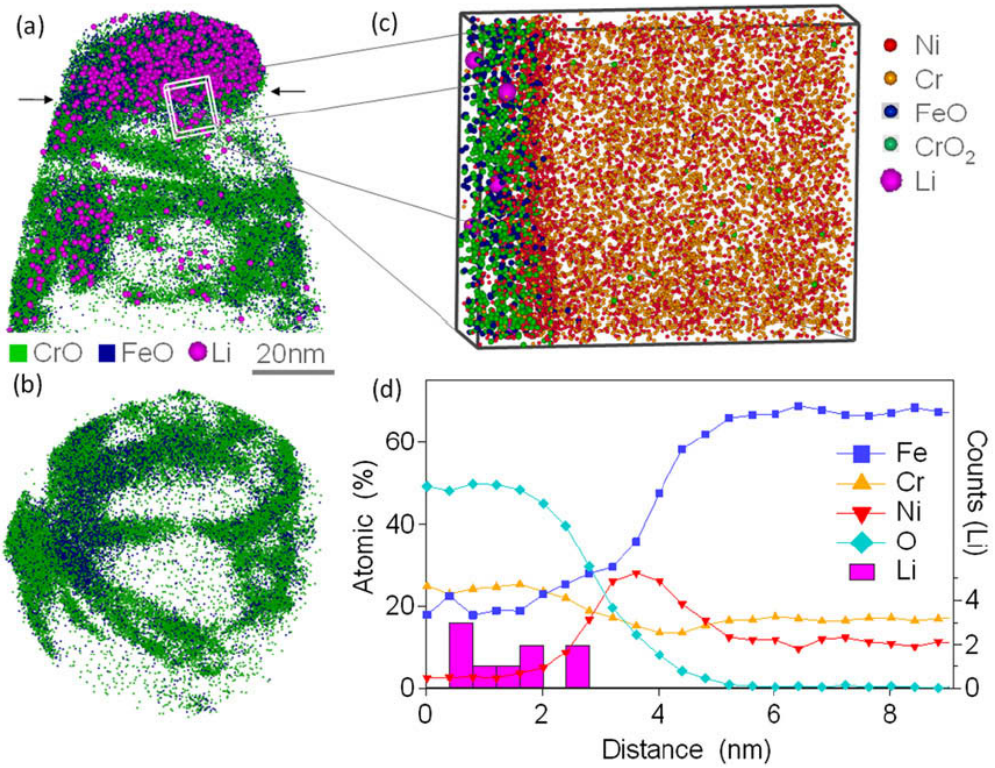

Figure 3.13: APT reconstruction demonstrating "atom by atom" on oxide formed on stainless steel 316L under primary PWR condition: (a) the cap and sub-interface oxides; (b) top-view of sub-interface region removing the cap oxide; (c) sub-volume showing the detected species taken form the cap-oxide-metal interface, square region in figure(a); (d) concentration profile across the oxide-metal interface using Proxigram analysis [25].

3.1.D.2 Influence of pH

Recent studies [42, 43] were performed on the oxide film formed on the nickel-based alloy and the stainless steel 304 at high temperature in aqueous solution and borated and lithiated water, respectively. For the stainless steel under primary PWR water, they show that in the safe E-pH zone ($pH_{300°C}$ between 7.7 and 9.1), the density and the size of crystallite (Fe-rich oxide) decrease with the increasing pH while the composition of the inner protective layer (Cr-rich oxide) is nearly not affected.

However, the influence of pH cannot be simply dragged out, because it depends on other parameters, such as temperature, the aqueous chemistry, etc.

According to Montemor *et al.*, chromium decreases in the oxide film formed on 316L and nickel based alloy in high temperature aqueous environment, from pH 8 to 10 [13]. They say that the pH effect does not change the double layer structure of oxide film. However, the composition may be somewhat affected. Iron content in the oxide film seems to increase with the increasing pH. Consequently, the chromium concentration decreased in the oxide film leads the oxide film less protective. The same conclusion was made for alkaline media at room temperature, in which pH varies from 9 to 13 [44].

Carmezim *et al.* [45] have studied the electrochemistry, the composition and the semiconducting properties of the passive film on austenitic stainless steel 304 at room temperature under different environments contain NaOH, KOH and H_2SO_4 separately in order to achieve different pH, 4.5, 8 and 0.6. They demonstrate that:

- Corrosion potential (E_{corr}) becomes more anodic as pH decreases. Corrosion current depends on pH slightly and it increases with the decreasing pH.
- Chromium oxide strongly depends on the acidic condition, the content of Cr(III) oxide in the oxide film decrease dramatically with the increasing pH, revealing that an enrichment of chromium oxide in a more acid environment. Subsequently, iron oxide enriches when the solution is less acid. In other words, the ratio of Cr/Fe increase significantly with the decreasing of pH, at pH = 0.6, the film is nearly all chromium oxide.
- The capacitance behaviours are different at pH= 4.5 and 8, and the difference is mainly related by the donor density, N_D, it augments with the pH. Therefore, the film is enriched in iron oxide with the increasing pH while the chromium oxide gradually decreases, which is in accordance with the composition study. Nevertheless, pH at 0.6 seems to be too acid to perform a capacitance measurement.

In brief, the influence of pH can be based on the different temperatures and various environments.

3.1.D.3 Influence of surface state

Surface state is an important parameter which can affect the oxide film, more precisely, the substructure under the oxide film. The presence of a recrystallised area under oxide layer has been reported [46]. The surface state, either polished or ground can influence this recrystallised area.

The metal under the oxide layer is recrystallised in a fine elongated nano-grains structure, as pictured in Fig.3.14. The study was done for 304L, but it can also be adapted to our case, 316L. When the surface is rough, the recrystallised area is larger and the oxide layer is relatively thinner.

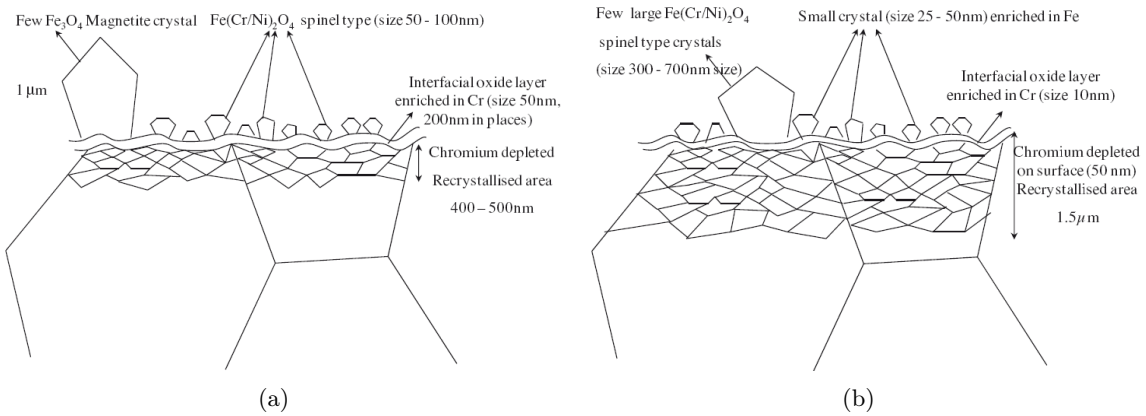

Figure 3.14: Diagrammatic sketch of the oxide formed on a 304L sample under simulated PWR primary water at 340°C for 500 hours: (a) polished surface; (b) ground surface [46].

.

As already shown by Tapping *et al.* in Fig.3.7 [4], the thickness of oxide layer is much higher for polished samples than pickled ones at same exposure time.

3.1.D.4 Influence of Chromium Content

The chromium content in stainless steel causes several related consequences:

- the size of crystal formed on the outer layer;
- the thickness of oxide film;
- the chromium content in the protective oxide scale;
- the corrosion rate.

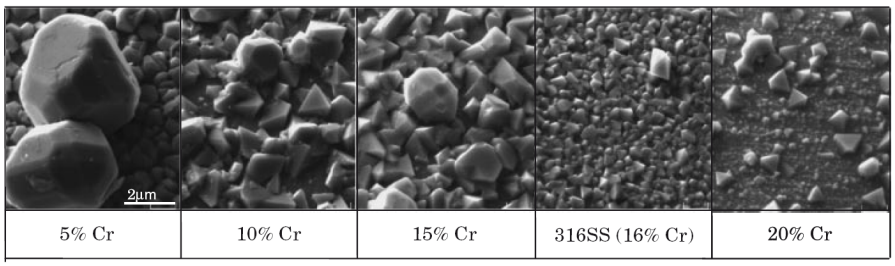

Figure 3.15: SEM images of oxide film after immersion in the primary PWR water at 320°C for 380 hours [10].

Fig.3.15 demonstrates that bigger size of crystal for lower content of chromium. At 5% of Cr, the big crystals may have 4 to 5 μm, and for 316L which has nearly 16% of Cr, the crystal sizes seem to be less than 1 μm. Fig.3.16 shows the relationship between the total oxide film thickness and Cr content which appears to be linear decrease. Other than the morphology and thickness, Fig.3.17 shows that the structure of the spinel oxide may also be affected by chromium content. The peaks shift gradually from Fe_3O_4 to $FeCr_2O_4$ with the increase of Cr% in the alloy.

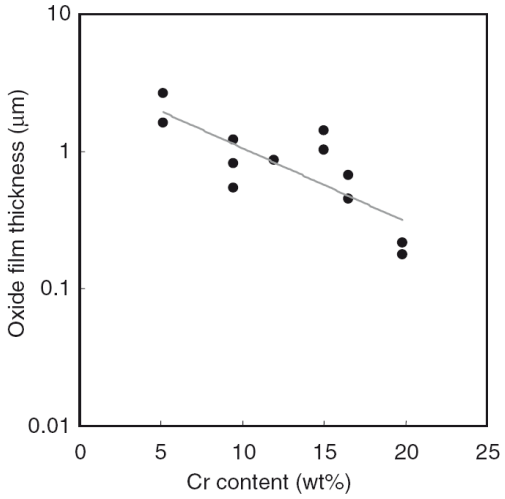

Figure 3.16: Oxide film thickness as a function of Cr content: formed under primary PWR water at 320°C for 380 hours [10].

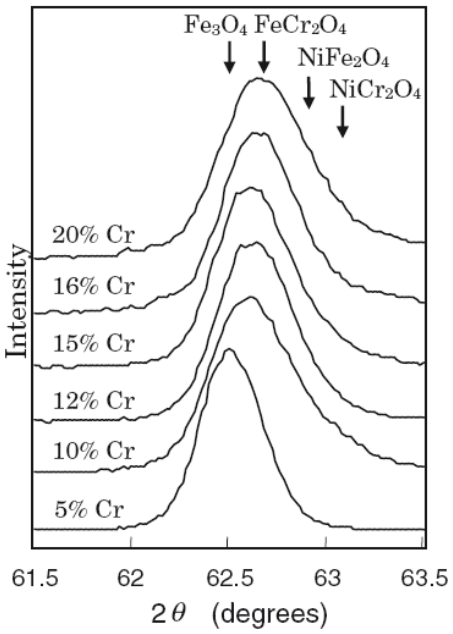

Figure 3.17: XRD analysis of 316L formed under PWR simulated conditions, 320°C, 380 hours: diffraction peaks of the spinel structure for different Cr% content alloy [10].

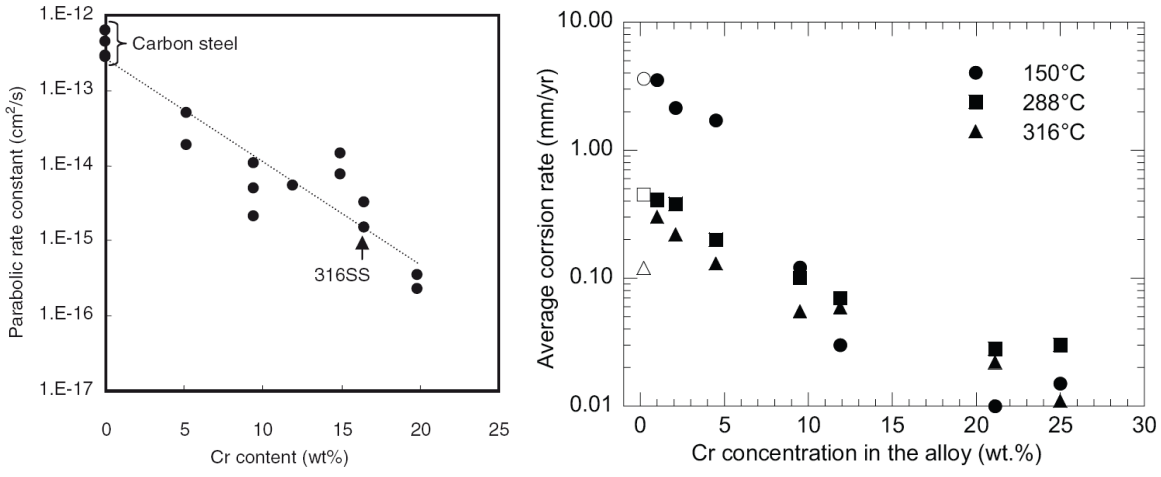

Figure 3.18: The effect of chromium content on the corrosion rate : (a) the parabolic rate constant as a function of Cr% in the alloy under simulated PWR primary condition at 320°C for 380 hours [10]; (b) average corrosion rate of steels as a function of Cr%, in boric acid solution at different temperatures [39].

.

Fig.3.18 (a) & (b) on the other hand give the proof that average corrosion rate decreases with chromium content in the alloy [10, 39]. (a) demonstrates the relationship between Cr% and k_p, which is the parabolic constant in the Eq.3.3. (b) shows directly the corrosion rate of various steels at different temperatures all decrease with chromium content in the alloy. In other words, more chromium in the alloy results in a lower global corrosion rate.

Briefly, the increase of Cr content in the alloy leads to a decrease of oxide film thickness. And the chromium content of the protective oxide scale increased with chromium content in the alloy [10]. Furthermore, the inner chromium-rich layer may not be a continuous and compact structure when Cr% in the alloy is lower than 10% [47]. In summary, the increase of Cr content in the alloy mitigate the corrosion rate. Therefore, in the aspect of corrosion, it is a beneficial effect.

3.1.D.5 Influence of Stress and Strain

Stress and strain have strong influences on the oxide film, and stress cracking corrosion (SCC) susceptibility of austenitic stainless steel can also be traced back to them.

The electrical resistance of oxide film increases with the strain level [8]. Fig.3.19 shows the stress/ strain curve and the dependence of the average contact resistance of the oxide film on 316L on the strain level. It can be identified into three steps of strain levels, 0 - 0.03, 0.03 - 0.08 and 0.08 to 0.18 the end of the experiments showing in the figure:

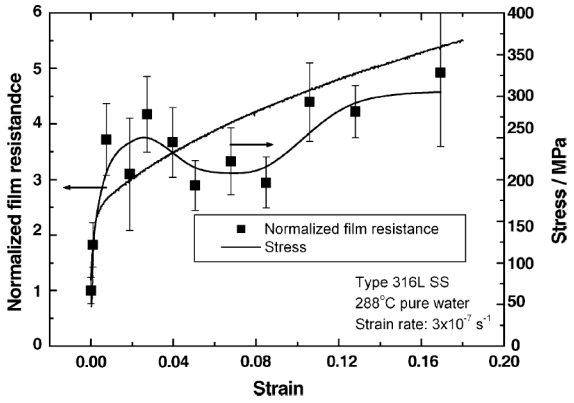

Figure 3.19: Normalised film electrical resistance (left) and stress (right) as function of strain level on stainless steel 316L without cold work, strain level up to 0.18 [8].

- The first maximum of film electrical resistance at strain level around 0.03, is actually correlated to the increase of Cr(III) concentration in the inner oxide layer [48]. Töpfer *et al.* [49] have explained this phenomenon by the conductivity of the inner layer which can actually control and affect the transport of ions and charge through the whole oxide film. As mentioned before, the conductivity decreases with its Cr content in the inner layer and hence the resistance increases.
- The decrease of film electrical resistance at strain level between 0.03 and 0.06, is linked to the decrease of Cr content in the whole oxide film [50]. It can be explained by the increase of the density of both donors and acceptors and leads to an increase in conductivity and thus a decrease in resistance [51].

- The last increase above 0.08 strain level is possibly linked to artefacts of the measurements [8].

In short, the inner layer seems to be more sensitive to the mechanical stress than the outer layer. Furthermore, it also shows that stress may enhance the vacancy concentration in the oxide layer and leads to an augmentation of conductivity [51].

The morphology and thickness between stressed and unstressed oxide film are quite similar. Though the size and the density of grains are relatively bigger on the unstressed oxide film, and thus result in the difference of the thickness. With the presence of cold work (CW), it may enlarge the slight difference [8].

The composition of oxide film is influenced by the stress. For the inner layer, the content of Cr(III) is higher in the unstressed and without cold work surface. It is because the transpassive dissolution of chromium may be enhanced by the strain. For the outer layer, the ratio of Fe/Ni is much higher for the stressed surface than the unstressed one while the cold work does not seems to affect the outer layer significantly. It is thought that the Fe dissolution has also been enhanced by the strain and thus more iron will be deposited on the outer layer.

On the other hand, a recent study [11] says that due to the cold work, the inner Cr-rich oxide is discontinuous, and hence the cold worked materials are less protected. This conclusion is in accordance with the previous interpretation of composition.

Thereby, the susceptibility of SCC can be enhanced by strain hardening. It increases with the increasing cold work and localised plasticity [11, 52]. More precisely, IGSCC is enhanced by strain localisation [53].

3.1.D.6 Influence of Temperature

Temperature is always an important parameter which has a strong effect on the oxide formed. With increasing temperature, the double structure of the oxide film is not affected while the thickness will increase sharply.

Secondly, temperature influences the open circuit potential. With an increase of temperature, the open circuit potential may shift either to a more negative or more positive value until it reaches a steady state, respectively. It has been shown that in lithiated water containing H_2, the open circuit potential goes down [3] while it goes up in a borate buffer solution [31].

Fig.3.20 (a) & (b) illustrates the temperature influence on semiconducting properties [3, 31], (a) is for capacitance measurements and (b) is for photoelectrochemical results.

Temperature (°C)	ambient	50	150	250	350	450
N_D (10^{20} cm^{-3})	2.5	2.6	1.5	0.9	0.5	0.3
N_A (10^{20} cm^{-3})		2.8	2.7	2.3	2.3	2.2

Table 3.3: Donor and Acceptor densities (N_D & N_A) of oxide film formed on 304 stainless steel at different temperature, using the dielectric constant $\varepsilon = 12$ for the calculation [3, 31].

In Fig.3.20(a), it can be noticed that:

- The electronic structure for the oxide film formed on austenitic stainless steel does not changed with the increasing temperature: inner layer, chromium rich oxide, with a p-type semiconductiv-

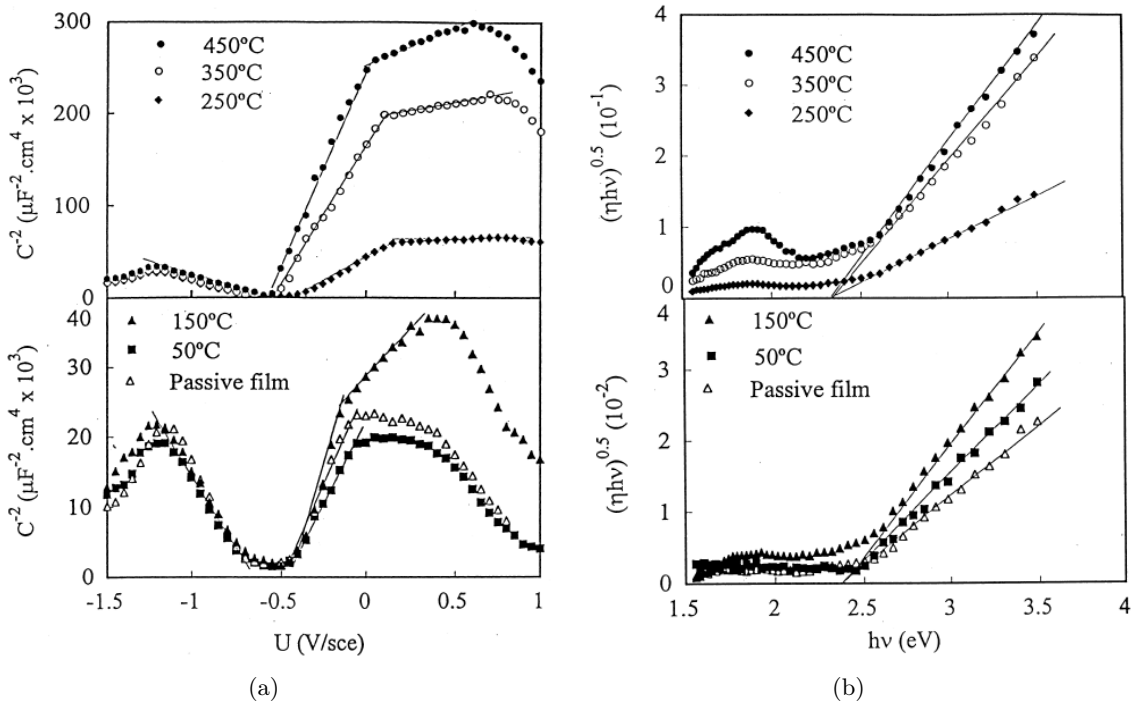

Figure 3.20: The effect of temperature on electrochemical behaviour of oxide formed 304 stainless steel in the temperature range from 50 to 450°C, with the presence of passive film formed at 0.8 V/SCE in borate buffer solution : (a) plot of $1/C^2$ as a function of applied potential U; (b) plot of $(\eta h\nu)^{0.5}$ versus the incident light energy $h\nu$ [31].

ity; outer layer, iron rich oxide, n-type semiconductor. It is still a classical p-n heterojunction, the flat band energy stays at −0.5 V.

- According to the plot and Eq.3.4, estimation of donor and acceptor densities can be done, as exhibited in Tab.3.3. The donor density, N_D, depends on the temperature during the oxide formation, whereas the acceptor density appears to be indifferent. Note that the N_D for passive film is actually close to the one for oxide film formed at 50°C.

- Due to the decrease of N_D, the transport of Fe^{2+} seems to be less important through the oxide film and result in an increase of Fe^{3+} content in the film. In another word, the ratio of Fe^{3+}/Fe^{2+} increases with the temperature of oxide formation.

- The break at 0 V remains with the increasing temperature, it is considered as a second donor level formed by Fe^{2+} ions placed in the octahedral sites in the spinel as mentioned previously. The oxide film can be thought as a semiconductor electrode containing multiple donor level in the bandgap. The changes in the slopes from 150°C to higher temperature, imply that a decrease of the concentration of Fe^{2+}_{oct} in the oxide film, especially between 150 to 250°C.

- The thickness of space charge layer, W, can also be estimated by the expression:

$$C = \varepsilon\varepsilon_0/W$$

where the definition for C, ε, ε_0 are the same as in Eqs.3.4 & 3.5. It has been concluded that the space charge layer in the outer region is closely related to the thickness of iron oxide, meaning the outer oxide layer. Meanwhile, the space charge layer is independent of either the thickness and the temperature. It seems that the inner thickness is not relevant with the temperature of oxide formation.

The quantum efficiency (η) increases with the temperature during the oxide formation, shown in the Fig.3.20(b). As expressed in Eq.3.5, no wonder it augments with the increase of space charge layer, W, and it is the case when temperature rises. The band gap energy is the same for all the temperatures, 2.3 eV, which is also the same value for thin passive film. However, a peak become more significant at about 1.9 eV with the increasing temperature which is associated with transitions from the valence band to the second donor level in the bandgap. Together with the capacitance results, the second donor level is formed by Fe^{2+} place in the octahedral sites in unit cell of the spinel oxide. The intenser peaks imply that the content of Fe^{2+}_{oct} in the oxide film decreases with the increasing temperature. It is in agreement with the capacitance measurements.

The explanation for the increase of quantum efficiency (η) is related to the donor density. The decrease of donor density with temperature also decrease the film defects, and subsequently decrease the electron-hole recombination processes. Therefore, the quantum efficiency (η) become more significant at higher temperature.

3.1.D.7 Influence of Dissolved Hydrogen

The dissolved hydrogen plays an important role on the oxide formation under PWR conditions. In general, it can be distinguished into two parts: the oxide film itself and the electrochemical behaviours of 316L .

The structure and composition of oxide film is not affected by the dissolved hydrogen in the solution, nevertheless the thickness and the corrosion rate of oxide layer appear to increase with dissolved hydrogen [10].

Cation diffusion in the oxide needs to be brought into consideration. According to Dieckmann [49, 54], cation vacancies and cation interstitials are the majority defects at high and low oxygen activities, respectively. The oxygen activity dependence of the tracer diffusion coefficient in magnetite-based spinels can be written as Eq.3.6.

$$D^*_{Me} = D^0_{Me(v)} P^{2/3}_{O_2} + D^0_{Me(I)} P^{-2/3}_{O_2} \tag{3.6}$$

Based on this diffusion equation, V-shaped curves can be obtained in D^*_{Me}. Fig.3.21 illustrates the diffusion rate of Fe at 320°C. And as concluded by Dieckmann, the diffusion of Cr and Fe are governed by cation vacancies at high oxygen activities; otherwise, they are governed by cation interstitials at low oxygen activities. However, in the same conditions, the diffusion of Fe is much more significant than that of Cr.

As explained, when the partial pressure is relatively low, $D_{Fe(I)}$ takeover the dominant position for iron cation diffusion in the spinel which is actually enhanced by the increasing dissolved hydrogen. Therefore, the corrosion rate increased by dissolved hydrogen might be caused by this augmented

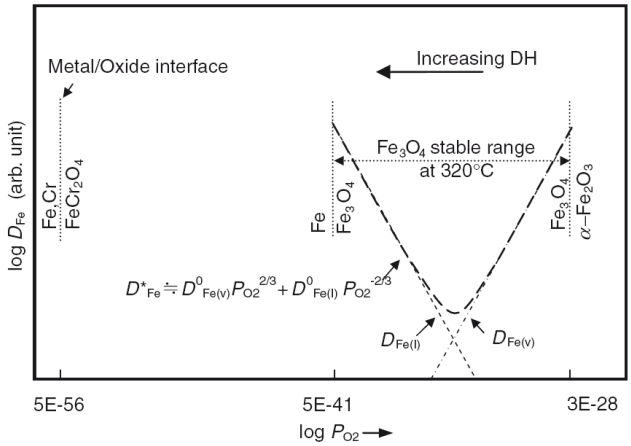

Figure 3.21: Diffusion rate of Fe in spinel oxide versus oxygen partial pressure, calculated for metal/oxide and oxide/oxide interfaces at 320°C [10].

interstitial iron diffusion in the spinel.

From the point view of electrochemical behaviour, there is no direct study the effect of dissolved hydrogen on stainless steel. By comparing with the low-alloy steel [55], and the Alloy 600 [56], several points should be noticed:

- With the increase of dissolved hydrogen, the corrosion potential, E_{corr} becomes more negative;
- With the increase of dissolved hydrogen, cathodic process can be promoted and result in a higher critical and passive current. Therefore, the protective performance of the oxide film can drop dramatically;
- With the increase of dissolved hydrogen, ion diffusion is much easier and the iron release rate may increased as a consequence, and the corrosion may be accelerated subsequently;
- With the increase of dissolved hydrogen at high temperature, more H_2 diffuses through the porous outer layer and comes into the inner protective layer. The more it reacts with, the less stable the oxide film will be. The decrease of stability of oxide film may also enhance the corrosion rate.

3.1.D.8 Influence of other parameters

Other parameters than those detailed before (boron, lithium, pH, dissolved hydrogen, etc.), have influence on the oxide film formed on 316L under primary PWR conditions, such as the dissolve oxygen, Mo, Zn, etc.

Dissolved Oxygen With the increase of dissolved oxygen in high temperature water, spinel oxide seems to be less stable. Furthermore, Cr content in the oxide film is certainly decreased with the increasing dissolved oxygen and the inner layer become less protective due to this Cr dissolution subsequently [57].

Mo For austenitic stainless steel 316L, the content of Mo in the substrate alloy is about $2 \sim 3\%$. Mo is beneficial to promote the corrosion resistance in chloride environments. The presence of Mo brings an enrichment of chromium oxide in the film between 250°C and 450°C [58]. Metallic Mo is also in the oxide/ film interface: it can act as a diffusion barrier for Fe and Cr ions in the oxide [59]. Moreover, Mo affects the oxide capacitance. With the presence of MoO_4^{2-} in the outer layer even in very low concentration, the number of donors in the iron oxide decrease and hence the conductivity. Besides, it ameliorates the defect structure cause by Fe^{2+} of the inner chromium oxide layer [58, 60]. Overall, Mo is a positive effect to against corrosion in chloride environments.

Zn Zn is introduced in the primary PWR water. It has been proved that Zn has a positive effect on the release of cations in the primary medium. It can both incorporate in the inner layer and probably form a new Zn-rich phase in the outer region. The thickness of the oxide film decrease dramatically with the presence of Zn. Due to the Zn hydrolysis reaction, pH can be changed, and results in an important decrease of iron transport in the inner layer. Briefly, Zn is a beneficial element to decrease uniform corrosion and thus to decrease the contaminations of primary circuits by corrosion products [61].

Under primary PWR conditions, more impurities can be found, like chloride, sulphate, radiolytic products which are quite aggressive even though the concentrations are relatively low, few ppb, in order to avoid corrosion risks. With no doubt, the existence of chloride and sulphate can accelerate the corrosion process and in favour of the non-protective rust formation on the outer region [62]. The presence of the radiolytic products, such as hydrogen peroxide, only makes the corrosion issues more seriously, enhances the probabilities of pitting and cracking corrosion [63].

In summary, the oxide of 316L formed under primary PWR water is a double oxide, chromium rich, continuous inner layer and an outer layer is iron rich and porous. It can be regarded as a semiconductor with a classic p-n heterojunction electronic structure. The oxide is sensitive to various parameters during the oxidation process, like temperature, stress, pH, redox and so on.

The oxide film formed on 316L well resists the corrosion, and it is actually the case without considering irradiation. However, in presence of irradiation, this situation can be modified, which will be explained in the following section.

3.2 Stress Corrosion Cracking (SCC)

What is stress corrosion cracking? It is the interaction between corrosion and mechanical stress, and it may produce failures by cracking. This type of failure is called **Stress Corrosion Cracking**, SCC. It has been studied for decades, many processes have been made in order to get a better understanding of this failure. However, the mechanisms of SCC are still under discussion.

Why is SCC so important? SCC is an insidious and tricky corrosion. It can bring a markable loss of mechanical strength with little metal loss. In consequence, the damage of SCC is not evident from inspection, but it can trigger mechanical fast fracture and catastrophic failure of components

and structures. However, the occurrence of SCC acquires at least several parameters simultaneously: a susceptible material, an environment which can cause SCC for this material and a sufficient tensile stress to induce SCC.

There exists several basic models for the mechanism of SCC, for example:

- **Active Path Dissolution:** The probability of the accelerated corrosion is higher along a path than the bulk material which is basically being passive. This path, often refers to the grain boundary, where segregation of impurity elements can make the passivation more difficult to occur. It implies that the whole surface of the material may still remains passive and the grain boundaries have already been corroded. In the way, SCC may occur even without stress by intergranular corrosion.

- **Hydrogen Embrittlement:** Hydrogen atoms can diffuse and dissolve in the metal, subsequently they will assist in the fracture of metal, start with cracks and develop to some mechanical defaults. The cracking under this process may be either trans- or inter- granular. Nevertheless, in the case of austenitic stainless steel, the coefficient of diffusion of hydrogen is relatively low, thus it is thought as immune form the embitterment of hydrogen.

- **Internal Oxidation:** This mechanism of is actually concerned for IGSCC, proposed by Scott and Le Calvar [64]. It occurs when atomic oxygen dissolves into an alloy at the external oxide-metal interface and diffuses into the metal matrix to oxidise a more reactive alloying element than the solvent metal. Under certain temperature range, it becomes intergranular internal oxidation. In the case for cracking, the morphology of nickel separated from chromium oxide, formed ahead of resolvable crack tips and result in the absence of solution impurities [65].

There are many types of SCC, the most discussed in recent decades, without any doubt, are the IGSCC[1] and IASCC[2]. The former one is the SCC without considering irradiation effects. IASCC is otherwise with the presence of irradiation. Recently, a new name, EAC has comes into sight, which is actually meaning Environmentally Assisted Crack. In fact, it includes all the type of SCC together and considers their effects in the same picture, which is exact the case for primary PWR conditions.

3.2.A SCC without Irradiation

SCC without irradiation, mainly refers to TGSCC[3] and IGSCC.

3.2.A.1 TGSCC

TGSCC (Trans-Granular Stress Corrosion Cracking) is related to cracks which propagate inside the grains. It has been studied for a long time. In the case of austenitic stainless steel, it is usually associated with chloride-contaminated aqueous environments [66]. Under certain environmental conditions, the fracture mode will tend to be intergranular [67].

[1] **IGSCC:** Inter-Granular Stress Corrosion Cracking.
[2] **IASCC:** Irradiation Assisted Stress Corrosion Cracking.
[3] **TGSCC:** Trans-Granular Stress Corrosion Cracking.

3.2.A.2 IGSCC

IGSCC (Inter-Granular Stress Corrosion Cracking) is the most studied SCC phenomenon. Its occurrence in the PWRs can not be overlooked even though the observation of IGSCC in a good quality PWR primary coolant is not so evident [68]. But one of its specific case, PWSCC[4] should be mentioned.

PWSCC PWSCC (Primary Water Stress Corrosion Cracking) actually links to the water chemistry in the primary circuit of PWRs. However, concerning the cracking occurrence, pH, the presence of Li/B, impurities in the water may only bring very small changes on the crack growth. The major issue comes form the dissolved oxygen, or more preciously the precursor of oxygen, the hydrogen peroxide [69]. As known, the corrosion potential, E_{corr} decreases with H_2 and increases with O_2. With the presence of O_2, the crack growth rate increases dramatically. On the other hand, the concentration of dissolve hydrogen also has an effect on PWSCC initiation [70]. It appears that the PWSCC initiation time become longer with the decrease of dissolved hydrogen in the water. Fig.3.22 illustrates the effect of dissolved hydrogen and dissolved oxygen (or H_2O_2) on the corrosion potential, and the correlation of the crack growth rate and dissolved hydrogen. Both electrochemical potential and crack growth rate decrease with dissolved hydrogen, either slightly or significantly [71]. Contrarily, the electrochemical corrosion potential increases with the increasing O_2 (H_2O_2).

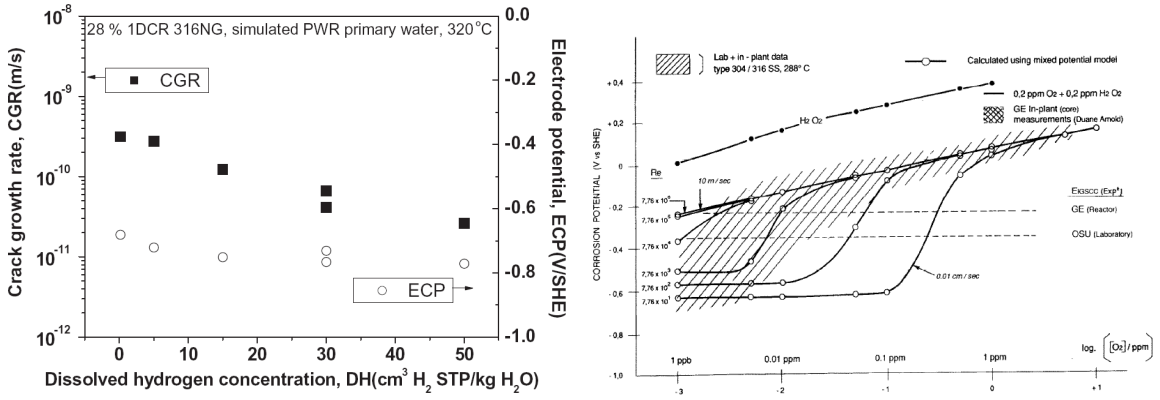

(a) (b)

Figure 3.22: Corrosion potential evolution in the presence of H_2, O_2 and H_2O_2. (a): Crack growth rate (left axe) and electrode potential (right axe) versus dissolved hydrogen for a 316L in a simulated primary PWR water at 320°C [71]; (b): Electrochemical corrosion potential versus the concentration of O_2 and H_2O_2 at 288°C in BWR conditions [72].

Usually, we separate the sensitised and annealed materials for discussion due to their different responses to SCC [67].

One of the explanations for the occurrence of IGSCC is linked to grain boundary compositions. Bruemmer *et al.* [73] have demonstrated its effect on promoting the IGSCC. Interfacial chemical composition can be changed by equilibrium and/or non-equilibrium process from the substrate matrix.

[4]**PWSCC:** Primary Water Stress Corrosion Cracking.

As a result, segregation and depletion of alloy/impurities elements can occur, and precipitated into second phases subsequently. Fig.3.23 shows the different parameters which can affect on the cracks.

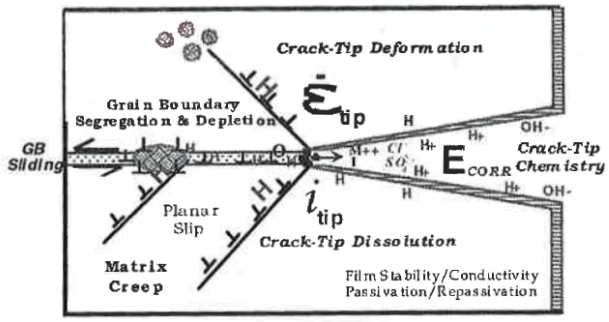

Figure 3.23: Diagrammatic layout of crack-tip process with different aspects of IGSCC [73].

For austenitic stainless steel, the change of interfacial Cr concentration is the dominant cause to promote IGSCC: the precipitation of Cr-rich $M_{23}C_6$ carbides at the interface leading a Cr depletion in the adjacent region. The extent of the gain boundary Cr depletion can directly control the IGSCC susceptibility of austenitic stainless steel. However, it still depends on some critical factors like the mechanical characteristics and environmental conditions.

The characteristics of Cr depletion depends on the material fabrication and heat treatments more precisely. For sensitised materials, they may have an equilibrium impurity segregation, among which the most known segregant is phosphorus, P. The content can reach 10% in the grain boundary. Others like sulphur and nitrogen may also segregate the gain boundary. The segregation of these impurity elements can promote hydrogen-induced cracking. However, in the case of austenitic stainless steel, it seems that the Cr depletion is not influenced by segregations [74]. For annealed materials, on the other hand, the segregation is considered as non-equilibrium. Elements like Cr and Mo are enriched on grain boundarys, Fe and Ni are decreased relatively. Actually, this *presegregration*, a non-equilibrium and vacancy drag process with the degree of boundary enrichment, can be linked to the annealing temperature and cooling rate during the fabrication [75, 76]. Other elements such as boron, carbon and nitrogen may also participate in the presegregration. With the Cr and Mo enrichment in the grain boundary, the resistance of IGSCC is enhanced.

Intergraular cracking happens to sensitised austenitic steel as well as to annealed ones. In the aspect of electrochemical behaviours, the annealed 316L shows two ranges of potentials over which TGSCC occurred whereas the sensitised material showed a wide range of potential for cracking and a transition from TGSCC to IGSCC with increasing applied potential at high temperature [77]. At high temperature, sensitised 316L show a lower strain requirement for crack initiation than annealed ones.

On the other hand, the presence of Ni and Mo in the substrate alloy are beneficial to against the SCC for both annealed and sensitised 316L. Especially Ni, it can be enhanced in the oxide film, and thus the resistance to SCC can be increased [77].

There are certainly many other parameters can influence the IGSCC, the following will be a short list of them: stress, applied potential, concentration of chloride, etc. Under a low stress, pitting, intergranular and transgranular corrosion cracking are possible. However, under high stress, only

intergranular cracking can be observed. It seems that IGSCC can only occur in a narrow range of potentials, above a critical potential and just below the pitting potential [78, 79]. Pitting corrosion on the other hand can occurs over a large range of potential, especially at higher applied potential, only pitting corrosion can be observed. As known, the presence of chloride can bring pitting corrosion. More preciously, with the increase of the chloride, the probability of pitting corrosion will be enhanced. Otherwise, IGSCC will be in predominant position together with TGSCC at lower chloride concentration and at more positive potential [67]. In general, the presence of IGSCC is always accompanied with pitting corrosion of stainless steel [80].

Generally the development of a IGSCC is divided into two stages: initiation and propagation. The crack tips which are extremely sharp and intergranular [81] is the main focus for the initiation stage. Many researches have reported that an enrichment of Ni is observed at the grain boundary ahead of the crack tip and beyond the Cr-rich oxide [82–84]. There also exists a B-rich region at the interface between the oxide and the boundary caused by the B segregation to the gain boundary [75, 82]. Oxidation deformations can be found along the crack path and their orientations likely respect to the propagation direction, which may play an important role. Influences as surface state, temperature, and potential are essentially important for the initiation process. Crack propagation is based on brittle fracture followed by localised oxidation and shearing near the crack tip [82]. The crack growth rate actually depends on the electrochemical potential and the apparent activation energy [81, 85].

Austenitic stainless steel is not susceptible to SCC unless under the oxygenated or irradiated conditions in PWR water. Surely, dissolved oxygen is eliminated under the primary PWR conditions, for the sake of radiolysis and also in the aspect of preventing SCC.

3.2.B IASCC - Irradiation Assisted Stress Corrosion Cracking

3.2.B.1 Introduction

The existence of IASCC, except in nuclear reactors, is rare. During the recent two decades, many scientists have contributed to this essentially complex subject [72, 86–91]. IASCC, a special case of IGSCC, can be referred as intergranular cracking showing little or no ductility which can occur in heavily irradiated structural components of nuclear reactor cores and/ or under irradiation [72]. IASCC is actually IGSCC combined with the presence of irradiation effects. The irradiation effects can be roughly considered into two major parts: effects on the metallic materials and on the water environment. More precisely, irradiation-induced changes in microstructures and microchemical content of alloys and also the environmental changes due to irradiation (radiolysis phenomenon) [89].

Fig.3.24 illustrates the different processes participated in the IASCC:

- **Radiation & Water:** the couple of radiation and water brings about water radiolysis which has been well explained in the previous chapter, Chapter 2.
- **Radiation & Material:** the radiation damage on materials can lead to changes in mechanical and metallurgical properties and subsequently in their resistances to SCC. It is generally thought as the most important factor for IASCC.

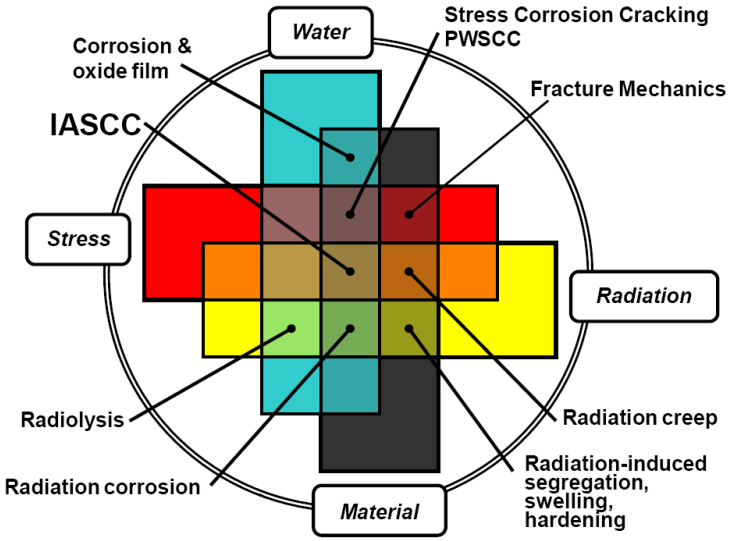

Figure 3.24: Diagram of different processes involved in radiation-induced stress corrosion cracking [92].

- **Radiation & Stress:** the combination of radiation and stress, often included in the *radiation & material*, which is linked to the applied stress. The applied stress can be affected by the dimensional changes due to creep or swelling induced by irradiation.

- **Radiation & Water & Material:** the presence of these three factors result in radiation corrosion. Indeed, the radiolytic products, the impurities in the water, may constitute an aggressive environment and accelerator the process of general corrosion. Moreover, without the presence of stress, the occurrence of IASCC may also possible.

- **Radiation & Water & Material & Stress:** when all the factors get together, it may lead to the IASCC.

The mechanism of IASCC, the main influence parameters, the crack growth rates and so on, have not been clarified yet. However, the effect of neutron fluence on IASCC has been established for a long time, as illustrated in Fig.3.25. One important point is related to the fact that the cracking is observed in BWR oxygenated water at fluence above 5×10^{20} n/cm^2 (E $>$ 1 MeV)[5] while a higher threshold about 2×10^{21} n/cm^2 (E $>$ 1 MeV) is needed in PWRs. This observation emphasises the role of the environment.

The specific radiation-induced microstructural and microchemical changes can promote IASCC susceptibility. Metallurgical, mechanical and environmental aspects which are considered to take part in the process for cracking propagation, as illustrated in Fig.3.26. It can be roughly separated into two aspects: the radiation damages on materials and the environmental changes.

[5]Another unit for fluence: **dpa**, meaning displacement per unit atom.

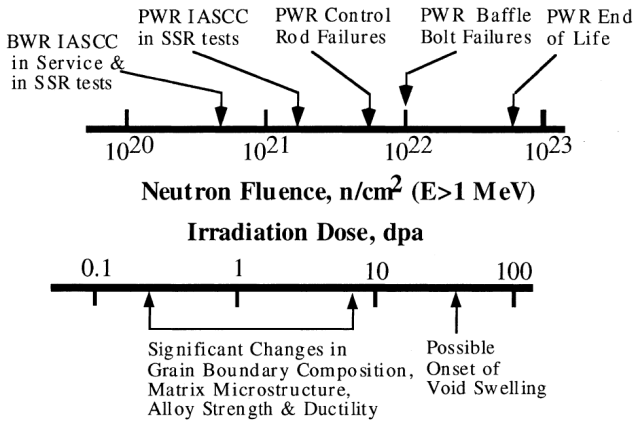

Figure 3.25: Neutron fluence effects on IASCC susceptibility of type 304SS in LWR environments [90].

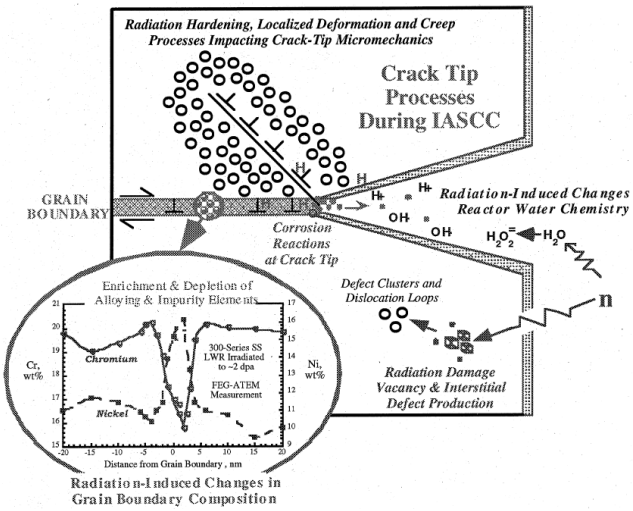

Figure 3.26: Schematic illustrating the different potential parameters on crack advance during IASCC of austenitic stainless steel [90].

3.2.B.2 Radiation Damages on Materials

Usually, radiation damages on materials are regarded as the most important factor for IASCC [72, 88, 90, 91].

The displacement of atoms from their lattice position caused by ionisation radiation is the basis for changes in the material, and results in creation of point defects in materials. Each displaced atom produces a *Frenkel pair*: one vacancy, one self-interstitial atom. The production, annihilation and migration of the point defects lead to changes in microstructure and microchemistry of the material.

- **Microstructural evolution:** starts by the partitioning of vacancies and self-interstitial atoms, and former clusters, dislocation loops and cavities.
- **Microchemical evolution:** caused by the migration of vacancies and self-interstitial atoms to sinks, like grain boundaries, dislocations, precipitations, or surfaces of second phase particles, and gives the local composition change.

Microstructure The mechanism of the microstructural evolution is not easy to predict: the cascade events as atomic displacement and cluster dissolution is rather rapid while the persistent growth of partitioned defect aggregates (the growth of interstitial loop and cavity, network dislocation development, etc.) are slower.

Material composition, thermomechanical treatment, irradiation temperature and dose rate may influence the changes in microstructure. For austenitic stainless steel:

- **Temperature:** is a significant parameter for microstructure evolutions:
  1. *Under* $300°C$, the change is dominanted by small clusters whose diameter is less than 4 nm and large dislocation loops with a diameter between 4 to 20 nm.
  2. *Between* 300 *and* $700°C$, the change is controlled by large faulted loops and network dislocations.
- **Dose** At high dose, cavities/voids[6] represents at the temperature above 350°C [91].

When the temperature is above 350°C, a second phase particles may be formed due to the irradiation, it is known as the radiation-induced precipitation. Nevertheless, the fabrication procedure may have an influence on the IASCC as well [87].

An irradiation at moderate dose and temperature below 350°C, leads to dislocation structure. Otherwise, cavities and voids become dominant at higher dose and higher temperature.

Microchemistry The microchemical evolution during the irradiation is due to *radiation-induced segregation* (RIS) [93]. It is often regarded as the precursor of IASCC. The RIS process is driven by the flux of radiation-produced defects to various sinks including grain boundaries, dislocations, or precipitates on the surfaces, and result in local composition change [73]. RIS is actually controlled by the strength of defect-solute interaction and the kinetics of back diffusion.

Most interstitials annihilate with the vacancies quickly during the irradiation. Major alloying and additional elements in stainless steel are fast diffusing species, such as Cr, Fe and Mo, they are depleted. Meanwhile, Ni as the slowest diffusing species, is enriched on the grain boundary. This is call *Inverse Kirkendall Segregation*, as represented in Fig.3.27 (a). Impurities elements, P and especially Si can bind with interstitials and migrate preferentially into sinks. That is *Interstitial Association segregation*, as delineated in Fig.3.27 (b).

Fig.3.28 illustrates the Cr depletion and Si enrichment on the grain boundary with fluence. Commonly, at 5 dpa, most stainless steel, shows a sharp decrease in Cr to nearly 13%wt, an increase in Si up to about 4% [93]. Therefore, Ni-silicide precipitation has often been observed at the region near sinks in irradiated stainless steel at high temperatures ($>$ 380°C) and high doses ($>$ 20 dpa). Without any doubt, the high concentration of Si at grain boundaries increases the susceptibility to IASCC. Furthermore, the Cr depletion, as stated for the IGSCC, is the major cause for the decrease of resistance to corrosion.

The predominant factors on microchemistry are still the temperature and dose. Mobility reduced at low temperature while back diffusion happens at high temperature. Therefore, in the intermediate

[6] clusters of vacancies and/ or gas bubbles

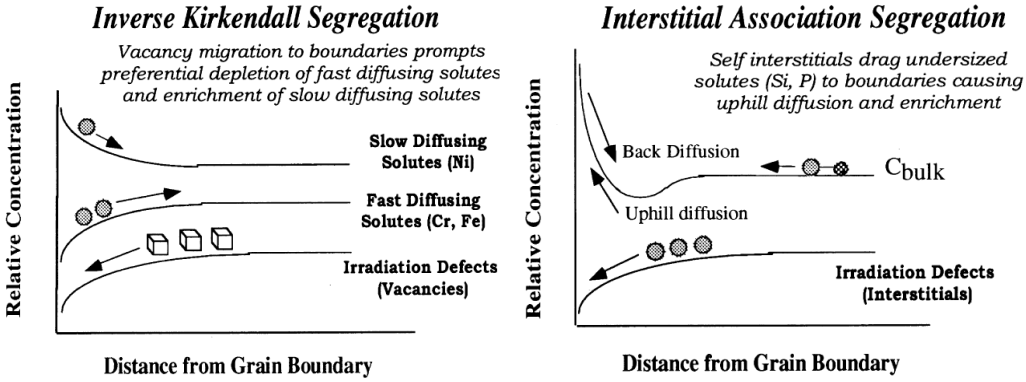

Figure 3.27: Diagrammatic sketch of solute-defect interactions on radiation-induced segregation (RIS): (a) Inverse Kirkendall segregation; (b) Interstitial Association segregation [90].

.

temperature, RIS comes to a maximum. For a specific dose, more RIS at lower dose rate. Between low and moderate dose, 0.1 - 5 dpa, RIS promotes a sharp change in interfacial composition.

Other elements segregate, like P, S, B and so on. However their effects are not significant, but they are still under debate.

Others: radiation hardening, yield strength, creep... The point defect cluster and precipitates produced by irradiation, act as obstacles to dislocation motion, leading to an increase in tensile strength and a reduction in ductility and fracture toughness of the materials. Cavities/ voids, Frank loops, small loops and bubbles can all serve as barriers to dislocation motion. The yield and ultimate stresses increase with irradiation and ductilities decrease [91]. It has been pointed out that hardening, yield strength and creep induced by radiation play an important role in IASCC [72]. It is suggested that a threshold hardening level may exist for the occurrence of IASCC, which corresponds to significant ductility loss and heterogeneous deformation mode [94].

In short, radiation perturbs the materials microstructure and microchemistry and leads to changes the threshold conditions for intergranular cracking. *Mechanistic factors*, deformation and fracture, are essential to interpret IASCC failure, followed by grain boundary chemistry. The third underpinning discipline will be the evolution of corrosion science due to the radiation-induced environmental change.

3.2.B.3 Environmental Change

As mentioned in the Chapter 2, both radical and molecular products can be produced during the water radiolysis. Their yields are dependent of mostly LET and temperature. Briefly, solutes reacting with e^-_{aq} or $H^\bullet$, reduce the yield of H_2, whereas those reacting with $HO^\bullet$ reduce the yields of H_2O_2 and O_2 subsequently.

The corrosion potential E_{corr} decreases with the presence of H_2 and increases with O_2. Therefore, the corrosion or redox potentials can be significantly shifted due to the radiolysis. It seems that the environmental changes induced by irradiation are quite clear. Under the consideration of water

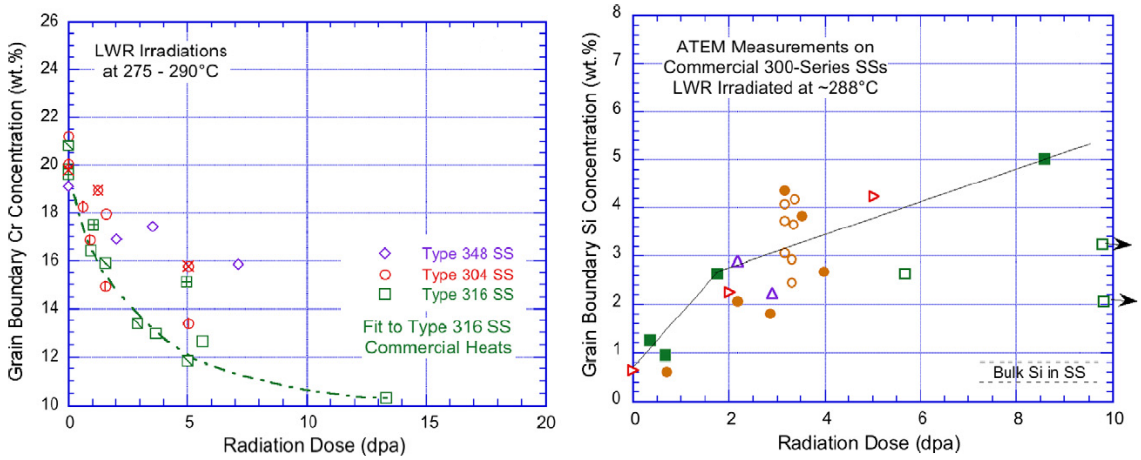

(a) (b)

Figure 3.28: Grain boundary compositions of different stainless steels versus the radiation dose: (a) Cr concentration; (b) Si concentration [91].

.

radiolysis, excess hydrogen is added/dissolved in the primary circuits of PWRs in order to suppress the oxidising species. Thus, the corrosion potential remains at a relatively low, reductive value.

However, things are not so simple in the case of IASCC. For example, the segregation of Si at the grain boundaries can increase the reducing potential in highly irradiated stainless steel, and thus enhances the susceptibility to IASCC [91]. Under this circumstance, a review on electrochemical corrosion potential (ECP) is quite necessary.

3.2.B.4 Electrochemical Corrosion Potential (ECP)

Electrochemical Corrosion Potential (ECP) measurement is a method to predicting the evolution of SCC occurred in nuclear reactors. Based on the tests have done in BWRs, it is believed that a ECP < -230 mV (SHE) can achieve potential SCC mitigation. Above -230 mV (SHE), the crack growth rate increases as the ECP increases. ECP measurement is largely employed in BWRs but not PWRs. It is mainly due to the absence of dissolved oxygen in PWRs. However, it has been pointed out that zero dissolved oxygen does not necessarily mean the ECP is less than -230 mV (SHE). A higher ECP value ($-50 \sim +50$ mV (SHE)) may also be obtained without the presence of dissolved oxygen [95].

ECP is actually a measure of the reduction/oxidation (redox) reactions which occur on the metal/solution interface. These reactions depend directly on the dissolved oxygen, hydrogen, and hydrogen peroxide concentration of the water, as indicated in Eqs.3.7, 3.8 and 3.9. It is also worth mentioning the anodic main reaction written in Eq.3.10.

$$H_2 \rightleftarrows 2H^+ + 2e^- \tag{3.7}$$

$$O_2 + 4H^+ + 4e^- \rightleftarrows 2H_2O \tag{3.8}$$

$$H_2O_2 + 2H^+ + 2e^- \rightleftarrows 2H_2O \tag{3.9}$$

$$M \rightarrow M^{n+} + ne^{-} \tag{3.10}$$

According to MacDonald [96], ECP is a mixed potential, can be calculated in MPM (Mixed Potential Model) as a crossing point between anodic and cathodic polarisation curves, and the redox species can be calculated by the **Butler-Volmer** equation, Eq.3.11.

$$i_{R/O} = \frac{e^{(E-E_{R/O})/b_a} - e^{-(E-E_{R/O})/b_c}}{\frac{1}{i_{o,R/O}} + \frac{e^{(E-E_{R/O})/b_a}}{i_{l,a}} - \frac{e^{-(E-E_{R/O}/b_c)}}{i_{l,c}}} \tag{3.11}$$

where E is the potential of electrode, $E_{R/O}$ the equilibrium potential for redox reaction, $i_{o,R/O}$ the exchange current density, $i_{l,a}$ and $i_{l,c}$ the mass transfer limited current densities or limiting current densities ofr anodic and cathodic reactions, b_a and b_c are the respective Tafel constants [97].

Meanwhile, the calculation of ECP in corrosive environments based on the conservation of charge at the interface, the net current is zero, as shown in Eq.3.12:

$$\sum_{j=1}^{n} i_{R/O,j}(E) + i_{corr}(E) = 0 \tag{3.12}$$

where E is the potential, $i_{R/O,j}$ is the partial current density due to the jth redox couple in the system and i_{corr} is the corrosion current density of the substrate.

As suggested by MacDondald, the key to understanding and predicting SCC lies in developing an understanding of origin and properties of the coupling current, as depicted in Fig.3.29. The coupling current enables direct interrogation of the processes that occur at the crack tip and provides information of crack tip dynamics in different systems.

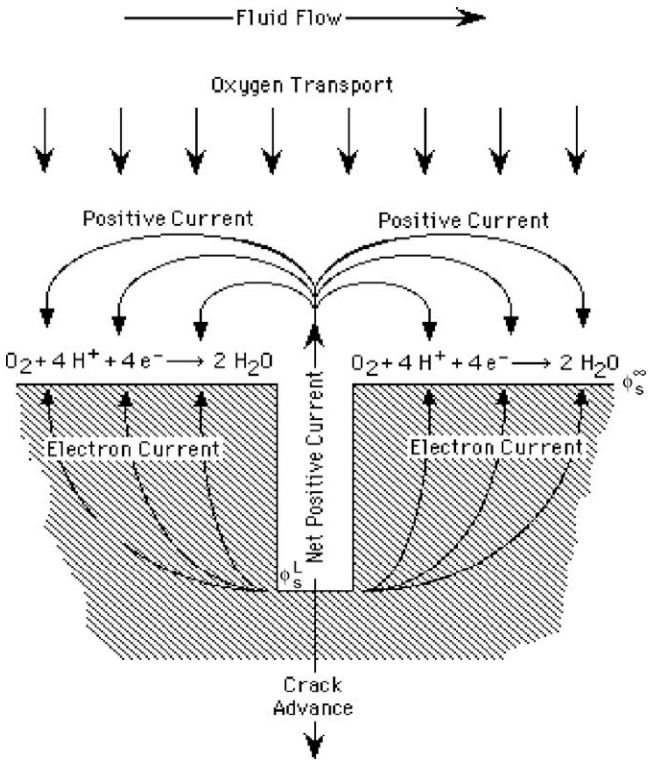

Figure 3.29: Coupling of crack internal and external environments [98].

Therefore, for IGSCC, shifting the ECP to a sufficiently negative value reduces the coupling current and thus the crack growth rate of IGSCC becomes negligible to a certain extent.

Concerning IASCC, MacDonald [97] has developed a code, CEFM, combining with the raidolysis model and mixed potential model, to predict coolant chemistry, ECP, and crack growth rate for any location in the coolant circuit for BWRs. Urquidi-MacDonald and MacDonald *et al.* [99] have developed a code, PWR-ECP, comprising chemistry, radiolysis, and mixed potential models to calculate radiolytic species concentrations and the corrosion potential of structural components at closely spaced points around the primary coolant circuits of PWRs.

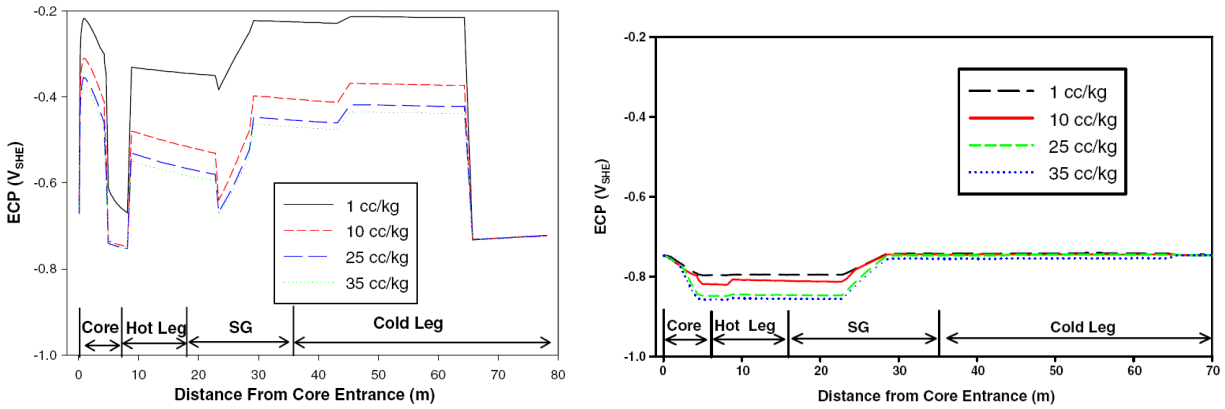

Figure 3.30: Calculated ECP in the primary circuit of a PWR, concentration of O_2 = 5 ppb, concentration of H_2 varied (1, 10, 25, 35 cc/kg): (a) Model uses *high* set of radiolytic yields; (b) Model uses *low* set of radiolytic yields [99].

.

Fig.3.30(a) & (b) illustrate the ECP in primary circuit of a PWR at constant O_2 concentration(5 ppb) and various H_2 concentration. It clearly shows that the sensitivity of the predicted ECP to the assumed values of radiolytic yields. No matter what the H_2 concentration is, the ECPs for *high* set radiolytic yields are always more positive than the ones at *low* set. Secondly, it also demonstrates that with the increasing concentration of H_2, ECP will be shifted to a more negative value.

For the calculation of ECP, only electro-active species presented at the highest concentrations will have a significant impact on ECP. Therefore, in the primary circuit of PWRs, for one thing, it traces back to the radiolytic yields, H_2O_2, $HO^{\bullet}$, $e^-_{aq}$and $H^{\bullet}$. For another, the dissolve hydrogen, added on purpose in the primary circuit, also needs to be take into account.

On the other hand, according to Ishigure *et al.* [100], the radiolysis in the diffusion layer give significant effects on the limiting current densities of the redox reactions of H_2O_2 and H_2, depending on factors as dose rate, flow rate and water chemistry. As a result, ECP can be increased importantly in hydrogen water chemistry conditions.

Briefly, measuring ECP is a good way to get a better understanding of the SCC circumstance, corrosion issues and radiolysis.

3.3 Summary

In this chapter, we have talked about the corrosion issues of 316L under primary PWR conditions. Its protective passive film is a double oxide film structure formed, chromium rich, continuous inner layer and iron rich, discontinuous outer layer. The oxide film also shows semiconducting properties, with a classic p-n heterojunction electronic structure.

With no doubt, influences like PWR chemistry, temperature, stress, pH and etc. can vary the oxide film. However, combining all the influences together, as in a real PWR conditions, stress corrosion cracking may occur. PWSCC and IASCC, two specific forms of IGSCC can be observed for stainless steel, including 316L. With the presence of PWR water and irradiation, corrosion issue becomes more complex.

This is actually the starting point of my thesis study, by including material, water radiolysis and corrosion issues into the same picture.

References

[1] Evans U. R. *The corrosion and oxidation of metals.* Edward Arnold, Londron, 1960.

[2] D.H. Lister and R.D. Davidson and E. McAlpine. The mechanism and kinetics of corrosion product release from stainless steel in lithiated high temperature water. *Corrosion Science*, 27(2):113 – 140, 1987.

[3] Szklarska-Smialowska Z. and Chou Kuo-chin and Xia Zaizhu. The Compostion and Properties of Oxide Films on Type 304 Stainless Steel on Exposure to Lithiate Water at 100-350°C. *Corrosion Science*, 32(5–6):609 – 619, 1991.

[4] Tapping R.L. and Davidson R.D. and McAlpine E. and Lister D. H. The composition and morphology of oxide films formed on type 304 stainless steel in lithiated high temperature water. *Corrosion Science*, 26(8):563 – 576, 1986.

[5] S.E. Ziemniak and M. Hanson. Corrosion behavior of 304 stainless steel in high temperature, hydrogenated water. *Corrosion Science*, 44(10):2209 – 2230, 2002.

[6] Kim Y. J. Characterisation of the Oxide Film Formed on Type 316 Stainless Steel in 288°C Water in Cyclic Normal and Hydrogen Water Chemistries. *CORROSION*, 51(11):849–860, 1995.

[7] Da Cunha Belo M. and Walls M. and Hakiki N. E. and Corset J. and Picquenard E. and Sagon G. and Noël D. Composition, structure and properties of the oxide films formed on the stainless steel 316L in a primary type PWR environment. *Corrosion Science*, 40(2–3):447 – 463, 1998.

[8] Takeda Y. and Shoji T. and Bojinov M. and Kinnunen P. and Saario T. In situ and ex situ characterisation of oxide films formed on strained stainless steel surfaces in high-temperature water. *Applied Surface Science*, 252(24):8580 – 8588, 2006.

[9] Cheng, Xuequn and Feng, Zhicao and Li, Chengtao and Dong, Chaofang and Li, Xiaogang. Investigation of oxide film formation on 316L stainless steel in high-temperature aqueous environments. *ELECTROCHIMICA ACTA*, 56(17):5860–5865, JUL 1 2011.

[10] Terachi T. and Yamada T., Miyamoto T., Arioka K., Fukuya K. Corrosion Behavior of Stainless Steels in Simulated PWR Primary Water - Effect of Chromium Content in Alloys and Dissolved Hydrogen -. *Journal of NUCLEAR SCIENCE and TECHNOLOGY*, 45(10):975–984, 2008.

[11] Féron D. and Herms E. and Tanguy B. Behavior of stainless steel in pressurized water reactor pirmary circuits. *Journal of Nuclear Materials*, 427:364–377, 2012.

[12] Hakiki N.E., Boudin S., Rondot B. and Da Cunha Belo M. The electronic structure of passive film formed on stainless steel. *Corrosion Science*, 37(11):1809–1822, 1995.

[13] Montemor M.F. and Ferreira M.G.S. and Hakiki N.E. and Da Cunha Belo M. Chemical composition and electronic structure of the oxide films formed on 316L stainless steel and nickel based alloys in high temperature aqueous environments. *Corrosion Science*, 42(9):1635 – 1650, 2000.

[14] Terachi T. and Fujii K., Arioka K. Microstructural Characterization of SCC Crack tip ans Oxide Film for SUS 316 Stainless Steel in simulated PWR Primary Water at 320°C. *Journal of NUCLEAR SCIENCE and TECHNOLOGY*, 42(2):225–232, 2005.

[15] Terachi T. and Totsuka N., Yamada T., Nakagawa T., Deguchi H., Horiuchi M., Oshitani M. Influence of dissolved hydrogen on structure of oxide film on Alloy 600 formed in primary water of pressurized water reactors. *Journal of NUCLEAR SCIENCE and TECHNOLOGY*, 40(7):509–516, 2003.

[16] Lobnig R. E., Schmidt H.P., Hennesen K. and Grabke H. J. Diffusion of Cations in Chromia Layers Grown on Iron-Base Alloys. *Oxidaation of Metals*, 37:81–93, 1992.

[17] Carrette F., Lafont M. C., Chatainier G., Guinard L. and Pieraggi B. Analysis and TEM examination of corrosion scales grown on Alloy 690 exposed to pressurized water at 325°C. *Surf. Interface Anal.*, 34:135–138, 2002.

[18] Soulas R., Cheynet M., Rauch E., Neisius T., Legras L., Domain C., Brechet Y. TEM investigations of the oxide layers formed on a 316L alloy in simulated PWR environment. *J Mater Sci*, 48:2861–2871, 2013.

[19] Jean-Philippe Berge. *Influence des traitement de surface sur la résistance á la corrosion des aciers inoxydables.* PhD thesis, Faculté de Université de Paris, 1968.

[20] Beverskog G. and Puigdomenech I. Revised pourbaix diagrams for iron at 25-300°C. *Corrosion Science*, 38(12):2121–2135, 1996.

[21] You D. Présentation du module de chimie pour pactole: Phreeqc-cea, private communication. Technical report, CEA, 2004.

[22] You D. Comportement thermodynamique des ferrites de nickel, de cobalt et de fer dans les réacteurs á eau pressurisée, private communication. Technical report, CEA, 1997.

[23] Beverskog G. and Puigdomenech I. Revised pourbaix diagams for nickel at 25-300°C. *Corrosion Science*, 39(5):969–980, 1997.

[24] Loïc Marchetti-Sillans. *Corrosion généralisée des alliages á base nickel en milieu aqueux á haute température: apport á la compréhension des mécanismes.* PhD thesis, Ecole Nationale Supérieure des Mines de Saint-Etienne, 2007.

[25] Sergio Lozano-Perez and David W. Saxey and Takuyo Yamada and Takumi Terachi. Atom-probe tomography characterization of the oxidation of stainless steel. *Scripta Materialia*, 62(11):855 – 858, 2010.

[26] Perrin S., Marchetti L., Duhamel C., Sennour M., Jomard F. Influence of Irradiation on the Oxide Film Formed on 316L Stainless Steel in PWR Primary Water. *Oxid. Met.*, 2013.

[27] Macdonald D. D. The Point Defect Model for the Passive State. *J. Electrochem. Soc.*, 139(12), 1992.

[28] Macdonald D. D. Passivity-the key to our metals-based civilization. *Pure Appl. Chem.*, 71(6), 1999.

[29] Macdonald D. D., Al Rifaie M. and Engelhardt G. R. New Rate Laws for the Growth and Reduction of Passive Films. *J. Electrochem. Soc.*, 148(9), 2001.

[30] Wilhelm S. M. and Hackerman N. Photoelectrochemical Characterization of the Passive Films on Iron and Nickel. *J. Electrochem. Soc.*, 128(8):1668–1674, 1981.

[31] Hakiki N.E. and Montemor M.F. and Ferreira M.G.S. and Da Cunha Belo M. Semiconducting properties of thermally grown oxide films on AISI 304 stainless steel. *Corrosion Science*, 42(4):687 – 702, 2000.

[32] Feng Zhicao and Cheng Xuequn and Dong Chaofang and Xu Lin and Li Xiaogang. Passivity of 316L stainless steel in borate buffer solution studied by Mott-Schottky analysis, atomic absorption spectrometry and X-ray photoelectron spectroscopy. *Corrosion Science*, 52(11):3646 – 3653, 2010.

[33] De Gryse R., Gomes W. P., Cardon F. and Vennik J. On the Interpretation of Mott-Schottky Polts Determined at Semiconductor/Electrolyte Systems. *J. Electrochem. Soc.*, 122 (5):711–712, 1975.

[34] Gärtner W. W. Depletion-Layer Photoeffects in Semiconductors. *Phys. Rev.*, 116(1):84–87, 1959.

[35] Butler M. A. Phtotelectrolysis and physical properties of the semiconduting electrode WO_3. *J. Appl. Phys.*, 48(5):1914–1920, 1977.

[36] Hamadou L., Kadri A., Boughrara D., Benbrahim N., Petit J. P. Influence of oxidation time on semiconductive behaviour of thermally grown oxide films on AISI 304L. *Applied Surface Science*, 252, 2006.

[37] Di Quarto F., Sunseri C., Piazza S., Romano M.C. Semiempirical Correlation between Optical Band Gap Values of Oxides and the Difference of Electronegativity of the Elements. Its Importance for a Quantitative Use of Photocurrent Spectroscopy in Corrosion Studies. *J. Phys. Chem. B*, 101(14):2519–2525, 1997.

[38] Sudesh T. L., Wijesinghe L. and Blackwood D. J. Electrochemical & optical characterisation of passive films on stainless steels. *J. Phys.: Conf. Ser.*, 28:74–78, 2006.

[39] Park J. H., Chopra O. K., Natesan K. and Shack W. J. Boric acid corrosion of light water reactor pressure vessel materials. In *Proceedings of the 12th International Conference on Environmental Degradation of Materials in Nuclear Power System - Water Reactors*, 2005.

[40] Lozano-Perez S., Schröder, Yamada T., Terachi T., English C. A., Grovenor C. R. M. Using NanoSIMS to map trace elements in stainless steels from nuclear reactors. *Applied Surface Science*, 255:1541–1543, 2008.

[41] Andresen P. L., Emigh P. W., Morra M. M. and Hickling J. Effects of PWR Primary Water Chemistry and Deaerated Water on SCC. In Allen T. R., King P. J. and Nelson L., editor, *Proceedings of the 12th International Conference on Environmental Degradation of Materials in Nuclear Power System - Water Reactors*, pages 989–1008, 2005.

[42] Huang J. B., Wu X. Q., Han E. H. Influence of pH on electrochemical properties of passive films formed on Alloy 690 in high temperature aqueous environments. *Corrosion Science*, 51:2976–2982, 2009.

[43] Sun H., Wu X. Q., Han E. H., Wei Y. Z. Effects of pH and dissolved oxygen on electrochemical behavior and oxide films of 304SS in borated and lithiated high temperature water. *Corrosion Science*, 59:334–342, 2012.

[44] Freire L. and Carmezim M. J. and Ferreira M. G. S. and Montemor M. F. The passive behaviour of AISI 316 in alkaline media and the effect of pH: A combined electrochemical and analytical study. *Electrochimica Acta*, 55(21):6174 – 6181, 2010. IMPEDANCE SPECTROSCOPY AND TRANSFER FUNCTIONS.

[45] Carmezim M. J. and Simões A. M., Montemor M. F., Da Cunha Belo M. Capacitance behaviour of passive films on ferritic and austenitic stainless steel. *Corrosion Science*, 47(3):581 – 591, 2005. Corrosion, Electrodeposition and Surface treatment of the 54th Annual Meeting of the ISE.

[46] Cissé, S., Laffont L., Tanguy B., Lafont M. C., Andrieu E. Effect of surface preparationon the corrosion of austenitic stainless steel 304L in high tmeperature steam and simulated PWR primary water. *Corrosion Science*, 56:209–216, 2012.

[47] Delabrouile F. and Legras L., Vaillant F., Scott P., Viguier B., Andrieu E. Effect of the chromium cotent and strain on the corrosion of nickel based alloys in primary water of pressurized water reactors. In Allen T. R., King P. J. and Nelson L., editor, *Proceeding of the 12th International Conference on Environmental Degradation of Materials in Nuclear Power System - Water Reactors* -, pages 903–909, 2005.

[48] Takeda Y., Bojinov M., hanninen H., Kinnunen P., Laitinen T., Mäkelä K. Saario T., Sakaguchi T., Shoji T., Sirkiä P., Toivonen A. Effect of Strain on Electric Properties of Oxide Films Growing on AISI 316L Steel in Simulated BWR Conditions. In *Proceedings of the 11th International Conference on Environmental Degradation of Materials in Nuclear Power System - Water Reactors*, 2003.

[49] Töpfer J., Affarwal S., Dieckmann R. Point defects and cation tracer diffusion in $(Cr_xFe_{1-x})_{3-\delta}O_4$ spinels. *Solid State Ionics*, 81, 1995.

[50] Takeda Y., Bojinov M., hanninen H., Kinnunen P., Laitinen T., Mäkelä K. Saario T., Sakaguchi T., Shoji T., Sirkiä P., Toivonen A. Effects of environmental factors on the electronic properties of interfacial oxide film on 304L stainless steel in high temperature pure water. *Key Eng. Mater.*, 925:261–263, 2004.

[51] Vignal V., Valot C., Oltra R., Verneau M., Coudreuse L. Analogy between the effects of a mechanical and chemical perturbation on the conductivity of passive films. *Corrosion Science*, 44, 2002.

[52] Cissé, S., Laffont L., Lafont M. C., Tanguy B., Andrieu E. Influence of localized plasticity on oxidation behaviour of austenitic stainless steels under primary water reactor. *Journal of Nuclear Materials*, 433:319–328, 2013.

[53] Couvant T., Legras L., Vaillant F., Boursier J. M. Rouillon Y. Effect of strain-hardening on stress corrosion cracking of AISI 304L stainless steel in PWR primary environment at 360°C. In Allen T. R., King P. J. and Nelson L., editor, *Proceeding of the 12th International Conference on Environmental Degradation of Materials in Nuclear Power System - Water Reactors* -, pages 1069–1081, 2005.

[54] Dieckmann R. Point defects and transport properties of binary and ternary oxides. *Solid State Ionics*, 12, 1984.

[55] Berge P., Ribon C., Paul P. S. Effect of hydrogen on the corrosion of steels in high temperature water. *Corrosion*, 33(5), 1997.

[56] Qiu Y. B., Shoji T., Lu Z. P. Effect of dissolve hydrogen on the electrochemical behaviour of Alloy 600 in simulated PWR primary water at 290°C. *Corrosion Science*, 53, 2011.

[57] Kuang W. J., Wu X. Q., Han E. H. Influence of dissolve oxygen concentration on the oxide formed on 304 stainless steel in high temperature water. *Corrosion Science*, 63, 2012.

[58] Montemor M.F. and Simões A. M. P., Ferreira M.G.S. and Da Cunha Belo M. The role of Mo in the chemical composition and semiconductive behaviour of oxide films formed on stainless steels. *Corrosion Science*, 41:17–34, 1999.

[59] Mathieu H. J. and Landolt D. An investigation of thin oxide films thermally grown in situ on $Fe_{24}Cr$ and $Fe_{24}Cr_{11}Mo$ by auger electron spectroscopy and X-ray photoelectron spectroscopy. *Corrosion Science*, 26(7), 2012.

[60] Taveira L. V. and Montemor M. F., Da Cunha Belo M., Ferreira M. G., Dick L. F. P. Influence of incorporated Mo and Nb on the Mott-Schottky behaviour of anodic films formed on AISI 304L. *Corrosion Science*, 52:2813–2818, 2010.

[61] Betova I., Bojinov M., Kinnunen P, Lundgren K. Saario T. Influence of Zn on the oxide layer on AISI 316L(NG) stainless steel in simulated pressurised water reactor coolant. *Electrochimica Acta*, 54, 2009.

[62] Pérez F. R., Barrero C. A., Hight Walker A. R., García, Nomura K. Effects of chloride concentration, immersion time and steel composition on the spinel phase formation. *Materials Chemistry and Physics*, 117, 2009.

[63] Bellanger G. . Localized corrosion of 316L stainless steel in tritiated water containing aggressive radiolytic and decomposition products at different temperatures. *Journal of Nuclear Materials*, 374(1–2):20 – 31, 2008.

[64] Scott P. M., Le Calvar M. Some possible mechanisms of intergranular stress corrosion cracking of Alloy 600 in PWR primary water. In *Proc. 6th Int. Symp. on Environmental Degradation of Materials in Nuclear Power System - Water Reactors*, pages 657–665, 1993.

[65] Scott P. M. An Overview of Internal Oxidation as a Possible Explanation of Intergranular Stress Corrosion Cracking of Alloy 600 in PWRs. In Ford P. N., Bruemmer S. M. and Was G. S., editor, *Proceedings of the 9th International Symposium on Environmental Degradation of Materials in Nuclear Power Systems - Water Reactors*, pages 3–14, 1999.

[66] Lantanision R. M. and Staehle R. W. From Conference on Fundamental As pecks of Stress Corrosion Cracking, Athens, Ohio. UNCL. Orig. Technical report, Ohio State Univ. Reasearch Foundation, Columbus, 1967.

[67] Cragnolino G. and Macdonald D. D. Intergranular Stress Corrosion Cracking of Austenitic Stainless Steel at Temperature Below 100°C- A Review. *Corrosion - NACE*, 38, 1982.

[68] Tice D., Platts N., Rigby K., Stairmand J and Fairbrother H. Environmentally assisted crack growth of cold-worked type 304 stainless steel in PWR environments. In Allen T. R., King P. J. and Nelson L., editor, *Proceedings of the 12th International Conference on Envirommental Degradation of Materials in Nuclear Power System - Water Reactors*, pages 1037–1048, 2005.

[69] Uchida S., Satoh T., Morishima Y., Hirose T., Miyazawa T., Kakinuma N., Satoh Y., Usui N. and Wada Y. Effects of Hydrogen Peroxide and Oxygen on Corrosion of Stainless Steel in High Temperature Water. In Allen T. R., King P. J. and Nelson L., editor, *Proceedings of the 12th International Conference on Environmental Degradation of Materials in Nuclear Power System - Water Reactors*, pages 19–29, 2005.

[70] DOZAKI K., AKUTAGAWA D., NAGATA N, TAKIGUCHI H., and NORRING K. Effects of dissolved hydrogen content in pwr primary water on pwscc initiation property. *E-Journal of Advanced Maintenance*, Vol. 2:p. 65 – 67, 2010.

[71] Meng F. J., Lu Z. P., Shoji T., Wang J. Q. Han E. H., Ke W. Stress corrosion cracking of uni-directionally cold worked 316NG stainless steel in simulated PWR primary water with various dissolved hydrogen concentrations. *Corrosion Science*, 53:2558–2565, 2011.

[72] Scott P. M. A review of irradiation assisted stress corrosion cracking. *Journal of Nuclear Materials*, 211:101–122, 1994.

[73] Bruemmer S. M. Grain Boundary Composition and Effects on Environmental Degradation. *Materials Science Forum*, 294-296, 1999.

[74] Andresen P. L. and Briant C. L. In Theus G. J. and Weeks J. R., editor, *Proc. 3rd Int. Environmental Degradation of Materials in Nuclear Power System - Water Reactors*, page 371, 1988.

[75] Karsson L., Nordén H., Odelius H. Overview no.63 Non-equilibrium grain boundary segregation of boron in austenitic stainless steel - I. Large scale segregation behaviour. *Acta Metallrugica*, 36:1–12, 1988.

[76] Bruemmer S. M. Grain Boundary segregation inaustenitic Stainless Steels and Effects on Intergranular Stress corrosion Cracking in Light-Water Reactor Environments. *Corrosion*, NACE Conference Papers, 1998.

[77] Congleton J. and Yang W. The effect of applied potential on the stress corrosion cracking of sensitized type 316 stainless steel in high temperature water. *Corrosion Science*, 37(3):429 – 444, 1995.

[78] Macdonald D. D. and Cragnolino G. The critical potential for the IGSCC of sensitized type 304 in high temperature aqueous systems. In Nelson J. L. and Cubicciotti D., editor, *Proceedings: Workshop on Initiation of Stress corrosion Cracking Under LWR Conditions*, pages 22–30, 1988.

[79] Andresen P. L. and Ford P. F. Life prediction by mechanistic modelling and system monitoring of environmental cracking of iron an nickel alloys in aqueous systems. *Mat. Sci. Eng. A*, 103(1), 1988.

[80] Lin L. F., Cragnolino G., Szklarska-Smialowska Z., Macdonald D. D. Stress corrosion Cracking of Sensitised Type 304 Stainless Steel in High Temperature Chloride Solutions. *Corrosion*, 37:616–627, 1981.

[81] Young G. A., Wilkening W. W., Morton D. S. richey E. and Lewis N. The mechanism and modeling of intergranular stress corrosion cracking of nickel-chromium-iron alloys exposed to high purity water. In Allen T. R., King P. J. and Nelson L., editor, *Proceedings of the 12th International Conference on Environmental Degradation of Materials in Nuclear Power System - Water Reactors*, pages 913–924, 2005.

[82] Lozano-Perez S. and Yamada T. and Terachi T. and Schröder M. and English C. A. and Smith G. D. W. and Grovenor C. R. M. and Eyre B. L. Multi-scale characterization of stress corrosion cracking of cold-worked stainless steels and the influence of Cr content. *Acta Materialia*, 57(18):5361 – 5381, 2009.

[83] Tolockzo M. B., Andresen P. L., Bruemmer S. M. In Curran Associates, Inc., editor, *Proceedings of the 13th International Conference on Environmental Degradation of Materials in Nuclear Power System - Water Reactors*, page 1672, 2007.

[84] Bruemmer S. M., Thomas L. E. High-Resolution Characterizations of Stress-Corrosion Cracks in Austenitic Stainless Steel from Crack Growth Tests in BWR-Simulated Environments. In Allen T. R., King P. J. and Nelson L., editor, *Proceedings of the 12th International Conference on Environmental Degradation of Materials in Nuclear Power System - Water Reactors*, page 189, 2005.

[85] Morton D. S., Attanasio S. A., Richey E., and Young G. A. In Search of the True Temperature and Stress Intensity Factor Dependencies for PWSCC. In Allen T. R., King P. J. and Nelson L., editor, *Proceedings of the 12th International Conference on Environmental Degradation of Materials in Nuclear Power System - Water Reactors*, page 189, 2005.

[86] Jacobs A. J. and Wozadlo G. P. Irradiation-Assisted Stress Corrosion Cracking as a Factor in Nuclear Power Aging. *J. Mater. Eng.*, 9:345–351, 1988.

[87] Chung H. M., Ruther W. E., Sanecki J. E., Hins A., Zaluzec N. J., Kassner T. F. Irradiation-assisted stress corrosion cracking of austenitic steels: recent progress and new approaches. *Journal of Nuclear Materials*, 239:61–79, 1996.

[88] McNeil M. B. Irradiation assisted stress corrosion cracking. *Nuclear Engineering and Design*, 181:55–60, 1998.

[89] Shoji T., Suzuki S. I., Raja K. S. Current status and future of IASCC research. *Journal of Nuclear Materials*, 258-263:241–251, 1998.

[90] Bruemmer S. M., Simonen E. P., Scott P. M., Andresen P. L., Was G. S., Nelson J. L. Radiation-induced material changes and susceptibility to intergranular failure of light-water-reactor core internals. *Journal of Nuclear Materials*, 274:299–314, 1999.

[91] Chopra O. K., Rao A. S. A review of irradiation effects on LWR core internal materials - IASCC susceptibility and crack growth rates of austenitic stainless steels. *Journal of Nuclear Materials*, 409:235–256, 2011.

[92] Vankeerberghen M. IASCC Modelling: phenomenological approach. In *Training symposium on Irradiation Effects in Structural Materials for Nuclear Reactors*, pages STR–6.1–1 – STR–6.1–5, 2012.

[93] Bruemmer S. M. In *Proc. 10th Int. Symp. on Environmental Degradation of Materials in Nuclear Power System - Water Reactors*, volume paper no. 0008V, 2001.

[94] Fukuya K., Nakano M., Fujii K., Torimaru T. and Kitsunai Y. Separation of Microstructural and Micorchemical Effects in Irradiation Assisted Stress Corrosion Cracking using Post-irradiation Annealing. *Journal of NUCLEAR SCIENCE and TECHNOLOGY*, 41:1218–1227, 2004.

[95] Hettiarachchi S. Advances in Electrochemical Corrosion Potential Monitoring in Boiling Water Reactors. In Allen T. R., King P. J. and Nelson L., editor, *Proceedings of the 12th International Conference on Environmental Degradation of Materials in Nuclear Power System - Water Reactors*, pages 3–17, 2005.

[96] MacDonald D. D. *Corrosion*, 48:194, 1992.

[97] MacDondald D. D. The Electrochemistry of Stress Corrosion Cracking in Water-Cooled Reactor Coolant Circuits. In *Presentation at OLI Systems INC, Morris Plains, NJ*, 2007.

[98] Maeng W. Y., Macdondald D. D. The effect of acetic acid on the stress corrosion cracking of 3.5NiCrMoV turbine steels in high temperature water. *Corrosion Science*, 50:2239–2250, 2008.

[99] Mirna Urquidi-Macdonald, Jonathan Pitt, and Digby D. Macdonald. The impact of radiolytic yield on the calculated ECP in PWR primary coolant circuits. *Journal of Nuclear Materials*, 362(1):1 – 13, 2007.

[100] Ishigure K., Nukii T., Ono S. Analysis of water radiolysis in relation to stress corrosion cracking of stainless steel at high temperatures - Effect of water radiolysis on limiting current densities of anodic and cathodic reactions under irradiation. *Journal of Nuclear Materials*, 350:56–65, 2006.